University of Iowa

Iowa Research Online

Theses and Dissertations

Spring 2012

Reaction kinetics of cellulose hydrolysis in subcritical and supercritical water

Kazeem Bode Olanrewaju
University of Iowa

Recommended Citation
Olanrewaju, Kazeem Bode. "Reaction kinetics of cellulose hydrolysis in subcritical and supercritical water."
PhD (Doctor of Philosophy) thesis, University of Iowa, 2012.
https://doi.org/10.17077/etd.vq2ldcuy

REACTION KINETICS OF CELLULOSE HYDROLYSIS IN SUBCRITICAL AND

SUPERCRITICAL WATER

by

Kazeem Bode Olanrewaju

<u>An Abstract</u>

Of a thesis submitted in partial fulfillment
of the requirements for the Doctor of
Philosophy degree in Chemical and Biochemical Engineering
in the Graduate College of
The University of Iowa

May 2012

Thesis Supervisors: Adjunct Associate Professor Gary A. Aurand
Professor David Rethwisch

ABSTRACT

The uncertainties in the continuous supply of fossil fuels from the crisis-ridden oil-rich region of the world is fast shifting focus on the need to utilize cellulosic biomass and develop more efficient technologies for its conversion to fuels and chemicals. One such technology is the rapid degradation of cellulose in supercritical water without the need for an enzyme or inorganic catalyst such as acid. This project focused on the study of reaction kinetics of cellulose hydrolysis in subcritical and supercritical water.

Cellulose reactions at hydrothermal conditions can proceed via the homogeneous route involving dissolution and hydrolysis or the heterogeneous path of surface hydrolysis. The work is divided into three main parts. First, the detailed kinetic analysis of cellulose reactions in micro- and tubular reactors was conducted. Reaction kinetics models were applied, and kinetics parameters at both subcritical and supercritical conditions were evaluated. The second major task was the evaluation of yields of water soluble hydrolysates obtained from the hydrolysis of cellulose and starch in hydrothermal reactors. Lastly, changes in molecular weight distribution due to hydrothermolytic degradation of cellulose were investigated. These changes were also simulated based on different modes of scission, and the pattern generated from simulation was compared with the distribution pattern from experiments.

For a better understanding of the reaction kinetics of cellulose in subcritical and supercritical water, a series of reactions was conducted in the microreactor. Hydrolysis of cellulose was performed at subcritical temperatures ranging from 270 to 340 °C (τ = 0.40-0.88 s). For the dissolution of cellulose, the reaction was conducted at supercritical temperatures ranging from 375 to 395 °C (τ = 0.27 - 0.44 s). The operating pressure for

the reactions at both subcritical and supercritical conditions was 5000 psig. The results show that the rate-limiting step in converting cellulose to fermentable sugars in subcritical and supercritical water differs because of the difference in their activation energies.

Cellulose and starch were both hydrolyzed in micro- and tubular reactors and at subcritical and supercritical conditions. Due to the difficulty involved in generating an aqueous based dissolved cellulose and having it reacted in subcritical water, dissolved starch was used instead. Better yields of water soluble hydrolysates, especially fermentable sugars, were observed from the hydrolysis of cellulose and dissolved starch in subcritical water than at supercritical conditions.

The concluding phase of this project focuses on establishing the mode of scission of cellulose chains in the hydrothermal reactor. This was achieved by using the simulated degradation pattern generated based on different scission modes to fingerprint the degradation pattern obtained from experiment.

Abstract Approved: _____
  Thesis Supervisor

  _____
  Title and Department

  _____
  Date

  _____
  Thesis Supervisor

  _____
  Title and Department

  _____
  Date

REACTION KINETICS OF CELLULOSE HYDROLYSIS IN SUBCRITICAL AND

SUPERCRITICAL WATER

by

Kazeem Bode Olanrewaju

A thesis submitted in partial fulfillment
of the requirements for the Doctor of
Philosophy degree in Chemical and Biochemical Engineering
in the Graduate College of
The University of Iowa

May 2012

Thesis Supervisors: Adjunct Associate Professor Gary A. Aurand
Professor David Rethwisch

Graduate College
The University of Iowa
Iowa City, Iowa

CERTIFICATE OF APPROVAL

_____

PH.D THESIS

_____

This is to certify that the Ph.D. thesis of

Kazeem Bode Olanrewaju

has been approved by the Examining Committee
for the thesis requirement for the Doctor of
Philosophy degree in Chemical and Biochemical
Engineering at the May 2012 graduation.

Thesis Committee: _____
                    Gary A. Aurand, Thesis Supervisor

                  _____
                    David Rethwisch, Thesis Supervisor

                  _____
                    Alec Scranton

                  _____
                    Julie L.P Jessop

                  _____
                    Daniel M.Quinn

To GOD the Father, the Son, the Holy Spirit and to my loving mother and my late father

ACKNOWLEDGEMENTS

First and foremost, I wholeheartedly acknowledged GOD ALMIGHTY for making it possible for me to complete this project and for showering upon me HIS boundless grace, mercy and wisdom during my studies at the University of Iowa. The success of this project is without doubt a result of the unwavering effort of my advisor, Prof. Gary Aurand, who took courage to get me on board his research group at a time when the prospect of continuing the Ph.D programme appear bleak. Words will not be enough to express my immense appreciation for what you did Sir. Thus, I will like to thank Prof. David Rethwisch for accepting to serve as co-chair on my Ph.D thesis defense committee and for offering valuable contributions during and after the defense.

I will like to express my deepest appreciation to Prof. Daniel Quinn, Prof. Alec Scranton, and Prof. Julie Jessop, for willing to be on my thesis defense committee and for offering valuable contribution during and after the thesis defense. I will forever be grateful to the Iowa Energy Center and the University of Iowa graduate college for their financial support. It is no gainsaying that the completion of this project would have been met with serious hitch without these monetary supports.

My sincere gratitude goes to the entire staff of the department of chemical and biochemical engineering, University of Iowa. Honor they say should be given to whom is due and that explain why I will like to specially thank Ms.Linda and Ms.Natalie for the amazing work they do in the department such as helping in acquiring chemical and materials for research, offering administrative assistance where necessary and a desire to see us finished our degree programs in accolade. I will like to say a big thank you to Mr. Steve Struckman and his late co-worker Mr. Herbert Dirks, in the machine shop for

helping with quick repair and machining of metallic parts of some of the equipment used in the laboratory. I owe a lot of debt of appreciation to my colleagues in the biorenewable and supercritical fluid reaction research group, Ashley D'Ann Koh and Kehinde Bankole for their academic and moral support. I also wish to express my gratitude to friends in Iowa City including the Alarapes, the Onwuamezes, the Ajiboyes, the Goshits, the Vasciks, Chioma Ibeawuachi, Patience Ezenwanne, and members of international and living spring fellowships for their camaraderie and social support in the course of my study. However, my compliments will be incomplete without expressing my profound gratitude to my Aunty in New York, Mrs Bosede Otulaja and her Husband, Dr. Femi Otulaja for their parental advice and support this couple of years spent so far in the US of A.

I will like to thank my siblings, Mrs Oluwatoyin Akintomide, Mrs Oluwabunmi Oloruntoba, Mr Abiola Adeniji, Miss Oluwabukola Adeniji and Mrs Lara for their moral and prayer supports. Lastly, many thanks to my late father, Pa Olatunji Olanrewaju (who died midway into my Ph.D programme) and my mother, Mrs Oluwakemi Olanrewaju for instilling in me, through GOD's grace, the values that have carried me through these years.

ABSTRACT

The uncertainties in the continuous supply of fossil fuels from the crisis-ridden oil-rich region of the world is fast shifting focus on the need to utilize cellulosic biomass and develop more efficient technologies for its conversion to fuels and chemicals. One such technology is the rapid degradation of cellulose in supercritical water without the need for an enzyme or inorganic catalyst such as acid. This project focused on the study of reaction kinetics of cellulose hydrolysis in subcritical and supercritical water.

Cellulose reactions at hydrothermal conditions can proceed via the homogeneous route involving dissolution and hydrolysis or the heterogeneous path of surface hydrolysis. The work is divided into three main parts. First, the detailed kinetic analysis of cellulose reactions in micro- and tubular reactors was conducted. Reaction kinetics models were applied, and kinetics parameters at both subcritical and supercritical conditions were evaluated. The second major task was the evaluation of yields of water soluble hydrolysates obtained from the hydrolysis of cellulose and starch in hydrothermal reactors. Lastly, changes in molecular weight distribution due to hydrothermolytic degradation of cellulose were investigated. These changes were also simulated based on different modes of scission, and the pattern generated from simulation was compared with the distribution pattern from experiments.

For a better understanding of the reaction kinetics of cellulose in subcritical and supercritical water, a series of reactions was conducted in the microreactor. Hydrolysis of cellulose was performed at subcritical temperatures ranging from 270 to 340 °C (τ = 0.40-0.88 s). For the dissolution of cellulose, the reaction was conducted at supercritical temperatures ranging from 375 to 395 °C (τ = 0.27 - 0.44 s). The operating pressure for

the reactions at both subcritical and supercritical conditions was 5000 psig. The results show that the rate-limiting step in converting cellulose to fermentable sugars in subcritical and supercritical water differs because of the difference in their activation energies.

Cellulose and starch were both hydrolyzed in micro- and tubular reactors and at subcritical and supercritical conditions. Due to the difficulty involved in generating an aqueous based dissolved cellulose and having it reacted in subcritical water, dissolved starch was used instead. Better yield of water soluble hydrolysates, especially fermentable sugars, were observed from the hydrolysis of cellulose and dissolved starch in subcritical water than at supercritical conditions.

The concluding phase of this project focuses on establishing the mode of scission of cellulose chains in the hydrothermal reactor. This was achieved by using the simulated degradation pattern generated based on different scission modes to fingerprint the degradation pattern obtained from experiment.

TABLE OF CONTENTS

ix

LIST OF TABLES

xiii

xiv

CHAPTER 1. PROJECT INTRODUCTION

1.1 Project Overview

This project investigates the detailed reaction kinetics of crystalline cellulose in subcritical and supercritical water. These media offer conversion of cellulose to fermentable sugars via two routes: 1) a homogenous route involving dissolution and hydrolysis or 2) a heterogeneous route involving surface hydrolysis. Information obtained from the mechanism of cellulose conversion in these routes will aid in the design of a reaction flow path that will improve yield of fermentable sugars.

Extracting valuable products such as fermentable sugars and chemicals from cellulose has always been challenging. The challenges are largely connected to the structural integrity and recalcitrant nature of cellulose. As a result, the reaction kinetics describing the various methods of deconstructing its bonds, both on the intra- and intermolecular levels, will undoubtedly be complicated. Some of these methods include hydrolysis, ionic pretreatment, mechanical degradation, ammonia fiber explosion, and a thermochemical process.[1, 2] Thus, for any method adopted, a detailed understanding of its reactive behavior must be a necessary prerequisite. In this project, hydrolysis of cellulose in a hydrothermal environment will be adopted, and as a result the project will be guided by the following aims:

1. To conduct kinetics driven experiments on the conversion of cellulosic biomass to fermentable sugars following the dissolution and the hydrolysis routes.

2. To analyze the kinetics detailed of each step involved in the two reaction routes.

3. To design a reaction flow system that will be suited for optimizing yield of fermentable sugars.

4. To establish modes of scission of cellulose chains in a hydrothermal system by comparing its distribution pattern from modeling with the experimentally generated pattern.

To date, some questions regarding the hydrothermolytic conversion of cellulose to fermentable sugars still remain unresolved and, for this purpose, this research project has been designed to fill some of these gaps:

1. There are few scientific studies that adequately address characterization of the cellulose chains and their mode of scission in a hydrothermal system. Many studies on this subject have been conducted with such systems as enzymatic, acidic, and alkaline media but with the hydrothermal system, information is still very sparse.

2. There is still a substantial lack of clarity with respect to which of the steps along the route of cellulose dissolution and hydrolysis is rate-limiting. Is it the dissolution or the hydrolysis step? This work is set to contribute to the understanding and clarification of the kinetic details describing these reactions.

1.2 A Transition from Petroleum-based to Biobased Economy

The challenge posed to the socioeconomic and political stability of many nations by the crises-ridden oil-rich regions of the world is paving the way for an urgent transition from a petroleum-based to a biobased economy. This paradigm shift in the United States is largely driven by the need to avoid reliance on foreign oil and the accompanying national security risks. For some other regions such as the European Union, the shift is not only orchestrated by the need to reduce petroleum dependency but by an unwavering interest in environmental sustainability. A biobased economy utilizes

natural resources (biomass) as surrogates to all fossil-based feedstocks to generate valued end-products such as fuels and chemicals.[3] Table 1 shows the amounts of biomass utilized from various sources in 2003. A significant portion of it is from the forest products industry, which consists of wood residues and pulping liquors while the source with the least amount of biomass resources is from recycled or reused bioproducts. Biomass transformation results in far less emission of CO_2 to the atmosphere when compared with the fossil stock that releases CO_2 in excess of what is needed to maintain the greenhouse effect. Thus, excessive CO_2 loading on the atmosphere contributes to a phenomenon known as global warming.

In an effort to mirror every component describing the current petroleum based economy in the biobased economy, resources are being invested to design and construct a biorefinery* that will generate products that are ordinarily obtained from the traditional petroleum refinery. Adoption of the biorefinery is currently being viewed in phases based on the complexity and flexibility of the plant to process feedstock at a lower volume to a more complicated unit of processing lignocellulosic biomass at a higher volume. Phases in a biorefinery plant are described by the degree of complexity, level of flexibility and number of products being generated from the plant. For example, corn dry-mill ethanol process plant, designed solely to produce ethanol, is consider a phase I biorefinery unit because of its flexibility in generating other co-product, distiller's dry grains (DDG) used for animal feed. A corn wet milling ethanol plant, which is a bit more complex than the dry-mill, is portrayed as a phase II biorefinery because of its flexibility in generating

---

* A biorefinery is a facility that integrates biomass conversion processes and equipment to produce fuels, power, and chemicals from biomass[4]

Table 1: Amount of Biomass utilized from various sources in 2003

Biomass Consumption	Million dry tons/year
Forest products industry	
Wood residues	44
Pulping liquors	52
Urban wood and food & other process residues	35
Fuelwood (residential/commercial & electric utilities)	35
Biofuels	18
Bioproducts	6
Total	190

Source: U.S.D.A & U.S.D.O.E (2005) Biomass as Feedstock for a Bioenergy and Bioproducts Industry

multiple products including ethanol, starch, high fructose corn syrup, corn oil, and corn gluten meal.[4] As of now, corn is one of the strongest viable feedstock candidates in the emerging biorefinery plant. But the ultimate goal is to be able to utilize a wider range of biomass feedstocks to generate all products made available to us by the traditional petroleum-based refinery through biorefinery.

The future prospect of the current biofuel (bioethanol) generated from corn-starch is questionable due to speculated negative impact on food production[5]. The idea of corn starch utilization encroaching on the cost of the food supply is still not well founded as enough data have not been put together to support this trend. However, current efforts are channeled towards exploring cellulosic biomass as an alternative to increase the resource base for biofuel feedstock production and lessen the use of corn starch for ethanol production. Cellulosic biomass is grouped among feedstocks driving the current

advanced biofuel initiative for the expansion of biofuel production. Advanced biofuel is defined as biofuel generated from biorenewable sources other than corn starch, with the potential of emitting as much as 50% less greenhouse gases compared to the traditional fuel being replaced.[6] Cellulosic biomass, the most natural occuring organic matters, is seen as a strong prospect for salvaging future paucity of fossil fuel and a support for the ever increasing energy demand.

At the end of the twentieth century, it was estimated that 7% of total global biomass production, with an estimated record amount of 6.9×10^{17} kcal/yr, was utilized[7] while worldwide production of terrestial biomass was recently estimated to be 220 billion tons. Total energy content from this quantity (based on the analysis of heat of combustion) is roughly five times the energy content of the total crude oil consumed worldwide[4]. Table 2 depicts the relative abundance of different forms of biomass in Iowa, their equivalent energy content and potential.

Table 2. Energy Potential of Selected Biomass in Iowa

Material	Annual Amount (tons)	Energy Content (Btu/lb)	Energy Potential (10^9 Btu)
Switchgrass	11,200,000	8,000	179,200
Row crop residue	10,000,000	5,337	106,000
Wood and wood waste	165,000	4,800	1,580
Livestock byproducts	2,330,000	97	452
Cattle manure (dry basis)	1,600,000	6,760	21,600
Hog manure (dry basis)	2,700,000	7,300	39,400

Source : Iowa Biomass Energy Plan, **1994**.

Gasification of biomass to produce energy building blocks such as syngas (carbon monoxide and hydrogen) and biogas (methane) is one way of expanding biomass energy potential. Liquefaction of biomass through the hydrothermolysis process (subcritical and supercritical conditions), acidic hydrolysis, or enzymatic hydrolysis, is another route of generating fermentable sugars necessary for the production of liquid fuel used to power energy driven devices.

All the preceding indicators are currently driving the United States Department of Energy (USDOE) on a multiyear program[3, 8] focused at better understanding and utilizing biomass efficiently. USDOE is exploring potential technologies and improving on current techniques in transforming biomass to economically valuable products such as biofuels, and other bioproducts. One of the most crucial valued end points in the conversion of biomass to usable form is energy. As of 2008, about 93% of the energy supply in the United States is from non-renewable sources while 7% is from renewable sources. Roughly 50% of the renewable energy is biomass based and more than half of the biomass resources utilized, as indicated on Table 1, are from wood residues and pulping liquors.[9]

The renewed vision of USDOE is to reduce consumption of fossil fuel by 33% from 2010 to 2022, while investing more resources into biofuel production[8]. This vision presents itself as a modification of the initial goal of reducing fossil fuel consumption by 20 % from 2007 to 2017[3] which was the previously tagged vision "20 in 10". The possibility of reaching this feat is further encouraged by the introduction of the advanced biofuel initiative which expands resources for biofuel production. While there is this strong initiative to meet the above stated goal as a nation (USA), the techniques of

converting some of the newly adopted feedstock, such as cellulosic biomass, a highly recalcitrant feedstock, to valuable products, is of great concern.

To achieve this goal, efficient technology and approachs should be investigated to generate and optimize the yields of fermentable sugars from cellulosic biomass. The mode of converting biomass and the kinetics describing the conversion are essential in understanding ways of improving yield and selectivity of fermentable sugars. As of now, biomass, though thermally pretreated, is largely transformed biochemically[10] ; a process that is far more kinetically limited when compared with transforming biomass to fermentable sugars in an absolute hydrothermal process[11]. It is hereby proposed in this research work to investigate the kinetics of cellulose conversion in subcritical and supercritical water.

1.3 Biomass Model Compounds

The term "biomass" can be defined specifically as the total mass of living or recently dead (unfossilized) organic matter within a given environment[12]. More pertinently, biomass refers to all organic matter available on a renewable or recurring basis, including dedicated energy crops and trees, agricultural food and feed crops, animal waste, agricultural crop waste, wood and wood waste, aquatic plants, municipal wastes and other waste materials[13]. Plant biomass is an abundant renewable natural resource consisting mainly of crude organic matter such as cellulose, hemicellulose, lignin and starch[14]. Biomass model compounds that will be investigated in this work are cellulose and starch.

Cellulose is a long linear chain polymer of several monomeric D-glucose units linked by β-1,4-glycosidic bonds. It is the most abundant organic compound in nature and

does exist in the cell wall of plants as complex fibrous carbohydrates.   Starch is formed by α-1, 4 and/or α-1, 6 glycosidic bonding of several glucose units. The strength and chemical stability of these biopolymers differs due to different glycosidic bond types at the anomeric carbon. The β-type is more stable due to hydroxyl (-OH) group equatorial orientation at the anomeric carbon while the α-type, with a hydroxyl (OH) group axially positioned at the anomeric carbon and beneath the hemiacetal ring, displays less stability[15]. Their stability is ranked by resistance to biodegradability from microbes and enzymes.

Raw biomass (e.g. corn stover) comprises mainly cellulose, lignin, and hemicellulose. The biomass is deconstructed to produce chemical compounds such as cellulose, starch, ethanol, methanol, and other biomass-based chemicals. Some of the extracted macromolecular compounds, cellulose and starch, are further degraded to smaller chemical compounds such as glucose, maltose, cellobiose, maltotriose, cellotriose, etc. The degradation involves breaking of the glycosidic bond (primary covalent bond) between the monomeric residues and disruption of both the intra and inter-molecular hydrogen bonding amidst the polymer chains. Intra-hydrogen bonding in cellulose is responsible for its chain stiffnes[16]while inter-hydrogen bonding establishes its crystallinity. In Figure 1, the red dotted lines indicate the intra-chain hydrogen bonding while the blue dotted lines depict the inter-chain hydrogen bonding.
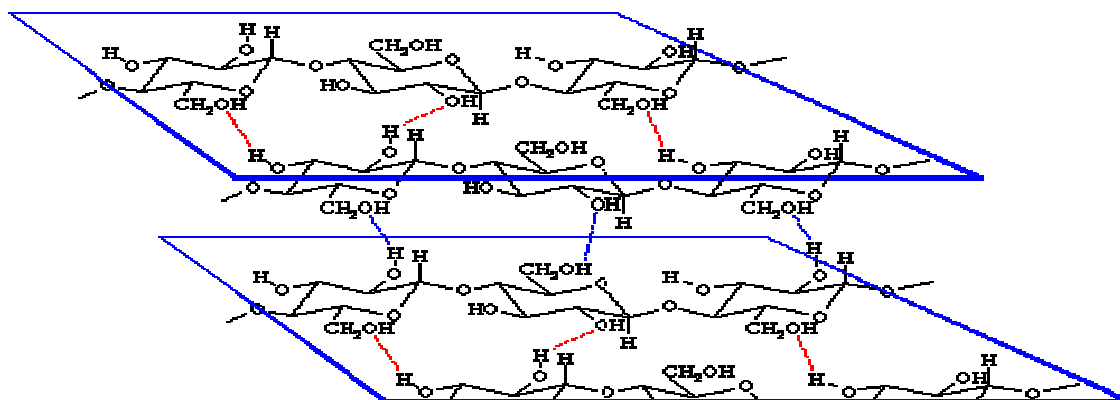
Figure 1. Crystalline Layers of Cellulose Structure (Department of Biology, University of Hamburg, Germany)

1.4 Subcritical and Supercritical Phases: Hydrolysis Media

In a pressure-temperature phase diagram, the critical point is the point where the equilibrium line for coexisting liquid and vapor ends. The region extending upwards, with temperatures and pressures exceeding their respective critical values,[17] as indicated in Figure 2, is depicted as the supercritical fluid. However, subcritical condition of the fluid describes a zone slightly below or near its critical pressure, and a temperature lower than its critical point. The data used for generating the equilibrium line on Figure 2 were obtained from the Chemistry WebBook published by the National Institute of Standard and Technology (NIST) for calculating thermophysical properties.[18, 19]

Most solvents can be characterized by their critical temperature and pressure [20-22]. For instance, water has a critical temperature and pressure of 374 °C and 22.1 MPa respectively. Ethanol and methanol also exhibit unique critical values despite belonging to the same aliphatic alcohol group. Table 3 displays critical temperatures, pressures and

densities for different solvents. Supercritical fluids have been used extensively in a number of applications ranging from supercritical fluid chromatography, supercritical fluid extraction, polymer processing, hydrothermal processing, and hydrothermal destruction of hazardous waste [23]. Supercritical water has been a primary medium for nuclear waste diminution and oxidative detoxification of organic waste [24].
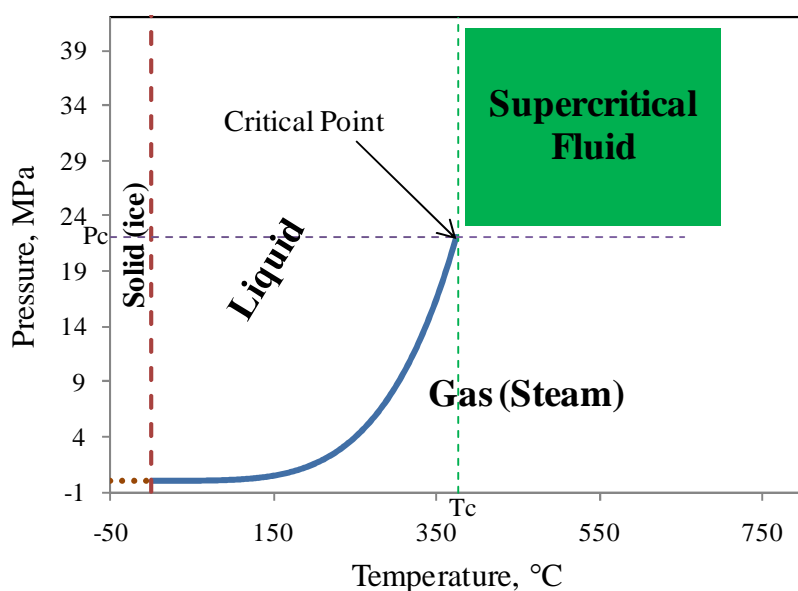
Figure 2. Pressure-Temperature Phase Diagram for Pure Water

Table 3. Critical Temperatures, Pressures, and Densities of Selected Fluids

Substance	T_c (°C)	P_c (atm)	ρ_c (kg m^{-3})
Ethylene	9.4	49.7	214
Trifluoromethane	26.1	48.1	322
Carbon dioxide	31.2	72.8	468
Sulfur hexafluoride	45.7	37.1	735
Propane	96.8	41.9	217
Ammonia	132.6	111.3	235
Methyl amine	157.0	73.6	222
Acetone	235.1	46.4	269
i-Propanol	235.3	47.0	273
Methanol	239.6	79.9	272
Ethanol	243.2	63.0	276
Water	374.3	217.6	322

Industrial applications of supercritical water started in 1994 when Eco Waste Technologies, a Canadian company, developed the first industrial-scale supercritical water oxidation (SCWO) process specifically to treat organic waste generated from a Huntsman petrochemical plant located in Austin, Texas[25].

The uniqueness of supercritical fluid (SCF) is portrayed by displaying both gas-like and liquid-like properties. The gas-like properties, including high diffusivity and low viscosity, enhance SCF mass transfer rates [20], while high density atypical of a gaseous compound characterizes its liquid-like behavior. Physical properties of most liquid solvents at ambient conditions (significantly below the critical point) display slight

variation with respect to corresponding changes in pressure and temperature. However, density and properties such as solubility parameter, partition coefficient, and viscosity change immensely at a slight variation in pressure and temperature both on short and long range within the critical region.[22, 26-28] The significant change in density at a slight change in pressure is due to the compressible nature of the supercritical fluid.

Thus, variation in macroscopic density-dependent solvent properties creates room for the tunability of subcritical and supercritical fluid physico-chemical properties to suit *in-situ* applications such as microscopic dissolution[27, 29] of cellulose. Invariably, the ability of fine a tuning supercritical fluid (SCF), by switching it on and off to a density suitable for dissolving and precipitating out the solute, makes SCF a perfect candidate in extraction processes and is mostly applied in the food industry. Figure 3 shows the phase diagram depicting variation of density of pure water with pressure. The data used for generating the plot were obtained from NIST Chemistry WebBook.[18, 19]
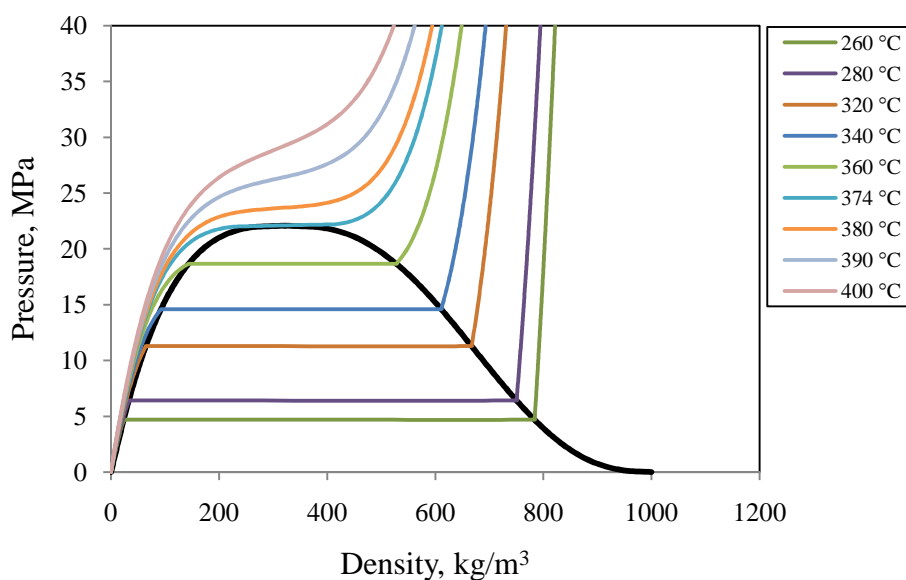
Figure 3. Pressure-Density Phase Diagram for Pure Water

The dome shape as depicted in Figure 3 is the region of a mixture of liquid and gaseous phases while the equilibrium lines from both left and right ends of the plot and merging to form a plateau at the critical point describe the saturation curves from the gaseous and liquid ends respectively. At an isothermal condition outside of the dome shape, increasing pressure results in a corresponding increase in the density. Also within the dome shape there is still a significant increase in the density of the liquid-gaseous mixture while maintaining a constant saturation pressure along an isotherm line. Moving beyond the critical point into the supercritical region, increasing pressure at a constant temperature leads to an increase in density while increasing temperature at constant pressure leads to a decrease in density of the fluid.

Modification of the dielectric constant opens opportunities for a normally polar solvent such as water to dissolve organic compounds.[24] For supercritical water, the dielectric constant is significantly lower and resides within the range common to most organic solvents. Figure 4 shows that the dielectric constant of supercritical water at a pressure of 300 bar and temperature of 375 °C is 12.03. Bewteen 2 and 30 , is a range typical for most organic solvents for dissolving organic macromolecules such as cellulose. Water at normal condition of 25 °C and pressure of 1 bar has a dielectric constant of about 78. From Figure 4, there is little or no change in the dielectric constant of water with respect to changes in pressure while following each isotherm except for 400 °C which displays some measurable direct variation with pressure in the range of 300 bar to close to 400 bar. However, at a constant pressure, changes in temperature reflect a significant change in the dielectric constant.
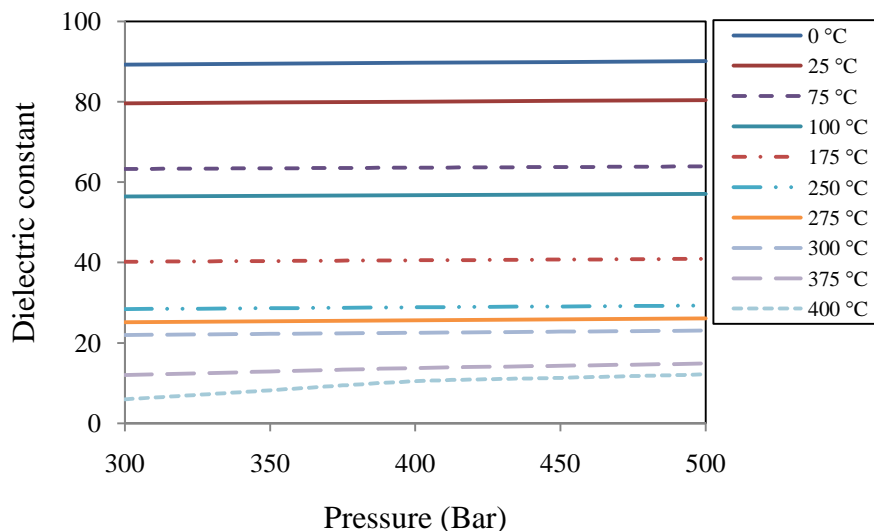
Figure 4. Variation of the Dielectric Constant (ε) of Water with Temperature and Pressure (NBS/NRC steam tables)

The ion product exhibited by supercritical water enhances the solvating power[27] needed to dissolve the compound in the medium. The ionic product is denoted as K_w and mathematically expressed as the product of the molar concentration of [OH⁻] and [H⁺] ($K_w = [H^+][OH^-]$). At neutral pH each has a value of 10^{-7} mol/l. At room temperature and pressure, the ion product of water is 10^{-14}(mol/l)^2 with a pH of 7 while at critical temperature and pressure its ion product is 10^{-11}(mol/l)^2 with a pH of 5.5. Figures 5 and 6 display the variation of the ion product of water at low and high pressure, respectively. In Figure 5, ion products appear to decrease monotonically as pressure increases except for isotherms of the four lowest temperatures in which the ionic product ($10^{-12.06}$(mol/l)^2) remains constant for pressure ranging from 200 bar to 500 bar. While at constant pressure, ion product increases with increase in temperature. Following the isotherms, 400 – 1000 °C, Figure 6 reflects a decreasing pattern in the ion product with pressure

within the range of 250 bar to about 3000 bar, while increasing pressure beyond this value, ion product decreases slightly. The effect of temperature on the ionic product of water in the high pressure region and at temperature range of 400 – 1000 °C, is less significant as portrayed in Figure 6. The ion product of water at a supercritical condition of about 3500 bar and 400 °C will be $10^{-9.5}$ $(mol/l)^2$, and the pH at this condition is 4.75. Both of these values, i.e. at critical and supercritical conditions, connote that water at these conditions will be slightly acidic. All the physico-chemical properties displayed by water at subcritical and supercritical conditions make it an excellent medium for converting macromolecular compounds to smaller valuable compounds.
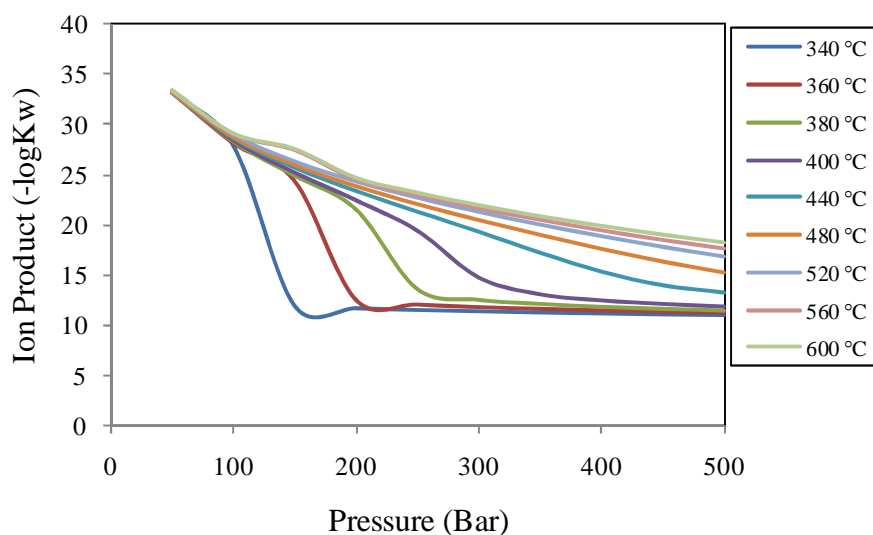
Figure 5. Ion Product of Water at Low Pressure
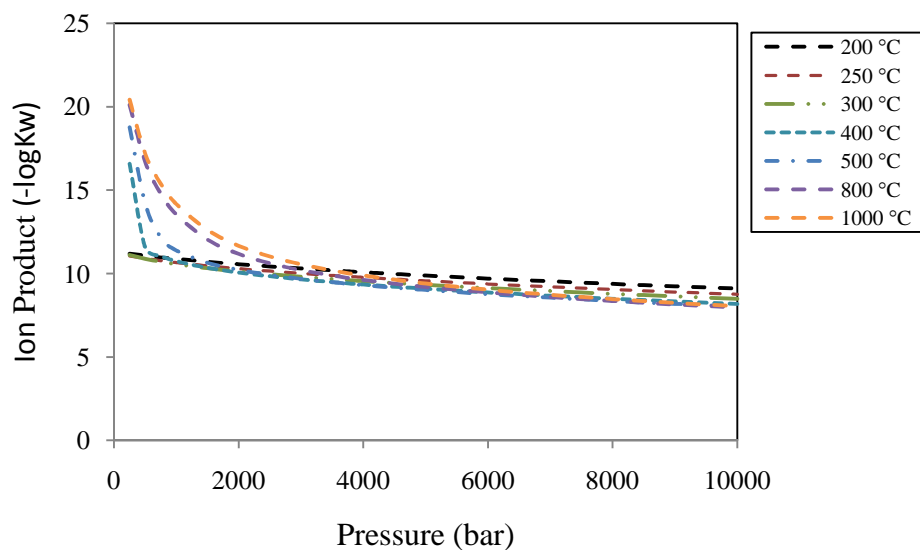
Figure 6. Ion Product of Water at High Pressure

In this age of environmental sustainability where most solvents that are toxic to the environment are being replaced with greener ones, supercritical fluids will be a very good replacement for many reactions and processes that involve solvents.

CHAPTER 2. RESEARCH BACKGROUND

In this chapter, the fundamentals of cellulose dissolution and hydrolysis will be discussed while exploring previous work on the reaction kinetics of cellulose hydrolysis in different media. Two of the different techniques of characterizing macromolecular compounds such as cellulose will be reviewed. Lastly, a thorough reviewed of the mode of scission of polymer molecules and the accompanying molecular weight distribution patterns in both organic and inorganic media will be conducted.

2.1 Cellulose Dissolution and Hydrolysis

Cellulose, a bioorganic linear polymer[15] and the most abundant renewable resource[30], is composed of D-glucose monomer units joined by β-1,4-glycosidic bonds. Native cellulose is built from several thousands (~10,000) of β-anhydroglucose residues to form a long linear chain molecule and that explains why its molecular weight is above 1.5 million. The linearly configured and highly dense cellulose chain molecules give rise to fibrillar structured material stabilized by inter-chain hydrogen bonding. The cellulosic fibril is a macro-picture of a smaller scaled unit called a microfibril[31] for all lignocellulosic biomass. This micro-scale unit, microfibril, is composed of orderly arranged crystallites with a cylindrical conformational structure.[32] The arrangement of cellulose molecules and the hydrogen bonding in fibrils are illustrated in Figure 7. The inter-chain hydrogen bonding between layers of longitudinally arranged microfibrils[33,34] establishs their crystallinity while intra-chain hydrogen bonding results in cellulose chain stiffness[16]. These properties justify why cellulose is ranked among recalcitrant compounds: substances that are very difficult to degrade. For most of these compounds, a special solvent or fluid such as supercritical fluid is needed for their dissolution.

Cellulose fibrils, though largely crystalline, exhibit amorphous structure at the ends of two adjoining microfibrils.
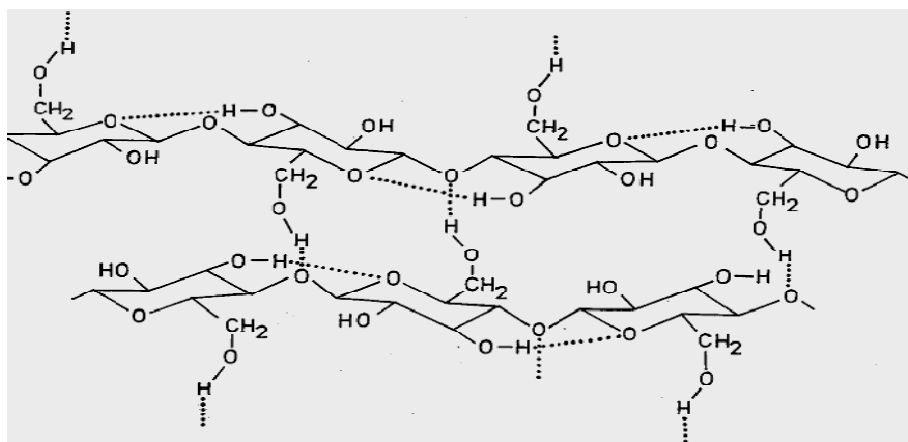
Figure 7. Arrangement of hydrogen bonds and cellulose molecules in fibrils (Cellulose Hydrolysis by Fan et al.)

Cellulose dissolution involves disengaging the inter-chain hydrogen bonding between layers of cellulose chains thereby making the hydroxyl (OH) on each of the glucose units available for bonding with the component of the dissolving solvent. The dissolution is preceded by swelling of the cellulose chain thereby facilitating accessibility of the degradative agent in breaking apart the inter-chain hydrogen bonding within the crystalline structure[31]. The dissolved cellulose can be further converted to lower molecular compounds such as the oligomers and fermentable sugars. Dissolution and hydrolysis of crystalline cellulose in media such as acid or supercritical water involve solvation of hydronium ions (protonated water molecules) around cellulose molecules. This process initiates protonation of either the cyclic oxygen (on one of the monomers) or

acyclic oxygen (glycosidic binding oxygen) along the polymeric chain[33]. The combined effect of solvation and protonation initiates rupturing of the inter-molecular hydrogen bonding (dissolution) and cleavage of intra-glycosidic and intra-hydrogen bonds (hydrolysis). The diagram below illustrates the dissolution and hydrolysis of crystalline cellulose.
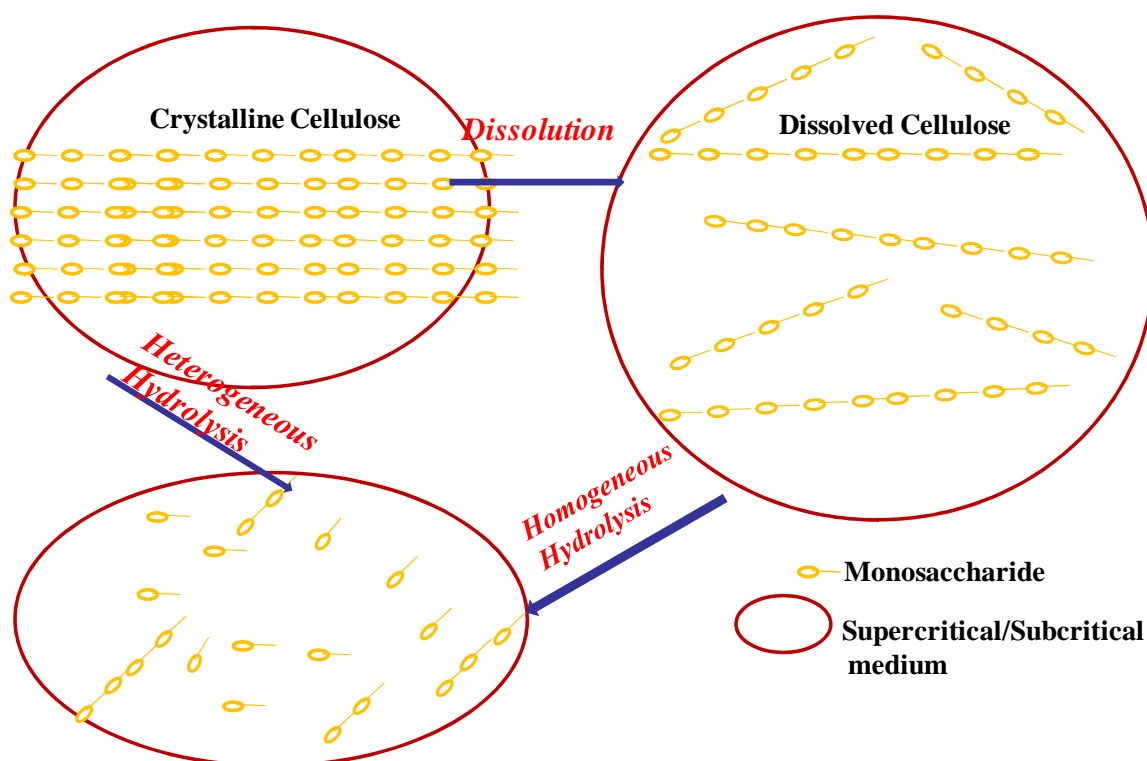
Figure 8. Schematic diagram of crystalline cellulose dissolution and hydrolysis

As depicted in the diagram above, direct hydrolysis of crystalline cellulose to smaller compounds such as glucose and water soluble oligosaccharides of DP less than 10 is probable but with relatively large cellulose chains yet undissolved. This type of

hydrolysis is termed heterogeneous while homogeneous hydrolysis is connoted by a complete dissolution of the crystalline cellulose[35]. The key issue which remains unresolved by most previous studies is a detailed kinetics evaluation of the rate of dissolution and rate of hydrolysis of crystalline cellulose under hydrothermal conditions. Considering the conversion of crystalline cellulose to simple sugars and water soluble oligosaccharides; which of the two steps could be considered rate limiting? Is it the dissolution step or hydrolysis step?   This is one major aspect of reaction kinetics of cellulose in hydrothermal conditions yet to receive serious attention by researchers but considered due for investigation in this research project.

2.2 Reaction Kinetics of Cellulose Hydrolysis in Different Media

The hydrolysis rate of cellulose largely depends on the medium of degradation. In other words, the rate at which cellulose and starch depolymerize in acidic, enzymatic and hydrothermal media differ.

2.2.1 Acidic Media

Degradation of celluloses in an acidic medium was enhanced by its ability to hydrolyze both the glycosidic bond and break the intra- and inter-molecular hydrogen bonding[33]. Acid-aided cellulose hydrolysis can either occur in a homogeneous or heterogeneous phase. Different models have been developed to better understand the kinetics of homogeneous and heterogeneous hydrolysis of cellulose and starch in acid. Cellulose hydrolysis is classically defined by a pseudo-homogeneous kinetics model, a term that in reality reflects that the hydrolysis process is heterogeneous. A very good example of such a model is the kinetics model[36] of Saeman et al. (1945) proposed for the hydrolysis of cellulosic wood biomass. The model assumed that the amount of cellulose

was the same as an equivalent quantity of dissolved glucose and that the reaction proceeds in two successive steps. A similar model approach was adopted in a study conducted by Girisuta et al. (2007).[37]

$$\underset{A}{Cellulose} \rightarrow \underset{B}{Glucose} \rightarrow \underset{C}{Decomposed\ glucose} \tag{1}$$
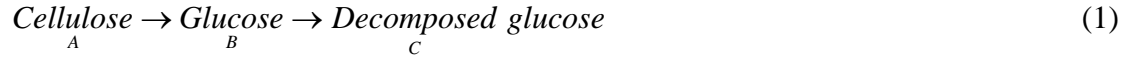
The kinetics expression of the schematic process above is as follows:

$$\frac{dC_A}{dt} = -k_1 C_A \tag{2}$$

$$\frac{dC_B}{dt} = k_1 C_A - k_2 C_B \tag{3}$$

$$\frac{dC_c}{dt} = k_2 C_B \tag{4}$$

Lack of detailed understanding of the kinetics of heterogeneous hydrolysis of celluloses in acid explains the rationale behind developing different forms of empirical and diffusion models[33]. These representative models are mostly predicated on significant experimental observations. Xiang et al. (2003)[38] developed exploration tools to understand the heterogeneous hydrolysis of microcrystalline cellulose in dilute acid by designing a simplistic modeling approach that coupled intrinsic, heterogeneous hydrolysis and transport rates together. The model was developed based on two assumptions: 1) total surface concentration of glucopyranose rings is constant and 2) glucopyranoses are considered part of either glucan or sugar. Transport rates of solubilized sugars (dissolved saccharides) and hydrolysis rates of glucan (undissolved saccharides) were used as parameters in simplifying the complexity surrounding the heterogeneous hydrolysis of microcrystalline cellulose in acid. The measured hydrolysis

profile of the cellulosic compounds correlated well with simulated hydrolysis profiles but caution should be exercised with high conversions obtained from simulation.

The use of acid as a hydrolytic medium for degrading compounds such as cellulose has been discouraged in recent times. This is because the corrosiveness of the acid requires the use of an expensive corrosion-resistant stainless steel reactor. The problem of acid disposal from an environmental perspective is also an issue of thoughtful consideration[33].

2.2.2 Enzymatic Media

Enzymatic degradation as reflected from the study conducted by Knauf, et al. (2004) was considered a promising option for depolymerizing pretreated cellulosic biomass and other carbohydrate macromolecules[10]. Complete biohydrolysis of cellulose requires combined influence of the complex cellulase system[39]. The cellulolytic enzyme formulations comprise exoglucanases (otherwise called cellobiohydrolase, CBH), endoglucanases (EG), and β-glucosidases. Exoglucanases degrade cellulose from either ends of the chain to release cellobiose while endoglucanases degrade the polymer chain randomly. The cellobiose produced by cellobiohydrolases is further hydrolyzed by β-glucosidases to generate glucose (the most desired product for fermentation). Due to substrate specificity of enzymes, starch is degraded by a different set of biohydrolytic catalysts such as bacterial thermophilic α-amylase, β-amylase, amyloglucosidase, and maltogenase[40].

Without prior treatment of cellulose for de-crystallization and gelatinization, bioconversion time for complete enzymatic hydrolysis of cellulose is quite long. Fan et al. (1987)[33] reported 30% conversion of cellulose in an optimal batch time of 16 h while

Eremeeva et al.[41] observed, in a 10% NaOH enzymatic medium, 75% formation of cellulose hydrolysate in 42 h. Another issue of concern in biohydrolysis is the huge cost incurred in the procurement of the enzymes. On this premise and other related matters, Genencor International, with the support of USDOE, embarked several years ago on developing low cost cellulases and thermophilic enzymes for ethanol production.[10]

The reaction in enzymatic hydrolysis sequentially occurs in about four to five stages depending on the enzyme-substrate interaction with solvent-medium. These stages include (1) diffusion of enzymes onto the substrate, (2) adsorption of enzymes by substrate, (3) enzymatic reaction on the substrate, (4) desorption of enzymes back into the bulk solution.[33, 42] The kinetics of the cellulose-enzyme system could be explained theoretically by Michaelis-Menten or McLaren models. The rate limiting step is mass transfer of enzymes from the bulk solution to the substrates. A further problem is inhibition[33] after formation of hydrolysate such as cellobiose. The disaccharide competes for enzymes needed to further hydrolyze the remaining cellulose residues.

2.2.3 Hydrothermal Media

To investigate the rate of cellulose depolymerization in a non-catalyzed high temperature and high pressure medium, Saka et al. (1999)[43] dissolved various cellulosic compounds in supercritical water. These celluloses were hydrolyzed in a reaction vessel immersed in a preheated tin or salt bath and subsequently quenched in a water bath. The study indicated an appreciable yield of glucose and other products of decomposition within a very short supercritical water treatment time ranging from 3-10 s. Many of the studies [35, 43-46] reviewed by Matsumura et al. (2006)[47] on the hydrothermolytic recovery

of energy and material from biomass support high hydrolysis rates of cellulose and starch in subcritical and supercritical water.

Studies conducted by Yesodharan,[24] Sasaki et al.[35], and Sasaki et al.[46] generally support that the decomposition rate of hydrolysate (e.g., glucose) is higher than its formation in the subcritical phase, while in the supercritical phase, the rate of hydrolysate formation is reported to be faster than the rate at which it decomposes. Ehara et al.[11] investigated the decomposition trend of cellulose in a two-step treatment, with a first step in supercritical water (400 $^{\circ}$C, 40 MPa) and a subsequent subcritical phase treatment (280 $^{\circ}$C,40 MPa). To avoid excessive decomposition of the hydrolysate in the first phase (supercritical), a short reaction tube was used. The aim was to first dissolve cellulose before saccharifying it in a long reaction tube where subcritical condition is maintained. Combined yields of hydrolysate and monomeric pyrolysate (93.9%) were observed to be higher in the supercritical phase than what was obtained under subcritical conditions (82.7%). However, the selectivity of pyrolysate generated via isomerization (fructose), fragmentation and dehydration[48] in the two phases differs. According to Ehara et al.[11], fragmentation dominates pyrolysis of glucose in supercritical water and dehydration mainly dictates glucose decomposition in subcritical phase. Products of dehydration as stated by Ehara and Saka,[11] Sasaki et al.[35], and Matsumura et al.[47] are levoglucosan (1,6-anhydroglucose), 5-hydroxymethylfurfural (5-HMF), and furfural while most of the remaining pyrolysate such as erythrose, methylglyoxal (pyruvaldehyde), glycolaldehyde, glyceraldehydes, and dihydoxyacetone are obtained from fragmentation.

Taiying Zhang's recent work[14] tends to disagree with the idea of an increase in the hydrolysis rate compared to the hydrolysate decomposition rate in hydrothermal

conditions, (380-400 °C). Maximum glucose yield was observed at temperatures ranging from 260 – 300 °C for most of the reaction scenarios, while at higher temperatures (370-400 °C) glucose degradation was dominant due to high activation energy. Figure 9 reveals that the hydrolysis rate of cellobiose is higher than the decomposition rate of glucose within the subcritical temperatures ranging from 260 °C to 340 °C.[49] Extending beyond the subcritical temperature range to supercritical region (400 °C) as indicated by the extrapolated dashed line, decomposition rate of glucose is higher than the hydrolysis rate of cellobiose.
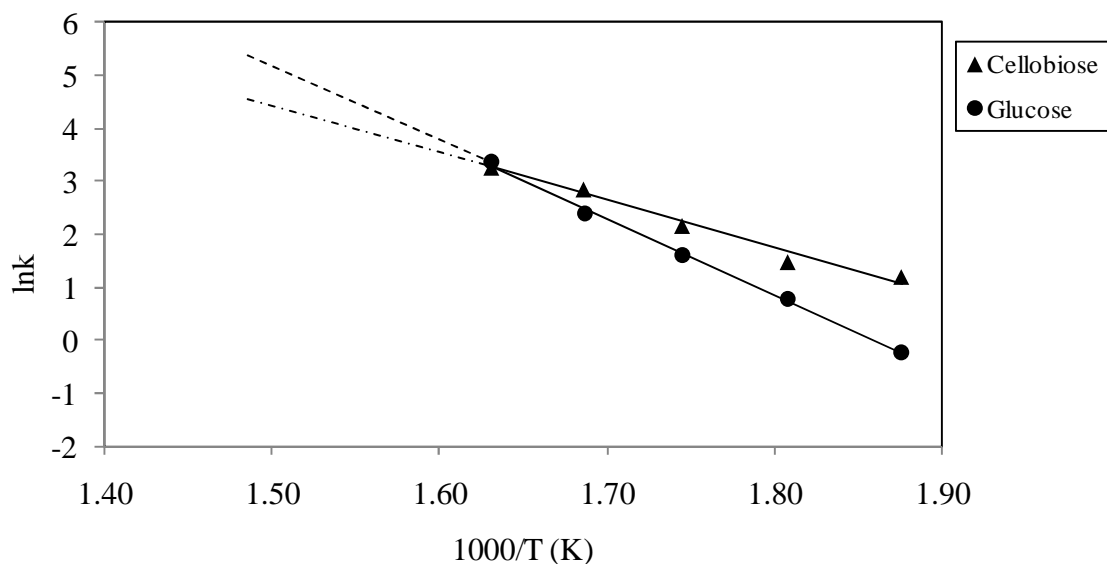
Figure 9. Rates of Cellobiose Hydrolysis and Glucose Decomposition

Nagamori et al.[50] hydrolyzed starch in a batch reactor at hydrothermal conditions of temperature ranging from 180-240 °C. An increase in yield in the decomposition product of glucose (e.g. HMF) at 220 °C was observed throughout the heating period

while glucose yield started to plummet after 50 % of the heating period had been expended. The decomposition behavior of cellulose and starch in subcritical and supercritical water is believed to be strongly influenced by an increase in the accessibility of the protonated water molecule to the various bonds[32, 34] and effectiveness of these hydrolytic agents in breaking these bonds.[31] Most of the work reviewed above revealed an in-depth understanding of the dynamics and kinetics of monosaccharide degradation, most especially in hydrothermal media. But much uncertainty still remains regarding the kinetics of the different stages that describe the monomerization of crystalline cellulose in subcritical and supercritical water. These stages include 1) dissolution of crystalline cellulose, 2) saccharification of dissolved cellulose, and 3) decomposition of saccharification product.

However, in an effort to offer insight to some of these ambiguities, Sasaki et al.[32] adopted a kinetics model that addresses both heterogeneous and homogeneous hydrolysis of crystalline cellulose at sub- and supercritical condition of water in a micro-reactor. The model which elucidates the mechanism of reaction on the surface of a solid particle is described as a shrinking core or grain model. They observed that heterogeneous hydrolysis of crystalline cellulose dominates under subcritical conditions in water, while homogeneous hydrolysis of crystalline cellulose prevails in supercritical water. The reason is that the solubility of macro-organic molecules such as crystalline cellulose increases as the phase condition of water changes from subcritical condition to supercritical condition. The low solubility level of crystalline cellulose in subcritical water results in surface hydrolysis of cellulose chains within the crystalline matrix to form water soluble cellooligosaccharide and simple sugars. As a result of swelling that

predominates on the surface of the cellulose chain while in supercritical water, the rate of dissolution is so high and rapid that the hydrolytic degradation of cellulose in this medium occurs homogeneously. The shrinking core model is thus expressed by the following equations.

$$\frac{dV(X)}{dt} = -k_s \cdot S(X) \tag{5}$$

where V and S are the volume and surface area of the cellulose particles respectively; and k_s is the surface reaction constant. The two size parameters (V and S) are both functions of conversion, X, and are mathematically related to V as $X = 1 - V(X)/V(0)$. The conversion, X, is afterward coupled into Equation (5) to obtain Equation (6).

$$\frac{dX}{dt} = 2 \cdot \frac{k_s}{r_{g,0}} (1 - X)^{1/2}$$

(6)

The shape of the cellulose particle is considered cylindrical and $r_{g,0}$ is the initial radius of the cellulose particle before hydrolysis. Equation 6 is integrated to obtain the following equation

$$k = \frac{k_s}{r_{g,0}} = \frac{1 - (1 - X)^{1/2}}{\tau} \tag{7}$$

where k (s^{-1}) is the overall conversion rate constant of the micro-crystalline cellulose and τ is the residence times.

2.2.4 Disadvantages of Conventional Hydrolysis Media

As interest continues to grow in bioenergy generation and biochemical production from biomass, more efforts are being put into researching other techniques in

transforming biomass to valuable end-points. These techniques, some of which have proven practicable on an industrial scale, include biomass gasification, hydrothermolysis of cellulose and starch, and pyrolysis of biomass. Excellent transport properties and fast reaction rate (low residence time) that characterized hydrolysis of cellulose and starch in a supercritical phase give it an edge over enzymatic hydrolysis. The problem of inhibition and mass transfer limitation (diffusion) in enzymatic hydrolysis are completely avoided in hydrothermolytic degradation of celluloses. Bottlenecks associated with acid hydrolysis such as waste disposal are avoided also in the hydrolytic depolymerization of cellulose in subcritical and supercritical water.

However, the quantity of heat required to power this reaction is a drawback for the hydrothermolysis process over enzymatic hydrolysis. But this issue could be resolved by way of process heat integration and recycling of waste heat from the boiler plant.

2.3 Polymer Molecules Characterization

Characterization of polymeric materials in terms of their molecular weight distribution, compositional and microstructural heterogeneity and degree of polymerization is challenging. This work will focus on the molecular weight distribution and the degree of polymerization. Molecular weight distribution is brought about by the variability in the molecular weights and chain lengths of the different molecules that constitute the polymer itself while the degree of polymerization describes the number of monomer units in a polymer chain. As polymer degrades, the degree of polymerization (DP) decreases. Therefore DP serves as a strong parameter in evaluating the extent of hydrolysis of cellulose and starch in a hydrothermal reactor. Degree of polymerization is evaluated in terms of molecular weight of the polymer per molecular weight of the

monomer. The molecular weight of polymer can be expressed[34, 51] as viscosity-average molecular weight ($\overline{M}_v$), weight-average molecular weight ($\overline{M}_w$), or number-average molecular weight ($\overline{M}_n$) and these reflect the three basic formats of expressing DP.

$$DP_n = \frac{\overline{M}_n}{MW_m} \tag{8}$$

$$DP_w = \frac{\overline{M}_w}{MW_m} \tag{9}$$

$$DP_v = \frac{\overline{M}_v}{MW_m} \tag{10}$$

Where MW_m is the molecular weight of the monomer and the molecular weight averages, $\overline{M}_n$, $\overline{M}_w$, and $\overline{M}_v$ are mathematically expressed as follows:

$$\overline{M}_n = \frac{\sum_{i=1}^{\infty} N_i M_i}{\sum_{i=1}^{\infty} N_i} \tag{11}$$

$$\overline{M}_w = \frac{\sum_{i=1}^{\infty} N_i M_i^2}{\sum_{i=1}^{\infty} N_i M_i} \tag{12}$$

$$\overline{M}_v = \left[\frac{\sum_{i=1}^{\infty} N_i M_i^{1+a}}{\sum_{i=1}^{\infty} N_i M_i} \right]^{1/a} \tag{13}$$

Where *i* depicts each polymer molecule size, N_i is the number of molecules of size *i*, M_i is the mass of each polymer molecule and *a* is the Mark-Houwink constant that is polymer-solvent-temperature dependent. Degree of polymerization (DP) of cellulose can be obtained experimentally from the dilute solution viscometry method, size exclusion / gel permeation chromatography and other techniques ranging from light scattering to end group analysis and osmotic pressure.

2.3.1 Dilute Solution Viscometry

Dilute solution viscometry is a characterization technique for establishing the average molecular weight of polymer molecules based on their impact in changing the viscosity of the solvent. Studies have shown that the viscosity of a solvent is significantly altered by the introduction of a strand of polymer chain. Thus, the two major steps in evaluating the molecular weight of polymer molecules via dilute solution viscometry method are : 1) to determine the intrinsic viscosity of the dissolved polymer and next is 2) to introduce the value of the intrinsic viscosity into the Mark-Houwink-Sakurada Equation and then solve for the average molecular weight.

For a fluid flowing through a capillary tube, its viscosity can be evaluated by Equation 14.

$$\frac{V}{t} = \frac{\pi \bar{p} r^4}{8 \eta l_c} \qquad (14)$$

Where *V* is the volume of the liquid, *t* is the flow (efflux) time through the capillary, l_c is the length of the capillary, η is the viscosity of the liquid, and $\bar{p}$ which is expressed below in Equation 15 is the average hydrostatic pressure.

$$\overline{p} = \rho g \overline{h} \tag{15}$$

Introducing Equation 15, into Equation 14 and re-arranging to obtain t as depicted in Equation 16

$$t = \frac{8V\eta l_c}{\rho g \overline{h} r^4 \pi} \tag{16}$$

Where ρ is the density of the liquid, g is the acceleration due to gravity and $\overline{h}$ is the average value of the liquid head. All the variables in Equation 16 are constant except for t and η. Thus, Equation 16 can be simplified as :

$$\eta = Ct\rho \tag{17}$$

where C is a constant for a particular viscometer and is commonly referred to as the viscometer constant. For example, a Cannon Fenske viscometer of size 50 (a size defined based on the Cannon Fenske calibration) typically has a viscometer constant of about 0.004 (centistokes/second). Equation 17 will only be valid if the total pressure difference applied across the column overcomes the viscous force, meaning that, the potential energy of the liquid in capillary tube should not at any rate affect the kinetic energy to the efflux. But in the real sense, this is not true. To correct for this contribution, Equation 17 is rewritten in a new form as depicted in Equation 18 and the second term on the right is the term responsible for the correction.

$$\frac{\eta}{\rho t} = C - \frac{D}{t^2} \tag{18}$$

The flow of liquid in the capillary is assumed laminar with a no-slip boundary condition on the capillary wall. This is an accurate assumption for the case of a dilute polymer solution. Most commercial viscometers are designed to minimize the effect of the kinetic

energy constant *D* so that Equation 17 can be applied. After measuring the viscosity η of a polymer solution, the next step is to calculate the intrinsic viscosity $[\eta]$ of a dilute polymer solution. This involves evaluating the increase in the viscosity of a solvent brought about by the introduction of polymer molecules. The first step is to solve for the relative viscosity which is the ratio of the viscosity of the solvent and polymer solution with respect to the viscosity of the solvent only. Relative viscosity symbolically denoted as η_r, expressed as

$$\eta_r = \frac{\eta}{\eta_0} \tag{19}$$

Where η_0 is the viscosity of the solvent without polymer (solute). Following the format of Equation 17, Equation 19 can be rewritten in the form

$$\eta_r = \frac{t\rho}{t_0\rho_0} \tag{20}$$

At an extremely dilute solution, the density of the polymer solution will be approximately equal to the density of the solvent, so that Equation 20 can be reduced to

$$\eta_r = \frac{t}{t_0} \tag{21}$$

Infinite dilution is a way of approximating the effect of the increase in the viscosity of the solvent caused by the polymer presence to the barest minimum, so that the value of η_r approaches unity. Specific viscosity (η_{sp}) is therefore evaluated on the basis of this condition and is mathematically expressed in Equation 22.

$$\eta_{sp} = \eta_r - 1 = \frac{t - t_0}{t_0} \tag{22}$$

The next step is to obtain the reduced viscosity (η_{red}) which is defined simply as the ratio of the specific viscosity to the concentration of the polymer solution;

$$\eta_{red} = \frac{\eta_{sp}}{c} \tag{23}$$

Physically, this ratio (η_{sp}/c) evaluates the specific capacity of the solute (polymer) to augment the relative viscosity. To finally set the stage for the evaluation of the intrinsic viscosity[η], inherent viscosity must be calculated. Inherent viscosity (η_{inh}) is defined as the ratio of the natural logarithm of relative viscosity (η_r) to the concentration c.

$$\eta_{inh} = \frac{(\ln \eta_r)}{c} \tag{24}$$

Due to the logarithmic component of Equation 24, it is referred to, following the IUPAC* terminology, as the logarithmic viscosity number.

Reduced and inherent viscosities are the two respective independent variables in Huggins and Kraemer equations, as depicted in

$$\frac{\eta_{sp}}{c} = [\eta] + k'[\eta]^2 c \tag{25}$$

$$\frac{\ln \eta_r}{c} = [\eta] + k''[\eta]^2 c \tag{26}$$

---

* IUPAC: International Union of Pure and Applied Chemistry

Where k' and k'' are Huggins and Kraemer coefficients. After obtaining the intrinsic viscosity, it is then coupled into the Mark-Houwink-Sakurada (MKS) equation as expressed in Equation 27 to obtain the viscosity average degree of polymerization (DP_v) of the polymer.

$$[\eta] = K(DP_v)^{\alpha} \tag{27}$$

Where K and α are constants specific for a particular polymer, solvent and temperature. Equations 25 and 26, needed to graphically solve for the intrinsic viscosity. Intrinsic viscosity $[\eta]$ can be describe as the limit at infinite dilution of the polymer solution and it is portrayed by simply setting the limit of concentration terms in Equations 25 and 26 to approaching zero. In essence, it is expressed mathematically as $(\eta_{sp}/c)_{c\rightarrow0}$ and $(\ln \eta_r/c)_{c\rightarrow0}$. Therefore, intrinsic viscosity is evaluated, following Huggins or Kraemer equations, respectively, as the average of the intercepts obtained after extrapolating the plots of η_{sp}/c and $\ln(\eta_r/c)$ with the polymer concentration c onto the ordinate axis.

An example is shown in Figure 10, which relates how the value of intrinsic viscosity was obtained in this research work for crystalline cellulose (as received) in cupriethylenediamine hydroxide and at 25 °C. The intrinsic viscosity which is the average of the two intercepts (1.30 and 1.31 g/dl) is 1.305 g/dl . The intrinsic viscosity is introduced into the MKS equation, i.e. Equation 27, to obtain 228 as the average DP_v of polymer (crystalline cellulose as received). Details of the experiment will be discussed later in the results section.
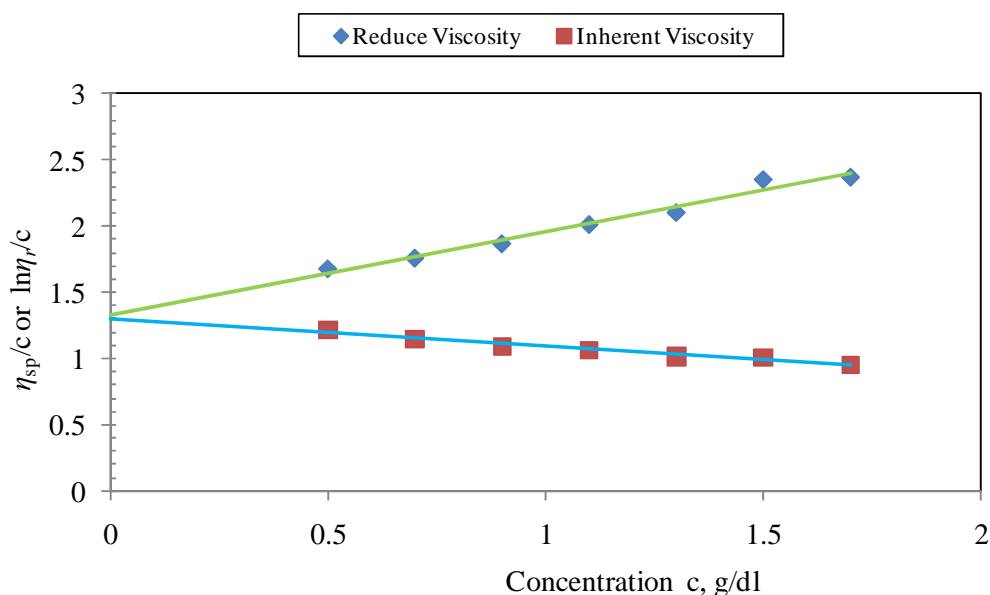
Figure 10. Plot of η_{inh} ($\ln\eta_r/c$) and η_{red} (η_{sp}/c) versus c for a crystalline cellulose in cupriethylenediamine at 25 °C with shared intercept as [η]

2.3.2 Size Exclusion Chromatography

Size-exclusion chromatography was a scientific breakthrough in the field of analytical techniques of separating macromolecular compounds in the mid twentieth century[52]. The name has always been gel permeation chromatography (GPC) but not until recently that researchers adopted size exclusion chromatography (SEC) as a name as definitive and descriptive as GPC. According to Varian Incorporation, the term *"GPC[53] is used to describe the analysis of polymers in organic solvents such as tetrahydrofuran while SEC is used to describe the analysis of polymers in water and water-based solvents (buffer solutions)"*. It is applied in analyzing the molecular weight distribution of synthetic polymers and oligomers, lipids, natural macromolecules such as proteins,

glucans, and cellulose derivatives. SEC is extremely useful in studying processes accompanied by changes in the hydrodynamic volume of polymers. These processes include hydrolysis of biopolymers (cellulose and starch), polymerization, and refolding of protein molecules.

SEC separates macromolecular chains or polymer chains according to their size or hydrodynamic volume.[51] The normal chromatographic column is packed with spherical microporous material (rigid) and the material most often used for packing is crosslinked polystyrene particles with pore sizes ranging from 3 to 20 μm. The sample solutes are dissolved in a suitable eluting solvent (mobile phase), and partitioning is created between the mobile phase flowing within the interstitial spaces and the mobile phase stationary within the volume of the particle pores. The larger the size of the sample solutes (polymer) within the eluting media, the more probably it is to flow past many porous volumes and the less it is for the solute to be retained within the column. Larger molecules (larger sizes) flow more within the interstitial mobile phase than the porous mobile phase while the smaller molecules (smaller sizes) partition more into the porous mobile phase than the interstitial mobile phase within the column. These exclusion activities exhibited by both large and small sized molecules determine their retention time and volume within the column. Large molecules meander less within pores of the stationary phase thereby eluting faster than small molecules which spend more time within the porous volume than in the interstitial spaces. Eluting solutes are sensed by a detector or a series of detectors connected to the outlet of the SEC column. The diagram below illustrates SEC separation process.[54]

Time Sequence

Retention time
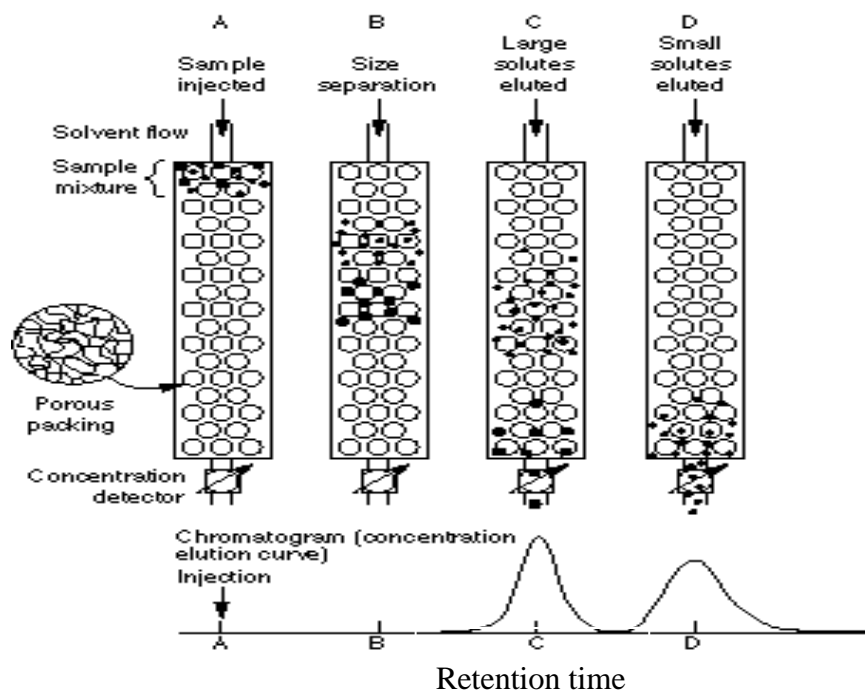
Figure 11. Illustrative diagram of separation mechanism in SEC column

Most commonly used detectors in size exclusion chromatography include a differential refractometer and/or a light scattering detector. The laser light scattering technique will directly measure the average molecular weight while a differential refractometer will aid in generating a chromatogram for the molecular weight distribution. A differential refractometer operates by measuring the difference in the refractive index of the pure solvent (mobile phase) and the polymer solution eluting from the column.

2.3.3 Effect of Hydrolysis on Molecular Weight Distribution and Degree

of Polymerization

Chang et al.[55] performed gel permeation experiments to investigate cellulose degradation in acid while establishing a connection between the hydrolysis rate of cellulose, its molecular weight distribution and the degree of polymerization (DP). Cellulosic material, cotton linter, was subjected to periodic hydrolysis in 1 N hydrochloric acid at 80 ^{o}C. The end products of the hydrolysis, the polymeric residues, and the acid-soluble hydrolysate were analyzed for molecular weight distribution using gel permeation chromatography. Figure 12 depicts the hydrolysate chromatogram at different time intervals. Considering the DP with the corresponding peak maxima as reflected on the chromatograms, it could be observed that at the initial stage of the degradation, the hydrolysis rate was high. But as the degradation continues and hydrolysis time increases, the hydrolysis rate gradually slows due to a limiting DP value as indicated by clustered peak maxima of the chromatograms on the extreme right of the plot. The point at which there is little or no change in the DP is referred to as the leveling-off degree of polymerization (LODP). On the chromatogram, after the original sample on the far left, the degraded samples from left to right correspond respectively to the treatment times of 6 min, 18 min, 60 min, 4 h, 11 h, 24 h, and 120 h.

$$\overline{DP}$$
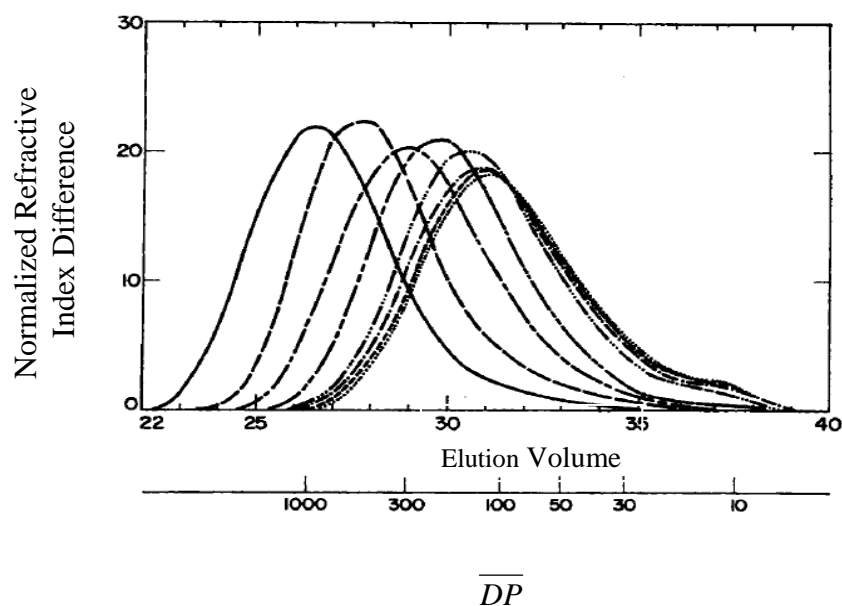
Figure 12. Chromatograms of cellulose residue (cotton linters) degraded with 1 N HCl at 80 °C. After the original sample on the far left, samples converted from left to right correspond respectively to the treatment times of 6 min, 18 min, 60 min, 4 h, 11 h, 24 h and 120 h.

2.3.4 Hydrolysis Rate of Crystalline Cellulose Based on Glycosidic Bond

Concentration

Hydrolysis rates of crystalline cellulose can be addressed more specifically by looking at changes in bond concentration with respect to time while degrading cellulose in a hydrothermal system. Bond concentration (Cb) as expressed in this work is the number of bonds of polymer molecule per volume of solution. Number of bonds can be expressed mathematically as DP-1, but the DP used in this study is based on viscosity average. The bond concentration is given by

$$Cb = \left(\frac{Moles\ of\ polymer}{Volume} \right) \left(\frac{Number\ of\ bonds}{Chain} \right) \tag{28}$$

For a more useful representation, Equation 28 can be expressed as follows:

$$Cb = \left(\frac{M_{ce}/V_s}{MW_{ce}} \right)(DP - 1) \tag{29}$$

Where M_{ce} is the mass of cellulose, V_s is the volume of sample solution, DP is the degree of polymerization, and MW_{ce} is the average molecular weight of cellulose which can be expressed as:

$$MW_{ce} = (DP * 162) + 18 \tag{30}$$

Mass of cellulose and volume of sample solution are measured; viscosity-average degree of polymerization is experimentally determined, while viscosity-average molecular weight is evaluated using Equation 30.

First order kinetics are assumed for the hydrolytic splitting of the β-glycosidic bonds and the rate equation for the reaction is expressed by

$$-\frac{dCb}{dt} = kCb \tag{31}$$

Equation 31 is integrated to obtain a relationship between Cb and t

$$-\int \frac{dCb}{Cb} = \int k\,dt \tag{32}$$

yielding

$$c - lnCb = kt \tag{33}$$

The integration constant c is obtain by solving for the bond concentration Cbo when $t = 0$. Final expression between Cb and t is

$$-ln\frac{Cb}{Cbo} = kt \tag{34}$$

2.4 Degradation Pattern and Mode of Scission

Molecular weight distribution is one way of characterizing polymeric material. Polymer molecules of the same repeat unit often exhibit varied chain lengths and this explains why their weights are often expressed in a distributional form. Once any point along the polymer chain is broken, the distribution will be altered and the need to re-evaluate their molecular weight distribution will arise. However, this breakage or scission can take different modes. Thus, in this section, the effect of different modes of scission on changing the molecular weight distribution (degradation pattern) will be reviewed.

2.4.1. Pattern of Degradation

The degradation patterns of cellulose hydrolysis in acidic/alkaline and enzymatic media have been explored with limited understanding. The degradation pattern of polymeric chains is deduced from changes in the graphical display of the molecular weight distribution while undergoing degradation. Berggren et al.[56] studied the implication of cellulose degradation in pulp fibers on its molar mass distribution. Cotton linters and several pulps collected from industry and laboratory were subjected to different forms of degradation which include ozonation, acid hydrolysis, alkaline degradation, alkaline pulping (delignification), and soda anthraquinone degradation of wood polymer beads. Figure 13 shows the degradation pattern of cellulose and hemicellulose while delignifying wood. The initial bimodal molecular weight distribution changes into a monomodal distribution as alkaline concentration increases. The initial lower and higher peaks indicate hemicellulose and cellulose fractions respectively.
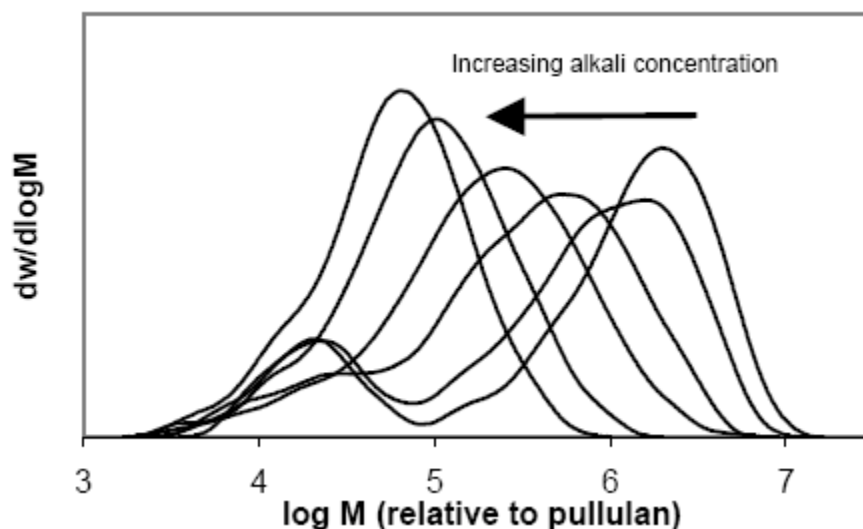
Figure 13. Molecular weight distribution of birch pulp (fibrous cellulose) with different alkaline concentration

2.4.2 Mode of Scission of Polymer Degradation

Modes of scission describe different ways of breaking bonds along the polymer chain and also aid in understanding the level of susceptibility of these bonds to cleavage. Enzymatic hydrolysis offers a much clearer view of the scission mode by virtue of the different type of enzymes and their specific activity[34, 57] in degrading biopolymer molecules. Two major categorized groups of enzymes used in cellulose depolymerization are: 1) exoglycosidases, that attack glycosidic bonds of cellulose from reducing ends, while 2) endoglycosidases, which randomly break any glycosidic bond of the cellulose chain.

Some studies[33, 56] reported that breakage of the glycosidic bond in acid follows a specific scission mode while other investigators indicated that hydrolysis of cellulose in acid occurs randomly. The mode of scissioning cellulose chains in alkaline medium is categorically reported as non-random: end-wise depolymerization.[33] Mechanical degradation of polymer, initiated by influence of shear forces on the polymer molecule, produced a non-random systematic scission at the center of the chain.[58] Guaita et al.[59] and Emsley et al.[60] both investigated polymer degradation based on Monte Carlo procedures using a BASIC program designed to systematically simulate polymer degradation. The latter studied different scission processes such as simple scission and scission with coupling, adopting polydispersity index (PI) as a tool to establish the randomness of bond scission along the polymer chain. The polydispersity index, a measure of spread of molecular weight distribution of polymer chains, is expressed as follows:

$$PI = \frac{\overline{M_w}}{\overline{M_n}} \tag{35}$$

Where $\overline{M_w}$ is weight-average molecular weight and $\overline{M_n}$ is the number-average molecular weight. It is random if the polydispersity index, after several stages of degradation, with respect to number of scissions per initial molecule approaches 2 and nonrandom if PI deviates from this limiting value. The number of scissions per initial molecule (S) is mathematically represented as

$$S = \frac{DP_{no}}{DP_n} - 1 \tag{36}$$

where DP_{no} denotes initial number-average degree of polymerization and DP_n is the number-average degree of polymerization after S scissions occur.

However, Emsley et al.[60] describe randomness to be a measure of linearity of the plot of the reciprocal of DP (1/DP) with respect to degradation time. Berggren et al.[56] tends to disagree with one of the definitions of Emsley et al., which states that slight variations in the position of the molecular weight distribution as degradation continues is indicative of a totally random scission. Berggren et al.[56] expounded that a significant shift in the molecular weight distribution from its distribution status to a lower molecular weight range typifies equal susceptibility of the cellulosic bonds to cleavage. Most studies[56, 59-61] agreed that broadening of the molecular weight distribution towards a peak higher than the mode of the initial molecular weight distribution is a result of coupling of the fragmented polymer chain molecules.

Montroll and Simha[62], one of the earliest groups investigating bond scission rate on a statistical basis, developed a depolymerization theory that is based on equal susceptibility of bonds to cleavage in long polymer chains. The theory was premised on three assumptions: 1) all intial polymer molecules have equal weight, 2) accessibility to reaction is independent of bond positions, and 3) all chains have equal access to reaction. A probability based expression relating average size distribution of polymeric chains as a function of initial polymer chain length and number of bonds split per molecule was developed. The average molecular weight of the degraded polymers was also expressed as a function of the number of bonds split per molecule. This work only addressed the probability of random scission but did not offer insight into situations where polymers of

varied chain length display unequal bond susceptibility to scission and the rate under those circumstances.

These issues were substantially addressed when Basedow et al.[63] and Mostafa et al.[64] developed similar kinetics schemes to evaluate analytically the degradation rate of polymers of different chain length. In this line of interest, Glynn et al.[65] designed a numerical scheme that fits molecular weight distributions generated by three different probability based breakage models (random, center, and Gaussian) with experimentally determined MWD. Ballauf et al.[66, 67] advanced further on the Basedow et al. kinetics schemes[63] by not only formulating an exact solution to obtain the rate constants for degrading individual polymer chains, but also generating scission rate constants for each bond in the polymer chain. The general kinetics equation for individual polymer chains is

$$\frac{dn_i}{dt} = -\left(\sum_{j=1}^{i-1} k_{ij} \right) n_i + \left(k_{i+1,1} + k_{i+1,i} \right) n_{i+1} + \cdots + (k_{r,i} + k_{r,r-1}) n_r \tag{37}$$

where $\frac{dn_i}{dt}$ is the rate of depolymerization of polymer i, k_{ij} is the individual rate constant of polymer i at bond point j, n_i is the number of molecules of polymer i, while r indicates the highest degree of polymerization of polymers under investigation. Individual rate constants were subsequently modeled for the three modes of scission which include random scission, central scission and Gaussian scission; the last two can be categorized as non-random.

The recent work on the mode of scission and probability rate of scission is the study conducted by Bose and Git on mathematical modeling and computer simulation of linear polymer degradation.[61] In this study, two different algorithms, a Monte Carlo method and an algebraic exact statistical formulation, were explored and developed.

Both, though different in their approach in estimating periodic scission outcome, are based on binary tree chain cleavage models. The model depicts chain rupturing as a sequence of probabilistic events and as a non-linear function of time. It assumes that one bond is broken at each step of degradation. The latter algorithm, which is the algebraic exact statistical formulation, is adopted and served as the mathematical formulation basis for the simulation in this research project. This approach utilizes an algebraic equation to express the expected fragmentation outcome of finite sets of chains from a large population. The equations are formulated from a list of logically defined degradation schemes that are specific to a particular mode of scission. Under this formulation, two probability-based criteria of selecting the affected polymer chain were considered: 1) chain length frequency, and 2) bond density. Highlighted below are the probability-based mathematical models describing each criterion.

Chain length Frequency:

$$P(n,t) = \frac{d(n,t)}{T(t) - d(1,t)}, \qquad 2 \le n \le N \tag{38}$$

Bond density :

$$P(n,t) = \frac{(n-1)d(n,t)}{\sum_{i=1}^{N}(i-1)d(i,t)} \quad 1 \le n \le N, \quad 1 \le i \le N \tag{39}$$

At the end of each cycle of degradation the total probability must be 1:

$$\sum_{n=2}^{N} P(n,t) = 1 \tag{40}$$

$P(n,t)$ is the probability of selecting polymer chain of size (DP) n at cycle t for scission, while $d(n,t)$ is the number of molecules of size n at cycle t and $T(t)$ is the number of molecules of all sizes in the system at cycle t .The size of the molecule is denoted with i.

These concepts were used in developing models used to simulate different types of scission such as unzip (peeling–off of polymer ends), midpoint, percent cut, and random scission. The algebraic equations representative of the different modes of scission formulated by Bose and Git can be expressed as follows:

Random scission:

$$d(1, t+1) = d(1,t) + \sum_{k=2}^{N} \frac{2P(k,t)}{k-1}, \; n = 1 \tag{41}$$

$$d(n, t+1) = d(n,t) - P(n,t) + \sum_{k=n+1}^{N} \frac{2P(k,t)}{k-1}, \; 1 \le n \le N-1 \tag{42}$$

$$d(n, t+1) = d(n,t) - P(n,t), \quad n = N \tag{43}$$

Midpoint Scission:

$$d(n, t+1) = d(n,t) - P(n,t) + P(2n-1,t) + 2P(2n,t) + P(2n+1,t); \quad n (1 < n < N) \tag{44}$$

Percent Cut Scission

$$d(n, t+1) = d(n,t) - P(n,t) + P\left(\frac{n}{p}, t\right) + P\left(\frac{n}{1-p}, t\right), \quad n (1 < n < N) \tag{45}$$

Unzip Scission

$$d(n, t+1) = d(n,t) - P(n,t) + P(n+z,t); \quad n (1 < z < N) \tag{46}$$

Quantity $d(n,t+1)$ is the number of molecules of size n at cycle t+1, i.e. after one degradation cycle, while p and z assume a fixed percent and fixed number of monomers

to be unzipped from either end of the polymer chain. Mode of scission was used in line with the formulation to simulate an array of polymer chains that were ruptured and was also used to generate molecular weight distribution patterns specific to each scission mode. The initial distribution function for the simulated molecular weight distribution is normal distribution.

Extensive studies have been conducted on the mechanism and dynamics of converting oligosaccharides and simple sugars to simpler compounds, but yet to be fully resolved is an adequate understanding of the mode of scissioning of cellulose molecules and the subsequent molecular weight distribution of the degraded molecules in a hydrothermal medium. This research work is aimed at answering some of the questions attributable to cellulose conversion in such media.

2.4.3. MATLAB

The programming language adopted for the simulation part of this project is MATLAB which is an abridged form of Matrix Laboratory. The name reflects the original design and purpose of the language, which was to perform matrix calculations. As times progressed, its capability and scope was further expanded to perform a range of scientific and engineering calculations and solve virtually any technical problem. The advantages of MATLAB over other programming languages such as Fortran, or C include: 1) ease of use, 2) platform independence, which affords MATLAB the opportunity of being supported on virtually any operating system including Macintosh, Linux, Unix, Microsoft Windows and 3) availability of many predefined functions such as mean, mode, and standard deviation. Other advantage of programming in MATLAB include device-independent plotting that offers many integral plotting and imaging

commands and tools that makes it possible for MATLAB programmers to create an interactive graphical user interface (GUI). This feature enhances analysis and monitoring of sophisticated data.

CHAPTER 3. RESEARCH OBJECTIVES

Most pretreatment methods[2] such as autohydrolysis, steam explosion, liquid hot water, wet oxidation, ammonia fiber explosion, comminution, ball milling, and radiation are designed to streamline generation of biofuel precursors or fermentable sugars from biomass. The main goal of all pretreatment methods is to create a platform for optimizing yield of fermentable sugars from biomass while invariably increasing biofuel production. In the long run, proponents of biofuel believe if all relevant resources are well channeled that biofuel will, in the foreseeable future, rise to becoming a very strong competitor to fossil fuel. However, research is still ongoing with the development of cost effective pretreatment methods. This project is intended to contribute resourcefully to this on-going research and will be addressed holistically in three separate parts: 1) reaction kinetics analysis of crystalline cellulose hydrolysis in the hydrothermal reactor, 2) hydrolysis of dissolved starch (which will be used as a surrogate for dissolved cellulose) in subcritical and supercritical water, and 3) the degradation pattern and mode of scission of cellulose hydrolysis in subcritical and supercritical water.

Therefore, the overall objectives of this project are: 1) to conduct a detailed reaction kinetics study of the conversion of crystalline cellulose to fermentable sugars in subcritical and supercritical water and 2) to determine the mode and rate of scission of crystalline cellulose in the hydrothermal reactor by fingerprinting experimentally determined degradation patterns with a probabilistic based model-generated pattern. To put things in perspective, this research opens up the possibility of developing and designing a fast reaction pathway contrary to a much slower conventional enzymatic approach while enhancing yield of fermentable sugars.

The reaction kinetics at each phase will be investigated while product and molecular weight distribution at different temperatures will be studied by size exclusion and ion exchange chromatography. An algebraic exact statistical formulation coded in MATLAB is adopted to model hydrolytic degradation of polymer chains, and the molecular weight distribution obtained from this simulation will be compared with the experimental distribution. Finally, adequate understanding of the reaction kinetics, product distribution at the different critical temperatures, degradation pattern, and mode of scission will help to facilitate the development of a comprehensive kinetics model. This research is driven by the following hypotheses:

1. *Cellulose dissolution is a limiting step in the overall reaction kinetics of crystalline cellulose hydrolysis in supercritical water.*

2. *Glucose formation from dissolved cellulose is better optimized in subcritical water than supercritical water*

3. *Bond scission of cellulose in sub- and supercritical water is nonrandom.*

Descriptions of the specific aims to address each hypothesis are briefly stated respectively in 3.1, 3.2, and 3.3, while detailed descriptions will be elucidated in Chapters 4, 5, and 6, respectively.

3.1 Reaction Kinetics Analysis of Crystalline Cellulose in Subcritical and Supercritical Water

The reaction kinetics analysis of crystalline cellulose in a hydrothermal reactor will focus on the detailed reaction kinetics model describing cellulose hydrolysis. The kinetics parameters describing the overall conversion of crystalline cellulose in subcritical water based on a shrinking core model were explored. To establish the rate

limiting step of crystalline cellulose conversion in subcritical and supercritical water, the dissolution and the hydrolysis rate constants of crystalline cellulose conversion in these media were determined. The hydrolysis rate is based on the rate at which the glycosidic bonds break, while the dissolution rate is described by the amount of cellulose dissolved in supercritical water.

3.2 Hydrolysis of Dissolved Starch used as a Surrogate for Dissolved Cellulose in Subcritical Water

Data obtained from previous work reveal a better yield of glucose from hydrolysis of crystalline cellulose in subcritical water than in supercritical water. To improve glucose yield in the overall reaction, a reaction sequence is intended to first dissolve cellulose and later hydrolyze the dissolved cellulose in subcritical water. As dissolving cellulose is difficult, dissolved starch will be used as a surrogate for initial hydrolysis studies in subcritical water. This approach is adopted as a result of the similarities in the hydrolytic rate behavior of maltosaccharides and cellosaccharides in subcritical media as observed in the studies conducted by Taiying Zhang.[49] It does indicate that due to proximity in values of the activation energies for the two saccharides that hydrolysis rate of maltosaccharides and cellosaccharides in subcritical water could be predicted similarly. Based on these findings, hydrolysis reactions of starch and cellulose in subcritical water are invariably predicted to be similar. Dissolved starch will be hydrolyzed separately in subcritical water, and its yields evaluated. The water soluble product (hydrolysate) obtained in the course of these reactions will be analyzed with high performance liquid chromatography (HPLC).

3.3 Determining the Degradation Pattern and Mode of Scission of Cellulose Hydrolysis in Subcritical and Supercritical Water

The goal of this section is to determine the pattern of cellulose degradation and its mode of scission in subcritical and supercritical water. The most feasible way of approaching this task is modeling cellulose chain degradation based on different modes of scission, and simultaneously simulating the molecular weight distribution of the degraded chains. The modeled molecular weight distribution will be used to fingerprint the molecular weight distribution generated from experimentally degraded cellulose chains at the subcritical and supercritical conditions of water. MATLAB based code was used for the simulation, and size exclusion chromatography was used to generate the molecular weight distribution for the degraded cellulose chains in subcritical and supercritical water.

CHAPTER 4. KINETICS ANALYSIS OF CELLULOSE REACTION IN
SUBCRITICAL AND SUPERCRITICAL WATER

In this chapter, the kinetic parameters describing the reaction of crystalline cellulose in subcritical and supercritical water will be investigated. Studies from previous work[11, 32, 35] have shown that dissolution of crystalline cellulose dominates in supercritical water, while surface hydrolysis largely dictates the order of its reactive behavior in subcritical water. Figure 8 in Chapter 2 presents a pictorial view of how these reactions can proceed in two different routes: 1) a homogeneous route (dissolution and hydrolysis) and 2) a heterogeneous route (surface hydrolysis).

Due to the surface-based heterogeneous nature of cellulose reactions in subcritical water, detailed kinetic parameters describing its overall conversion will be investigated based on a shrinking core model. The next step will be to evaluate the kinetic parameters guiding the glycosidic bond hydrolysis of crystalline cellulose in the hydrothermal medium. However, unlike heterogeneous hydrolysis, that uses a shrinking core kinetics model, the glycosidic bond hydrolysis rate will be evaluated based on the bond concentration rate equation given in Equations 28 - 34. Lastly, the kinetics details expressing the dissolution of crystalline cellulose in supercritical water will be investigated.

The rate constants for the overall conversion of crystalline cellulose and hydrolysis of the glycosidic bonds in subcritical water and dissolution of crystalline cellulose in supercritical water will be obtained by plotting their respective conversion terms with residence times. The conversion term is a reflection of the kinetic rate equation adopted for each reaction. A first order rate equation, as it is applied to the

hydrolysis of the glycosidic bond, will be adopted for the dissolution rate. However, the hydrolysis rate will be based on bond concentration, while dissolution rate will be based on mass concentration. The glycosidic bond concentration analysis will be conducted by experimentally determining the degree of polymerization (DP) via dilute solution viscometry analysis and later solved for the number of bonds per volume of solution. The dissolution rate will be approached based on the amount of crystalline cellulose dissolved in supercritical water. The rate constants obtained from the conversion-residence time plots for these reactions will be introduced into the Arrhenius equation to obtain the kinetic parameters. To establish the rate limiting step in the dissolution-hydrolysis (homogeneous) route, the activation energy obtained for the dissolution will be compared with the energy needed to activate the hydrolysis of glycosidic bonds. The step with the higher activation energy is considered the limiting step following the homogeneous route: dissolution- hydrolysis.

4.1 Experimental Methods

The experimental methods present a detailed description of the experimental setup and the processing steps, sample product analysis and data analysis methods.

4.1.1 Experimental Setup and the Processing Steps

Cellulose reactions were conducted in the microreactor. Figure 14 is a photograph of the experimental setup for the reaction of crystalline cellulose in the microreactor. The same setup was used for the cellulose reaction in the tubular reactor; the only difference is the point at which feedstock is fed into the process stream. For the microreactor, the feedstock which is crystalline cellulose in water (slurry solution) is fed into the microreactor positioned midway along the process flow path. A schematic chart of the

process for the microreactor can be seen in Figure 15. Most of the reactions that will be

discussed in this chapter will be cellulose slurry reactions in the microreactor.
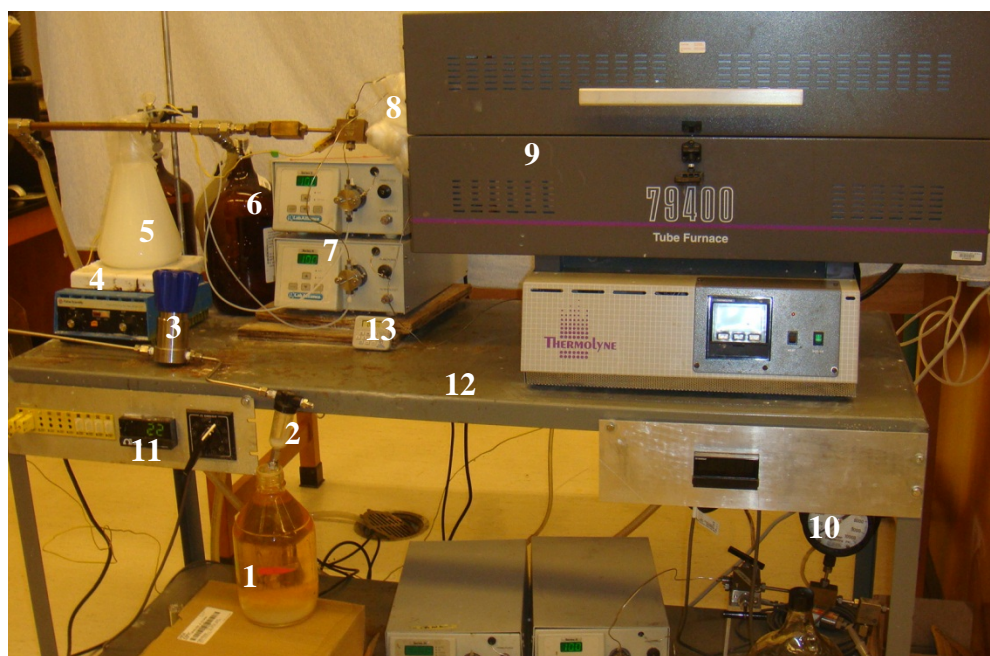
Figure 14. Experimental setup of the microreactor: 1) sampling bottle; 2) gas-liquid
separator; 3) back pressure regulator; 4) stirrer plate; 5)cellulose suspension;
6) deionized water; 7) pumps; 8) insulated microreactor; 9) furnace; 10)
pressure gauge; 11) temperature reader; 12) platform; 13)stopwatch

Deionized water obtained from a Nanopure infinity water purification system was

fed by Lab Alliance series II pump at flow rates ranging from 5 ml/min to 10 ml/min into

a tube enclosed within a tube furnace (Thermolyne 79400). Subsequently, the deionized

water was heated to subcritical temperatures ranging from 280 °C to 340 °C for separate

experimental runs. The pressure of the fluid was about 5000 psig and was set and

controlled by a 15,000 psig capacity Tescom back pressure regulator downstream. The

pressure gauge displays the operating pressure. Just after the pressure gauge is a rupture disc. This safety device, unlike the relief valve which opens when the maximum pressure is exceeded, is ruptured when the operating pressure exceeds its limit. In this experimental setup, the rupture disc can support a maximum pressure of 9000 psi, so therefore, any pressure beyond this limit can lead to rupture of the disc.
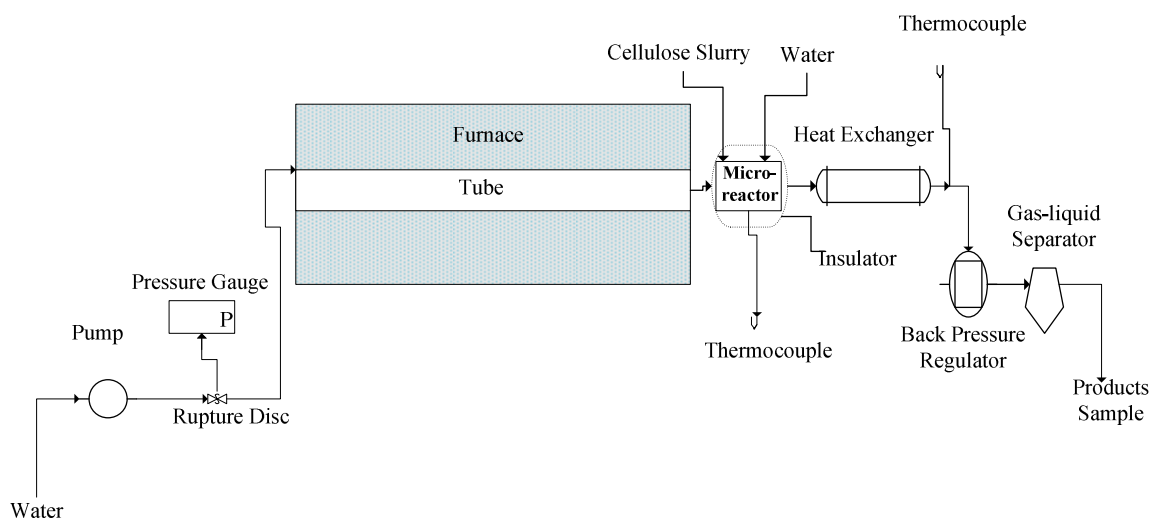
Figure 15. Schematic of cellulose hydrolysis in microreactor

The subcritical water exited into the glass fiber insulated microreactor and served as both hydrolytic agent and the reaction medium for the 2 wt% cellulose slurry solutions. The feedstock was fed into the microreactor at the upper inlet port closer to the outlet of the tube furnace. The temperature the furnace can support ranges from room temperature to 1200 °C. The cellulose slurry solution mixed with the subcritical water at equal volumetric flow rate, thereby diluting the slurry concentration to 1 wt%. The reaction was quenched by the deionized water entering from the other upper inlet port of

the microreactor and also by the shell and tube heat exchanger just at the outlet end of the microreactor. With the rapid heating and quick quenching of the cellulose reaction in the microreactor, the reacting volume within the microreactor is estimated to be 0.17 ml. The schematic flow detail in the microreactor can be seen in Figure 16. To address the dissolution rate of crystalline cellulose in supercritical water, some changes were made to the orientation of the microreactor, and variables such as the reacting volume, temperature, and wt% were altered. Detailed descriptions of these alterations will be elucidated in the dissolution rate section of this chapter. The samples were collected in the gas-liquid separator and analyzed for cellulose conversion, and weight and degree of polymerization of unreacted cellulose.
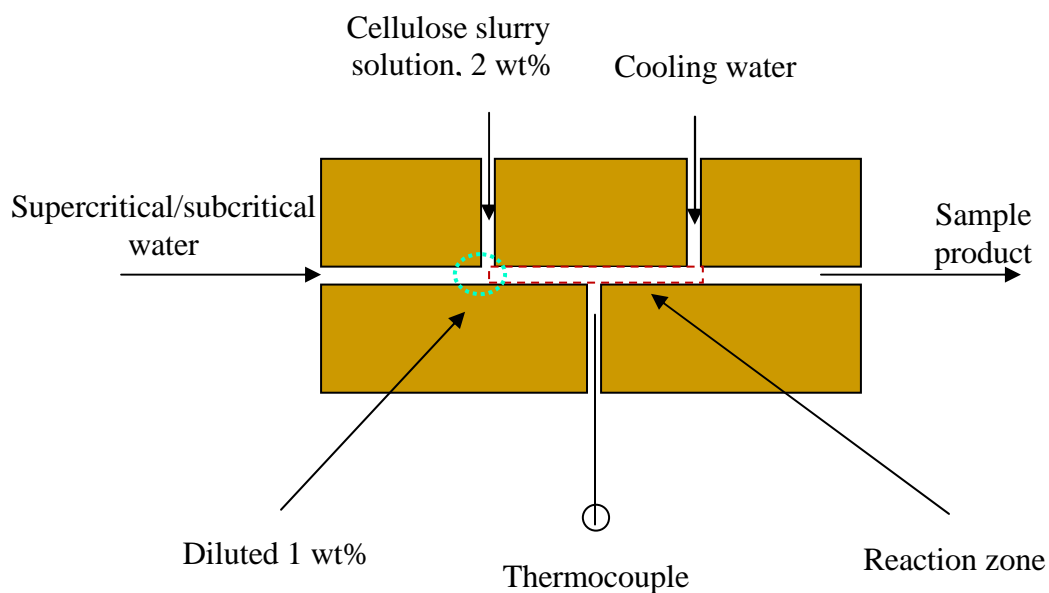
Figure 16. Schematic flow detail of reaction in microreactor

4.1.2 Product Sample Analysis Method

4.1.2.1 Materials

Sample solution of cellulose suspension in deionized water, and dissolved cellulose in bis(ethylenediamine)copper(II)hydroxide solution are the reactant and reagent solutions used in this section of the research project. The chemical compounds used for the experiments and standard solutions for calibration curves were all obtained from Sigma-Aldrich® and they are highlighted as follows: crystalline (sigmacell cellulose type, 20 μm), bis(ethylenediamine)copper(II)hydroxide solution, cellobiose (>98 %), maltose monohydrate (>98%), glucose (>99.5%), fructose (>98%), 5-(hydroxymethyl)-2-furfural and furfural .

4.1.2.2 Aqueous Products (Water Soluble Hydrolysate)

Cellulose were not subject to any pre-analytical test before being fed into the hydrothermal reactor. The products obtained from the hydrolysis reaction, which included water soluble, water insoluble, precipitate, and some gases, were analyzed by different analytical instruments. Water soluble hydrolysate was analyzed by ionic chromatography comprising: high performance liquid chromatography pump (LC-10ADvp), refractive index detector (RID-10A), SSI 505 LC column oven, aminex HPX-87H & HPX-42A (300 x 7.8 mm); mobile phase (5 mmol/L H_2SO_4 and water). The mobile phase operated at a flow rate of 0.6 ml/min and the oven temperature was set at 50 ^{o}C. Hydrolysate was quantified based on a standard calibration and identified by its characteristic retention time.

4.1.2.3 Water Insoluble Hydrolysate.

These are the solid portions of the sample products obtained from the hydrolysis reaction. The insoluble hydrolysate was mainly unreacted cellulose which is sometimes refered to as cellulose residue. These products were analyzed gravimetrically by 1) filtering the hydrolysate via Stericup® 0.22 μm Millipore GV PVDF membrane, 2) by centrifugation and decantation. The solid residues left after filtration were dried at room temperature till weight of the solid product remained constant. This method was adopted for knowing the mass (g) of unreacted cellulose per liter (L) of the hydrolysate solely for evaluating the conversion of crystalline cellulose in subcritical water. This gravimetric method was quite similar to how mass concentration of unreacted cellulose was assessed for the purpose of dissolution rate of crystalline cellulose in supercritical water. The only exceptions are 1) in place of the Stericup® 0.22 μm Millipore, a 15 ml centrifuge bottle was used and 2) samples in this case were not filtered but centrifuged and decanted to set the cellulose residue up for drying. The solid residues left after centrifugation and decantation were dried at a temperature of about 67 °C until the weight of the solid product remained constant.

For the viscometry analysis for cellulose characterization, the solid components of the hydrolysate were centrifuged and freeze dried with a 4.5 Labconco freeze dryer. Samples obtained from reaction were centrifuged to separate cellulose residue from the hydrolysate. The cellulose residue, after decanting the supernatant from the centrifuge bottle, was frozen at -20 °C and later freeze dried by the freeze drying system to obtain dried cellulose residue and weighed thereafter. The reason for freeze drying the cellulose residue needed for the

viscosity analysis is to avoid caking of the cellulose residue that may occur during drying in an oven or desiccator. In the case of freeze drying, the cellulose residue is obtained in powdery form which does allow for easy dissolution in bis(ethylenediamine)copper(II)hydroxide. The only disadvantage with freeze drying is the tendency to lose some residue during handling.

4.1.3 Data Analysis Method

In the microreactor, the average times the reactants spend in the reacting volume is referred to as residence time (τ) and can be expressed mathematically as:

$$\tau = \rho_c V/\rho_r F_r \tag{47}$$

where ρ_c is the density of the reactant mixture at reactor conditions, V is the volume of the microreactor, and ρ_r is the density of the reactant mixture at room temperature. F_r is the volumetric flow rate of the reactant solution being fed into the reactor. Other descriptive data analysis parameters include conversion, yield, and bond concentration. Conversion is denoted symbolically as X and is defined as the amount of solute (in solution/suspension) reacted with respect to the initial amount. It can be expressed by

$$X = \frac{Initial\ Mass - Final\ Mass}{Initial\ Mass} \tag{48}$$

Yield, commonly denoted as Y, is mathematically defined as

$$Y = \frac{Mass\ of\ product}{Mass\ of\ the\ feed} \tag{49}$$

Product in this case could be glucose, cellobiose, fructose, 5-(hydroxymethyl)-2-furfural (HMF), furfural, and organic acids while feed could either be cellulose suspension or starch solution. Cellulose and starch are polymers of glucose, and obtaining their

concentration in mole/liter may prompt an initial line of thought of finding the DP to obtain the molecular weight so as to obtain the moles of the polymer. The approach is logical but not necessary because these polysaccharides are polymers of glucose and concentration can be based on the mass of glucose units in the polysaccharides. Approximating the density of dilute aqueous solution at room conditions to be 1000g/L, the composition (mass ratio) of solute in terms of wt% is given by

$$mass\,ratio = \frac{mass\,concentration\,(g\,/\,L)}{1000\,g\,/\,L} \times 100\,wt\% \tag{50}$$

Bond concentration is another variable used in analyzing and describing some of the results obtained in this chapter. The detailed description of the theoretical approach of obtaining bond concentration in this research project was discussed in Chapter 2.

The Arrhenius equation is used significantly in this chapter:

$$k = Ae^{-\frac{E_a}{RT}} \tag{51}$$

where k is the rate constant, E_a is the activation energy, and A is the pre-exponential factor. Equation 51 can be expressed in linear form as:

$$\ln k = \ln A - \frac{E_a}{RT} \tag{52}$$

A plot of ln$k$ versus $1/T$ yields a slope of $-E_a/R$ and an intercept of ln$A$.

4.2 Conversion of Crystalline Cellulose in Subcritical and Supercritical Water

This section explores the reaction of crystalline cellulose in the microreactor at subcritical and supercritical conditions of water. As stated earlier, there are essentially two routes of hydrolyzing cellulose in hydrothermal media. It can either follow the homogeneous route (complete solubilization of the crystalline cellulose in supercritical water) or heterogeneous route (incomplete solubilization of the crystalline cellulose in subcritical water). For complete solubilization, two steps are involved and these steps include: 1) dissolution and 2) hydrolysis, while incomplete solubilization involves mainly surface hydrolysis.

Conversion of crystalline cellulose in subcritical water was studied with much emphasis on the kinetic detail describing the reaction in this medium. Thereafter, characterization of cellulose residues obtained from conversion of crystalline cellulose in subcritical water was conducted via dilute solution viscometry. The DP of unreacted cellulose was used to evaluate the rate of hydrolysis of glycosidic bonds. Lastly, conversions of crystalline cellulose in supercritical water were measured.

4.2.1 Conversion of Crystalline Cellulose in Subcritical Water

Reaction of crystalline cellulose in subcritical water is heterogeneous. This is due to the low solubility level of crystalline cellulose in subcritical water. Therefore, from a particulate standpoint, surface hydrolysis of crystalline cellulose is presumed to dominate in subcritical water. To describe the detail of this heterogeneous reaction at this particulate level, a rate equation based on the shrinking core model reported by Yoshioka et al.[68, 69] and later adopted by Sasaki et al.[32] was used. The conversion term based on this

reaction and its relationship with the residence time were established. The kinetics parameters were subsequently evaluated.

4.2.1.1 Experimental Description

Double distilled (deionized) water was fed into a tube enclosed within a tuber furnace at flow rates ranging from 5 ml/min to 10 ml/min. Subsequently, the temperature of the deionized water was raised from room temperature to subcritical temperatures ranging from 270 °C to 340 °C for separate experimental runs. The pressure of the fluid in the tube which was about 5000 psi was set and controlled by a back pressure regulator downstream. The subcritical water from the tube entered the microreactor and served as both the hydrolytic agent and reacting medium for the 2 wt% cellulose suspension. The cellulose suspension entered from the upper inlet port of the reactor closer to the tube furnace outlet. The 2 wt% cellulose suspension mixed with the subcritical water at an equal volumetric flow rate, thereby diluting it to 1 wt%. The reaction was quenched by the deionized water entering from the other upper inlet port of the microreactor and also by the heat exchanger just at the outlet end of the microreactor.

4.2.1.2 Cellulose Residue Data Analysis

Conversion was subsequently evaluated based on the amount of cellulose reacted with respect to the initial quantity of cellulose fed. The values obtained for the conversion at the different subcritical temperatures were coupled into the conversion term (numerator of Equation 7) and plots of the conversion term with residence times were made. The overall surface hydrolysis rate constants obtained from these plots were introduced into the Arrhenius equation to obtain the kinetics parameters.

4.2.1.3 Results and Discussions

The concentrations in g/l of the insoluble hydrolysates sampled at the subcritical condition were measured in accordance with the gravimetric analysis method discussed above in the sampling analysis section. The conversions obtained at each subcritical temperature per range of residence times can be seen in Table 4. At each subcritical temperature, conversion as observed from Table 4 increases generally with the residence times. Maximum conversion of 92.2 % is seen at a residence time of 0.56 s and at 320 °C. At residence times higher than 0.56 s at 320 °C, complete liquefaction of the 1 wt% cellulose suspension was observed. This explains why there are no experimental data (no residue to measured) due to complete conversion of the crystalline cellulose at 320 °C for residence times higher than 0.56 s.

As stated earlier in this section, the dominant reaction mechanism describing the conversion of crystalline cellulose to fermentable sugars in subcritical water is surface hydrolysis. The kinetics behind this mechanism are modeled after the shrinking core or grain model and detailed kinetics equations are expressed in Equations 5 to 7. The conversion term as shown in Figure 17 is plotted against the residence times to obtain the overall rate constants, k, for each subcritical temperature. The natural log of the rate constant was plotted with the reciprocal of the temperature to generate the Arrhenius plot as depicted in Figure 18. The kinetic parameters were subsequently evaluated.

Table 4. Conversion of 1 wt% Cellulose Suspension at Subcritical Temperatures in Microreactor

270 °C		280 °C		290 °C		295 °C		300 °C		320 °C	
τ	X	τ	X	τ	X	τ	X	τ	X	τ	X
0.00	0.00	0.00	0.00	0.00	0.00	0.00	0.00	0.00	0.00	0.00	0.00
0.445	0.165	0.437	0.234	0.438	0.330	0.424	0.316	0.402	0.465	0.400	0.723
0.498	0.257	0.489	0.262	0.469	0.324	0.453	0.431	0.494	0.487	0.437	0.831
0.537	0.186	0.559	0.177	0.545	0.455	0.525	0.377	0.534	0.306	0.495	0.868
0.601	0.202	0.606	0.237	0.612	0.431	0.623	0.581	0.582	0.464	0.555	0.922
0.725	0.289	0.712	0.327	0.745	0.553	0.691	0.855	0.684	0.565		
0.877	0.342	0.832	0.402	0.870	0.631	0.808	0.691	0.788	0.698		
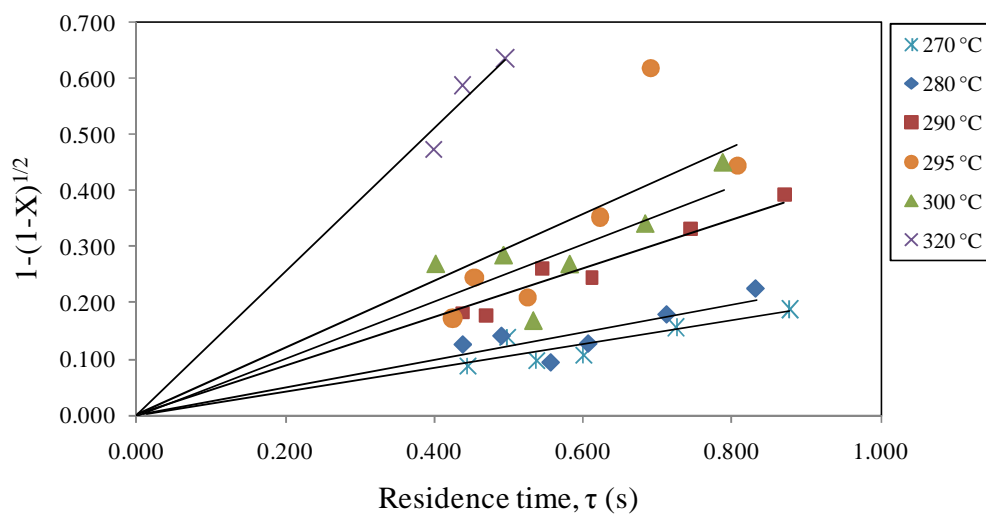
Figure 17. Relationship between $1-(1-X)^{1/2}$ and the residence time
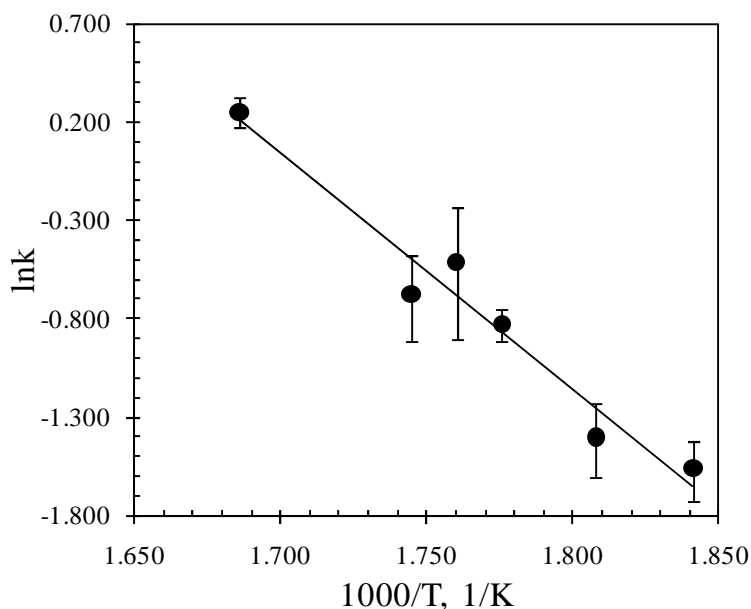
Figure 18. Arrhenius plot of the rate constant of the conversion of crystalline cellulose in subcritical water and at 5000 psig based on grain/shrinking core model

The activation energy, *EA*, and the frequency factor, *A*, evaluated based on the plot in Figure 18 are 99 ± 29 kJmol^{-1} and $10^{8.9 \pm 2.7}$ s^{-1} which are lower than 146 ± 5 kJ mol^{-1} and $10^{11.9 \pm 0.4}$ s^{-1} the values reported by Sasaki et al. [32] under subcritical condition. The error values were estimated based on 95 % confidence intervals.

4.2.1.4 Conclusion

Conversion of crystalline cellulose in subcritical water is heterogeneous due to its low solubility in this reaction medium. The reaction mechanism is surface based hydrolysis and can be best modeled after a shrinking core or grain model equation. The

kinetic parameters, including the activation energy and pre-exponential factor, obtained for the overall conversion of crystalline cellulose are 99 ± 29 kJmol^{-1} and $10^{8.9\pm2.7}$ s^{-1}, respectively. There is almost complete liquefaction of 1 wt % cellulose suspension at subcritical temperature of 320 °C and at a residence of 0.56 s in the microreactor. It is logical to categorically state that, all things being equal, if a residence time is increased above 0.56 s while at 320 °C, it is very possible to have 100 % liquefaction of the 1 wt % cellulose suspension. Thus, solubility of crystalline cellulose in subcritical water increases as the temperature increases.

4.2.2 Dilute Solution Viscometry Analysis of Crystalline and Unreacted Cellulose

To assess hydrolysis rates of glycosidic bonds in cellulose chains, the degree of polymerization (DP) of the crystalline cellulose as received and cellulosic residues obtained after reaction must be known. There are different characterization methods for knowing the DP of a polymer; examples include size exclusion chromatography, osmometry, dilute solution viscometry, and low-angle laser light scattering, to mention but a few. However, the characterization method adopted in this section of the project is dilute solution viscometry. The viscosity-average DP is obtained by dividing the viscosity-average molecular weight of the cellulose molecules with the molecular weight of the monomer, which is dehydrated glucose. A fundamental description of this characterization has been elucidated in Chapter 2.

4.2.2.1 Experimental Description

The ASTM International standard (ASTM 1795-96) for measuring intrinsic viscosity of cellulose[70] was adopted in evaluating the viscosity–average molecular weight

(MW_v) and viscosity-based degree of polymerization (DP_v) of cellulose. Crystalline cellulose as received was dissolved in the ASTM recommended reagent, 0.5 M cupriethylenediamine hydroxide solution (CED). After hydrolysis, cellulose residues left unreacted were separated from hydrolysate suspension through centrifugation, decantation and the solid residue was subsequently freeze-dried. The dried cellulose residue follows the same ASTM recommended steps for dissolution in 0.5 M CED. The dissolved cellulose was injected into a size 100 calibrated Cannon-Fenske viscometer from the bigger open end and suctioned up to cross over the marked line between the two smaller bulbs of the viscometer and later released to flow through the viscometer capillary passage. Viscosities were obtained for concentrations ranging from 0.1 to 3 g/dl. Similar procedure was followed for obtaining the kinematic viscosity (η_0) of the solvent (CED) void of any solid cellulose but with viscometer of size 50. The experimental procedure for evaluating the DP of unreacted cellulose was followed in like manner for cellulose residues obtained after hydrolysis in the microreactor.

4.2.2.2 Results and Discussions

Based on these data, intrinsic viscosity was deduced from the average of the intersection points resulting from the extrapolation of both inherent-viscosity-concentration and reduced-viscosity-concentration curves onto the ordinate axis. Figure 10 in Chapter 2 depicted the plot obtain for evaluating the intrinsic viscosity of crystalline cellulose as received from Sigmal Aldrich®.

Intrinsic viscosity obtained from Figure 10 is 1.31 dl/g and was subsequently introduced into the MKS equation (Equation 27) to evaluate the degree of polymerization (DP). The empirical Mark-Houwink constants are polymer-solvent specific and for

cellulose-cupriethylenediamine at dissolution temperature of 25 °C, their values[71] are K =1.7 cm^3/g and, α = 0.8. The DP_v evaluated for crystalline cellulose as received was approximately 228, and the viscosity-average molecular weight (MW_v) calculated for the cellulose was approximately 37 KDa. This average molecular weight agrees with the Sigma-Aldrich certified average molecular weight for cellulose which ranges between 36 and 40 KDa. The DP_v(s) evaluated for cellulose residues at different residence times and different subcritical temperatures during hydrolysis are highlighted on Table 5. A decreasing trend in the chain length of the cellulose molecules as temperature increases was observed with the lowest DP_v range obtained at 295 °C and 300 °C. The decrease in the chain length can be attributed to the reaction of the crystalline cellulose in subcritical water in the microreactor.

Table 5. Viscosity-Average Degree of Polymerization of Cellulose Residues at Subcritical Temperatures

270 °C		280 °C		290 °C		295 °C		300 °C	
τ(s)	DP_v	τ (s)	DP_v	τ (s)	DP_v	τ(s)	DPv	τ(s)	DP_v
0.00	228	0.00	228	0.00	228	0.00	288	0.00	228
0.445	78	0.437	125	0.438	90	0.424	47	0.402	89
0.498	87	0.489	108	0.469	68	0.453	42	0.494	43
0.537	91	0.556	115	0.545	76	0.525	42	0.534	55
0.601	85	0.606	127	0.612	73	0.623	26	0.582	49
0.725	69	0.712	57	0.745	72	0.691	7	0.684	39
0.877	53	0.832	50	0.870	72	0.808	13		

Figures 19 - 23 present some plots depicting how the value of intrinsic viscosity was obtained for cellulose residues obtained at subcritical water reaction temperature in the microreactor. The intrinsic viscosity, which is the average of the two intercepts on the ordinate axis, was introduced into the MKS Equation (Equation 27) to obtain the average DP_v of the cellulose residues as delineated on Table 5 for different residence times and at different subcritical temperatures.
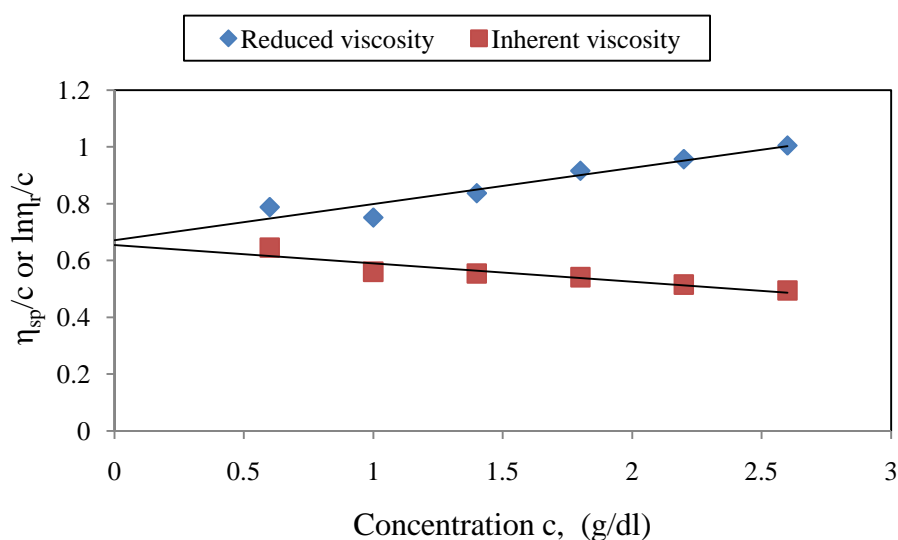
Figure 19. Plot of η_{inh} ($\ln(\eta_r/c)$) and η_{red} (η_{sp}/c) versus c for cellulose residues obtained at 270 °C and at flow rates of 8 ml/min and dissolved in cupriethylenediamine at 25 °C. The shared intercept is [η].
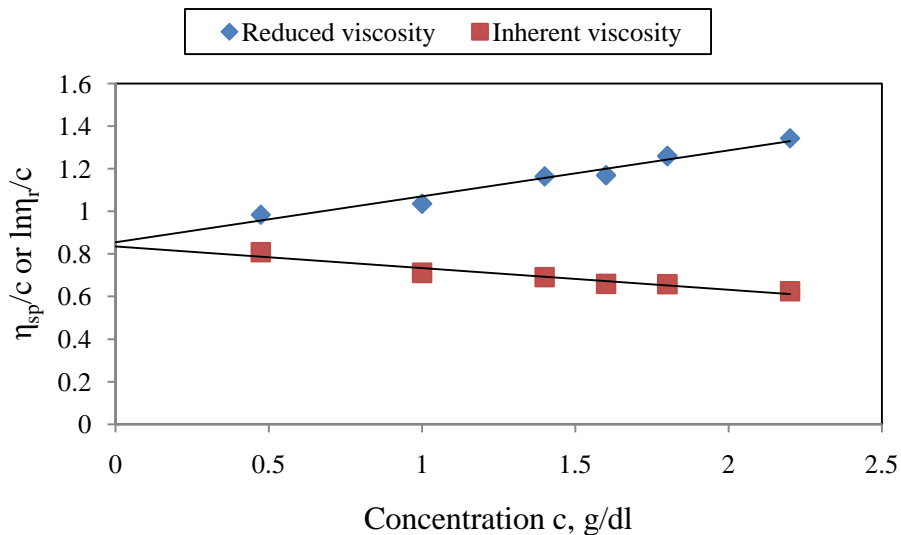
Figure 20. Plot of η_{inh} ($\ln(\eta_r/c)$) and η_{red} (η_{sp}/c) versus c for cellulose residues obtained at 280 °C and at flow rates of 7 ml/min and dissolved in cupriethylenediamine at 25 °C. The shared intercept is [η].
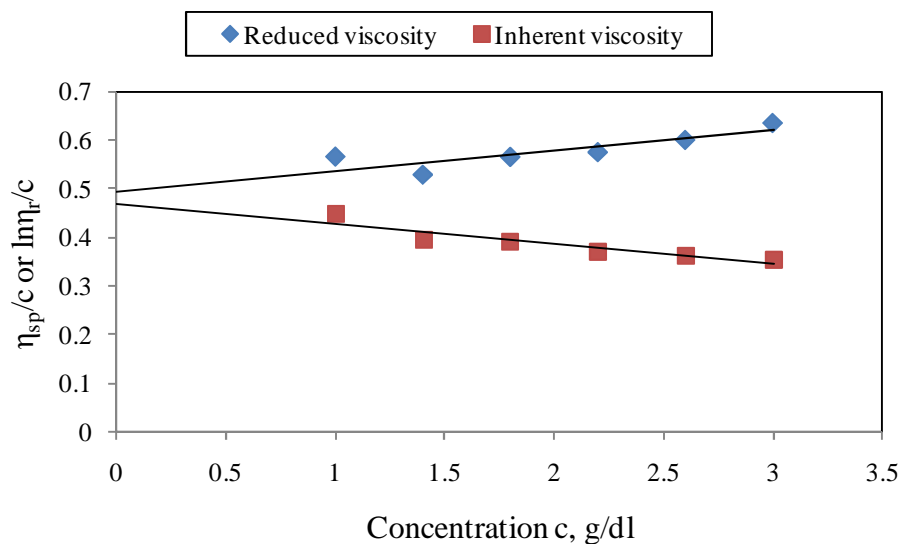
Figure 21.Plot of η_{inh} ($\ln(\eta_r/c)$) and η_{red} (η_{sp}/c) versus c for cellulose residues obtained at 290 °C and at flow rates of 9 ml/min and dissolved in cupriethylenediamine at 25 °C. The shared intercept is [η].
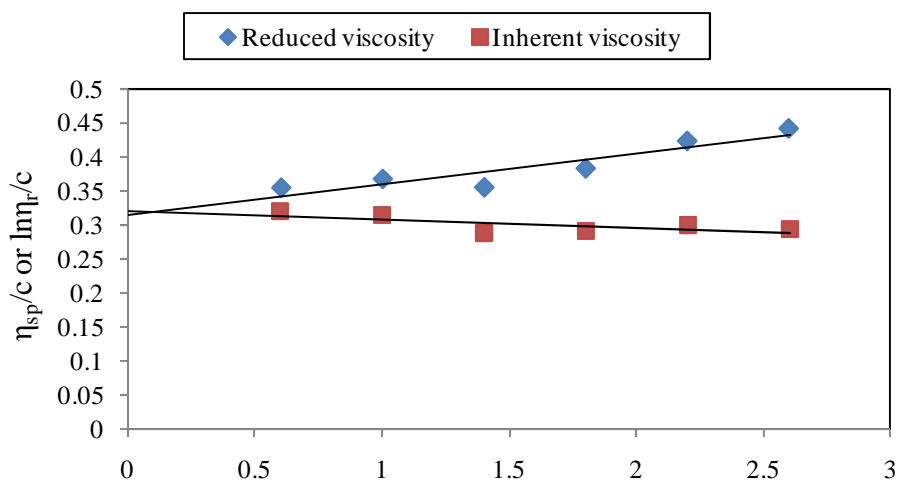
Figure 22. Plot of η_{inh} ($\ln(\eta_r/c)$) and η_{red} (η_{sp}/c) versus c for cellulose residues obtained at 295 °C and at flow rates of 9 ml/min and dissolved in cupriethylenediamine at 25 °C. The shared intercept is [η].
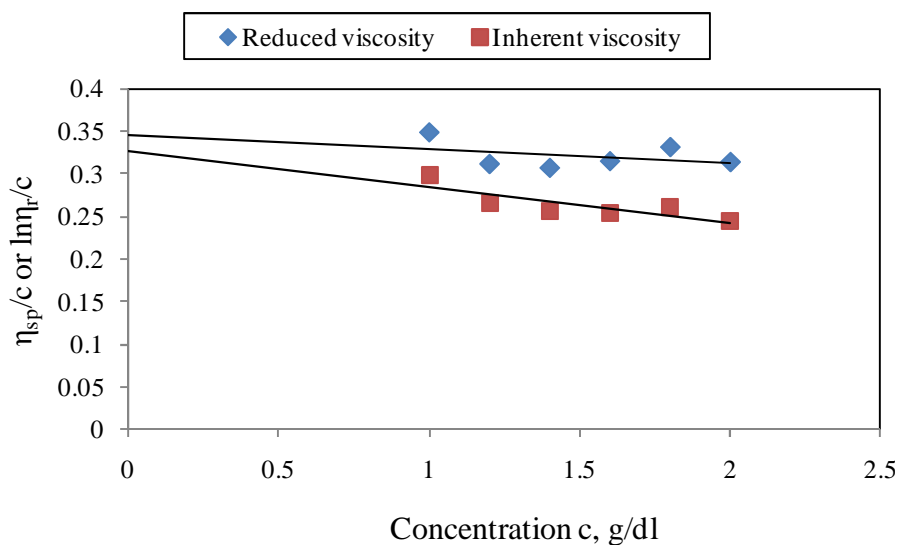
Figure 23. Plot of η_{inh} ($\ln(\eta_r/c)$) and η_{red} (η_{sp}/c) versus c for cellulose residues obtained at 300 °C and at flow rates of 9 ml/min and dissolved in cupriethylenediamine at 25 °C. The shared intercept is [η].

4.2.2.4 Conclusion

Crystalline cellulose as received and cellulose residues obtained from reaction were characterized by dilute solution viscometry. The viscosity-average degree of polymerization (DP_v) obtained for the crystalline cellulose was 228 while the DP_v obtained for the cellulose residues ranged from 127 to 7 for the temperature and flow rates considered. Having obtained the DP for the crystalline cellulose as received and for the cellulose residue obtained from reaction, we could then proceed to the next important step of evaluating the rate of hydrolysis of glycosidic bonds of the cellulose.

4.2.3 Hydrolysis of Glycosidic Bonds of Cellulose

The most logical approach to investigate the hydrolysis of crystalline cellulose in any medium, be it enzymatic, acidic, or hydrothermal, is to look at it from the standpoint of breaking its glycosidic bonds. To assess this hydrolysis rate, the initial and final number of bonds, and bond concentration must be known. Initial number of bonds is obtained from the DP of crystalline cellulose as received while the final number of bonds is obtained from the DP of cellulose residue after reaction. A detailed description of how the bond concentration is evaluated is discussed in section 2.3.4. The first order rate equation guiding the reactive behavior of breaking the glycosidic bonds was elucidated in the same section (2.3.4). This reaction was conducted in the subcritical phase, and based on the temperature range considered, it was largely heterogeneous.

4.2.3.1 Experimental Description

Deionized water was fed into a tube enclosed within a tube furnace at flow rates ranging from 5 ml/min to 10 ml/min. Subsequently, the water temperature was raised

from room temperature to subcritical temperatures ranging from 270 °C to 300 °C for separate experimental runs. The pressure of the fluid in the tube was about 5000 psig and was controlled by a back pressure regulator downstream. The subcritical water was injected into the microreactor and served as the reacting medium for the 2 wt% cellulose suspension entering from the upper inlet port of the reactor closer to the tube furnace outlet. The 2 wt% cellulose suspension mixed with the subcritical water at an equal volumetric flow rate thereby diluting it to 1 wt %. The reaction is quenched by the deionized water entering from the other upper inlet port of the micro-reactor and also by the heat exchanger just at the outlet end of the micro-reactor. The samples were collected in the gas-liquid separator and were analyzed.

4.2.3.2 Sample Analysis

The hydrolysate products were collected at different subcritical temperatures and the water insoluble portion were centrifuged, dried, and characterized. Centrifugation was conducted with SORVALL® RC 5B plus and samples were centrifuged at a speed of 8000 rpm and at duration of 10 min. The supernatant obtained after centrifugation were decanted leaving behind some cellulose residue which was later freeze dried with labconco freeze dryer. The dried cellulose residue was then dissolved in CED at 25 °C and subsequently characterized for viscosity-average degree of polymerization via dilute solution viscometry. Some of the cellulose residues were subject to size exclusion chromatography (SEC) analysis. The chromatography analysis allow for determination of the degree of polymerization and molecular weight distribution.

4.2.3.3 Results and Discussions

Figure 24 depicts the rate of cellulose hydrolysis at subcritical conditions of water in the microreactor. The $-\ln(C_b/C_{bo})$ values were plotted against residence times, τ, at subcritical temperatures ranging from 270 ℃ to 300 ℃ and at a pressure of 5000 psi. Rate constants, k, were evaluated at each reaction condition. Figures 25-29 show the Arrhenius plot for the k values obtained for the temperatures, 270 ℃ – 300 ℃. The k values were introduced into the Arrhenius equation to obtain the activation energy (EA) and pre-exponential factor (A) based on the different DPs used in calculating the bond concentrations. The activation energy and pre-exponential factors obtained for the bond concentration resulting from the DP(s) of cellulose residue evaluated experimentally from dilute solution viscometry and SEC are shown on Table 6. DP_p is the peak average degree of polymerization from the molecular weight distribution obtained in SEC. It is simply the molecular weight corresponding to the peak of the distribution. The idea of solving for the activation energy based on DP of cellulose residues obtained by these different characterization techniques is to validate that the activation energy corresponding to the DP obtained from dilute solution viscometry analysis. There is no significant difference in the activation energy obtained via both the dilute solution viscometry (DSV) and SEC. The corresponding activation energies for the viscosity average degree of polymerization obtained via DSV and SEC are quite close. Observing Arrhenius plots for each corresponding DP, there is a striking similarity in these plots and similar error bars; this further conferred a high level of confidence on the values of DP_v obtained via dilute solution viscometry.
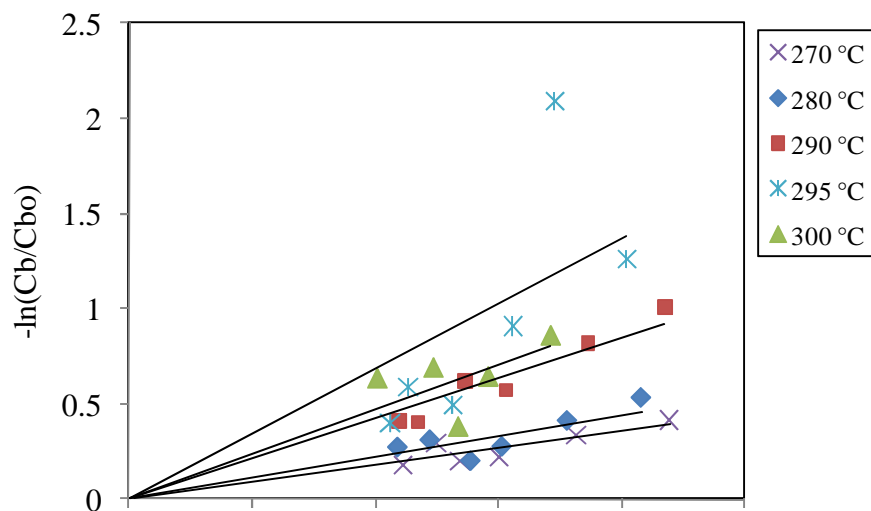
Figure 24. Conversion term based on bond concentration vs the residence time
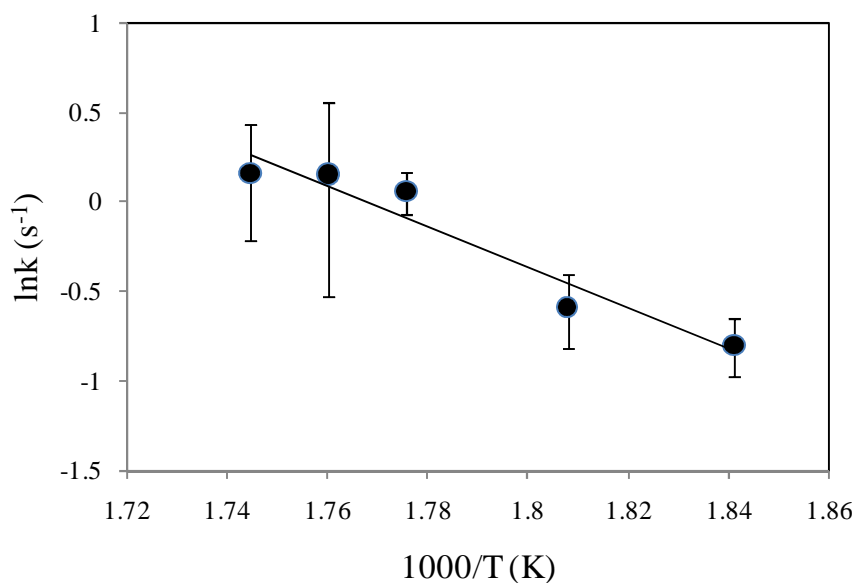
Figure 25. Arrhenius plot of the rate constant of crystalline cellulose
hydrolysis in subcritical water and at 5000 psi based on bond
concentration (DP_v from dilute solution viscometry experiment)
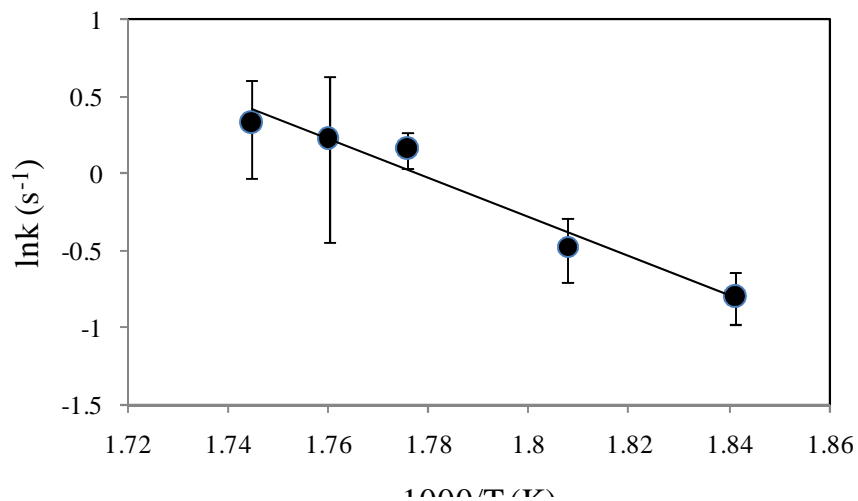
Figure 26. Arrhenius plot of the rate constant of crystalline cellulose hydrolysis in subcritical water and at 5000 psi based on bond concentration (DP_p from size exclusion chromatography experiment)
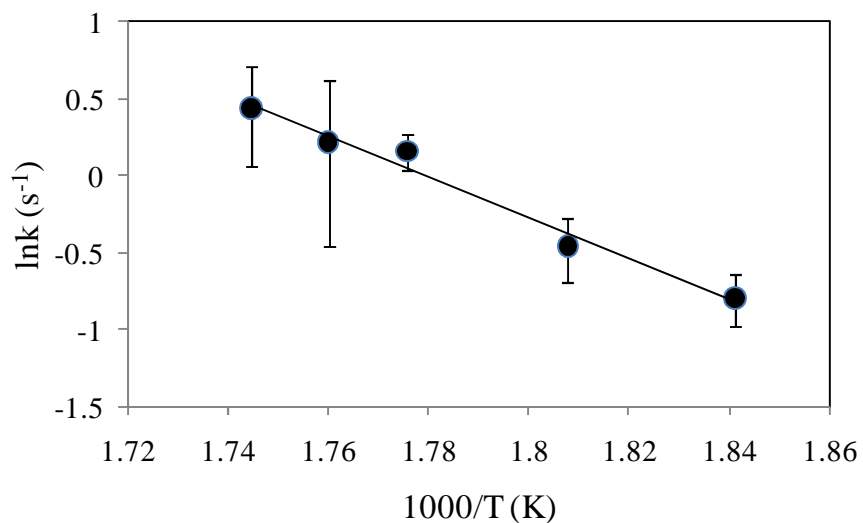
Figure 27. Arrhenius plot of the rate constant of crystalline cellulose hydrolysis in subcritical water and at 5000 psi based on bond concentration (DP_n from size exclusion chromatography experiment)
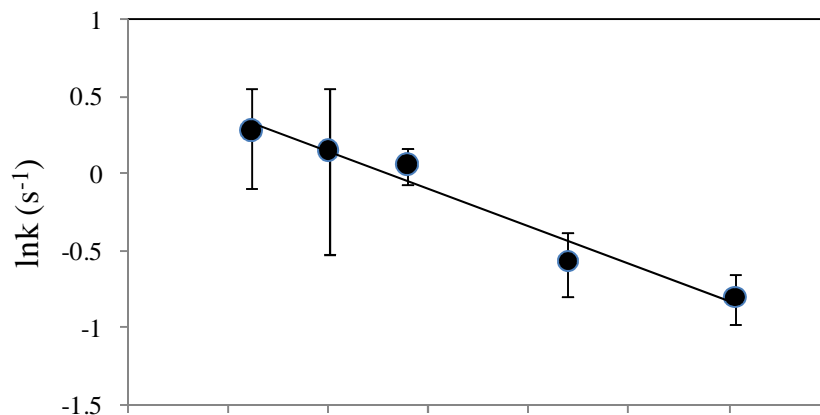
Figure 28. Arrhenius plot of the rate constant of crystalline cellulose hydrolysis in subcritical water and at 5000 psi based on bond concentration (DP_w from size exclusion chromatography experiment)
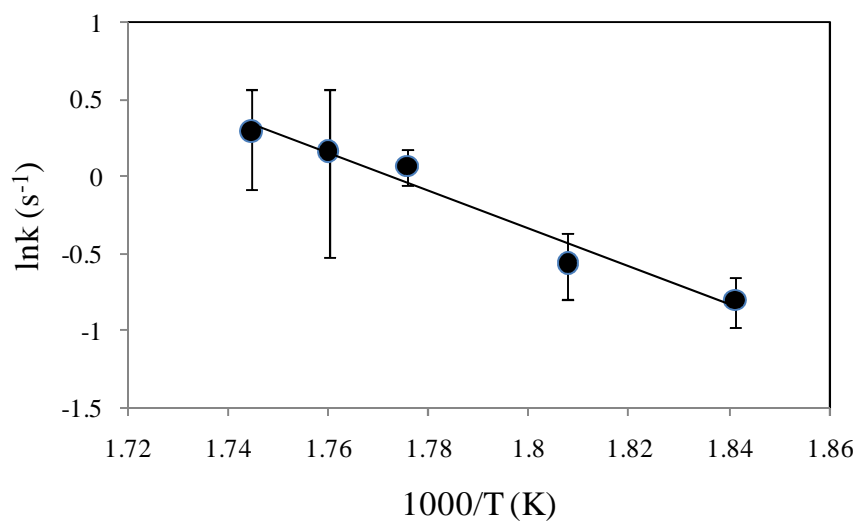
Figure 29. Arrhenius plot of the rate constant of crystalline cellulose hydrolysis in subcritical water and at 5000 psi based on bond concentration (DP_v from size exclusion chromatography experiment)
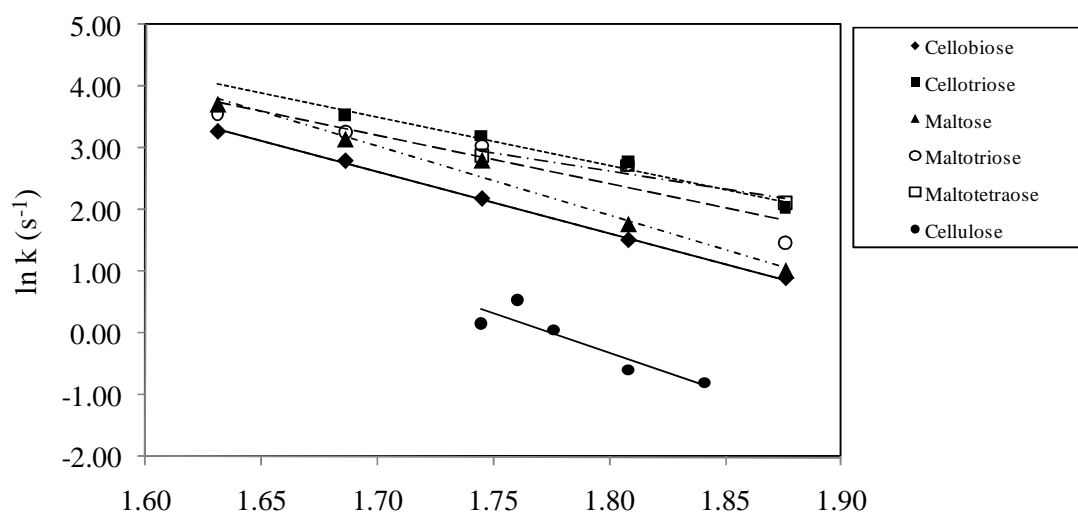
Figure 30. Arrhenius plot comparing rate constant of crystalline cellulose hydrolysis based on bond concentration with oligomers hydrolysis in subcritical water

Table 6. Kinetics Parameters obtained for the Glycosidic Bond Hydrolysis based on bond concentration evaluated from the DP of cellulose residues obtained from dilute solution viscometry and SEC

Degree of Polymerization	Characterization techniques	Activation Energy, EA (kJ/mol)	Pre-exponential factor, A (s^{-1})
DP$_v$	Dilute solution viscometry	108.24±89.09	$10^{10.04\pm4.65}$
DP$_p$	Size exclusion chromatography	104.98±36.48	$10^{9.75\pm1.91}$
DP$_w$	Size exclusion chromatography	101.17±35.46	$10^{9.36\pm1.85}$
DP$_v$	Size exclusion chromatography	102.04±34.59	$10^{9.45\pm1.81}$

Figure 30 displays an Arrhenius plot depicting the rate constants obtained for the hydrolysis of oligomers and cellulose in subcritical water. Hydrolysis rate constants for the oligomers are obtained from Taiying Zhang's PhD work[14] while hydrolysis rate constants for the cellulose are obtained from Figure 25. The activation energies obtained for the oligomers: maltose (93 kJ/mol), cellobiose (82 kJ/mol), cellotriose (65 kJ/mol), maltotriose (65 kJ/mol), and maltotetraose (52 kJ/mol), decreases with increase in the size of the monomeric units while activation energy for the hydrolysis of cellulose in subcritical water is higher than that of the oligomers.

4.2.3.4 Conclusion

Hydrolysates obtained as a result of hydrolyzing crystalline cellulose in subcritical water contained unreacted cellulose. These hydrolysates were centrifuged to separate the water soluble part via decantation from the sample as a whole. Subsequently, the cellulose residue was freeze dried and characterized to obtain the degree of polymerization (DP_v). Bond concentrations based on the DP(s) obtained from DSV and SEC were calculated and the detailed kinetics parameters based on a first order bond-concentration rate equation were evaluated. The activation energies (EA) and pre-exponential factors (A) obtained for the hydrolysis rate of breaking the glycosidic bonds in cellulose are 108 ± 89 kJ/mol and $10^{10.0\pm4.6}$ s^{-1} for DP_v obtained via DSV and 101 ± 35 kJ/mol and $10^{9.4\pm1.9}$ s^{-1} for DP_v obtained from SEC. The rate of breaking the glycosidic bonds is crucial to understanding the kinetics of converting crystalline cellulose to fermentable sugars.

4.3 Conversion of Crystalline Cellulose in Supercritical Water

Conversion of crystalline cellulose occurs by disintegrating the intermolecular hydrogen bonding binding each layer of cellulose chains within the crystal structure. As a result of the disintegration, the hydroxyl (OH) group on each of the glucose units reacts with the protonating component of the solvent. In this section, we shall be investigating the kinetics parameter defining the conversion of crystalline cellulose in supercritical water.

Considering the reaction volume of the microreactor (0.17 ml) coupled with the maximum flow rate the available pumps at our disposal could deliver, it proved to be unrealistic to obtain unreacted cellulose in supercritical water. Therefore, to obtain some cellulose residue after reacting crystalline cellulose in the microreactor at supercritical condition of water, there is the need to either significantly increase the maximum deliverable flow rates or substantially reduce the reaction volume. The latter option based on the available resources was chosen. The modification also involves changing the orientation of the microreactor. Details of the modification will be elucidated in the experimental set-up and processing steps. Experimental description of the conversion of cellulose in the microreactor and at the supercritical condition of water will be discussed. Subsequently, methods adopted in analyzing the sample will be presented while results and discussion section will follow immediately. Lastly, conclusions based on findings and a summary of experiments will complete this chapter.

4.3.1 Experimental Setup and the Processing Steps

This section describes the experimental setup and processing steps of converting crystalline cellulose in the microreactor in supercritical water. The essence of this reaction is to have some quantity of the crystalline cellulose reacted and leaving behind some residues. The experimental setup for the reaction of crystalline cellulose in the microreactor is similar to the experimental setup in Figure 14, the only difference is the orientation of the microreactor and extra heat exchanger unit in the setup for this experiment. The feedstock (slurry solution) is fed into the microreactor positioned midway along the process flow path. A schematic chart of the process for the reaction in the microreactor can be seen in Figure 31.

Deionized water (18 mohm) obtained from a Nanopure infinity water purification system was fed into a tube enclosed within a tube furnace (Thermolyne79400) by Lab Alliance series II pumps at flow rates ranging from 9 ml/min to 14 ml/min. Subsequently, the water was heated to supercritical temperatures ranging from 374 ℃ to 390 ℃ for separate experimental runs. The pressure of the fluid in the tube was about 5,000 psig and was controlled downstream by a 15,000 psig capacity Tescom back pressure regulator. The pressure gauge displays the operating pressure. Just after the pressure gauge is a rupture disc. This safety device, unlike the relief valve which opens when the maximum pressure is exceeded, is ruptured when the operating pressure exceeds its limit. In this experimental setup, the rupture disc can support a maximum pressure of 9000 psig, so therefore, any pressure beyond this limit can lead to rupture of the disc.
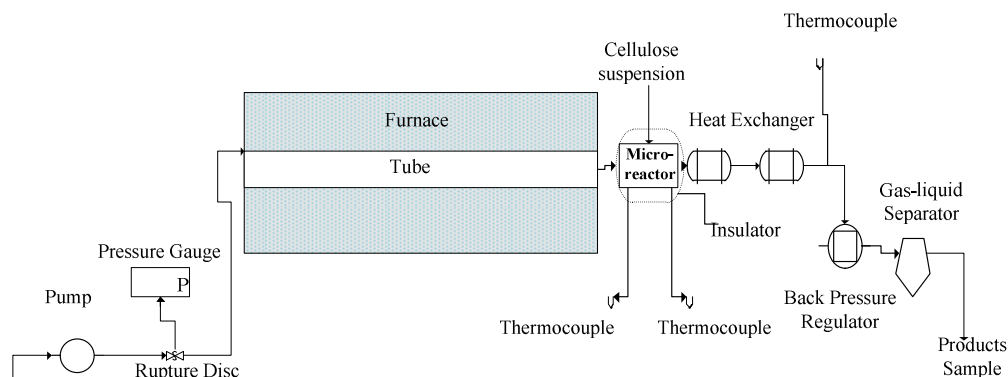
Figure 31. Schematic chart of the conversion of crystalline cellulose in microreactor at supercritical condition

The supercritical water exited into the glass fiber insulated microreactor and served as both hydrolytic agent and the reaction medium for the 2 wt% cellulose slurry solutions. The feedstock was fed into the microreactor at the inlet port oriented upward and located midway in the microreactor. The maximum temperature limit the furnace could support was 1200 °C. The cellulose slurry solution with flow rates ranging from 9 to 14 ml/min mixed with the supercritical water with a constant flow rate of 10 ml/min, thereby diluting the slurry concentration to values ranging from 0.947 to 1.167 wt%. The reaction was quenched by a heat exchanger just at the outlet port of the microreactor and also by the shell and tube heat exchanger placed just downstream from the first heat exchanger. With the rapid heating and quick quenching of the cellulose reaction in the microreactor, the reaction volume within the microreactor is estimated to be 0.088 ml. The schematic flow detail in the microreactor can be seen in Figure 28. Alterations made to the microreactor were mainly to reduce the reaction volume and allow the reaction to occur as indicated in Figure 32.

The reaction volume for the conversion of cellulose at supercritical conditions is this low because of the need to allow the reaction to occur at very low residence times to avoid complete disappearance of the crystalline cellulose in supercritical water. Cellulose residues left behind were measured gravimetrically. Detail of the gravimetric analysis for the sole purpose of evaluating the rate of cellulose conversion in supercritical water will be discussed in the subsequent sections. The samples were collected in the gas-liquid separator and analyzed for conversion and weight of unreacted cellulose (residue).
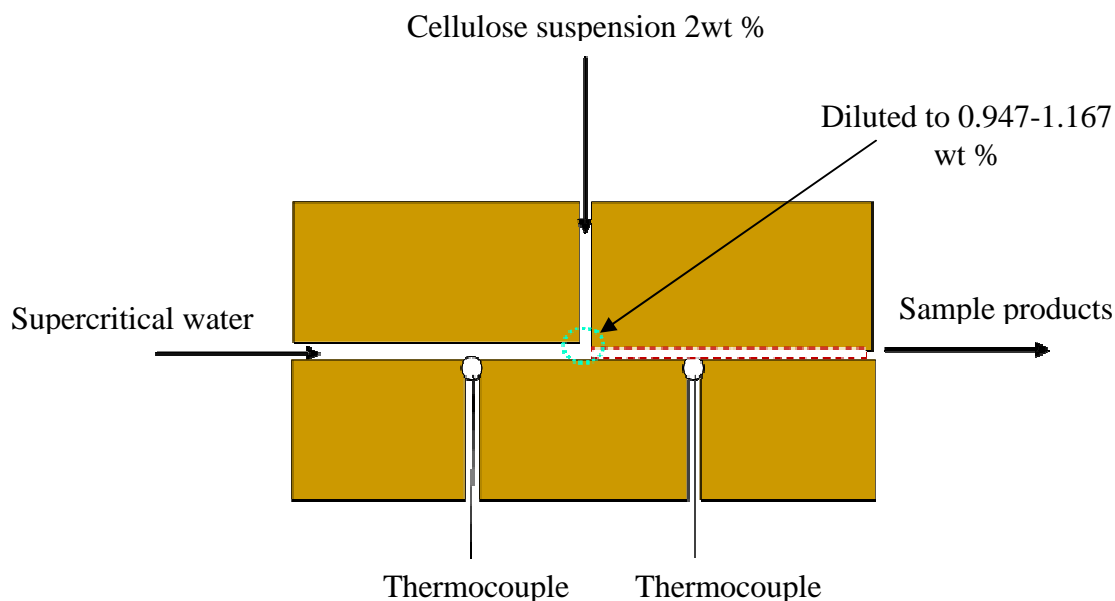
Figure 32. Microreactor system set-up for cellulose conversion at supercritical condition

4.3.2 Sample Analysis

The hydrolysate products were collected at different supercritical temperatures, and the water insoluble portions were centrifuged, dried, and analyzed gravimetrically. Centrifugation was conducted with SORVALL® RC 5B plus and samples were centrifuged at a speed of 8000 rpm for 10 min. The supernatant obtained after

centrifugation was decanted leaving behind the cellulose residue, which was later dried in an oven within the temperature range of 42 °C – 67 °C . Cellulose residues were measured gravimetrically to determine the mass that reacted. The results were used to calculate the conversion.

4.3.3 Results and Discussions

The concentrations in g/l of the insoluble hydrolysates sampled at the supercritical conditions were evaluated by gravimetrically measuring the amount of cellulose residue contained within the volume of the sampled hydrolysate. Conversions were evaluated and the values obtained at each supercritical temperature per residence times can be seen on Table 7. At each supercritical temperature, conversion as observed from Table 7 increases generally with the residence times. Maximum conversion of 90 % is seen at residence time of 0.154 s and at supercritical temperature of 390 °C, while a minimum conversion of 38.5% was observed at 374 °C and residence time of 0.142 s.

Table 7. Conversion of Cellulose Suspension at Supercritical Temperatures in Microreactor

374 °C		378 °C		380 °C		382 °C		388 °C		390 °C	
τ(s)	X	τ(s)	X	τ(s)	X	τ(s)	X	τ(s)	X	τ(s)	X
0.00	0.00	0.00	0.00	0.00	0.00	0.00	0.00	0.00	0.00	0.00	0.00
0.142	0.368	0.139	0.414	0.137	0.413	0.135	0.526	0.129	0.538	0.126	0.560
0.145	0.460	0.142	0.394	0.140	0.415	0.138	0.452	0.132	0.642	0.129	0.715
0.149	0.411	0.145	0.484	0.143	0.404	0.141	0.543	0.135	0.510	0.132	0.620
0.152	0.412	0.149	0.557	0.147	0.472	0.145	0.617	0.138	0.684	0.136	0.715
0.156	0.458	0.152	0.531	0.150	0.482	0.148	0.654	0.141	0.520	0.139	0.572
		0.160	0.572	0.154	0.588	0.165	0.750	0.149	0.692	0.154	0.895
		0.169	0.629	0.158	0.571			0.157	0.885		

Conversion of cellulose in this medium is modeled after a first order reaction rate equation. The conversion term, –ln(1-X), as shown in Figure 33 is plotted against the residence times to obtain the rate constants, *k*, for each supercritical temperature considered. The natural log of rate constants was plotted with the reciprocal of the temperature to generate the Arrhenius plot as depicted in Figure 34. The kinetic parameters were subsequently evaluated by equating the slope and the intercept of the Arrhenius plot with $-E_A/R$ and lnA respectively (Equation 52).
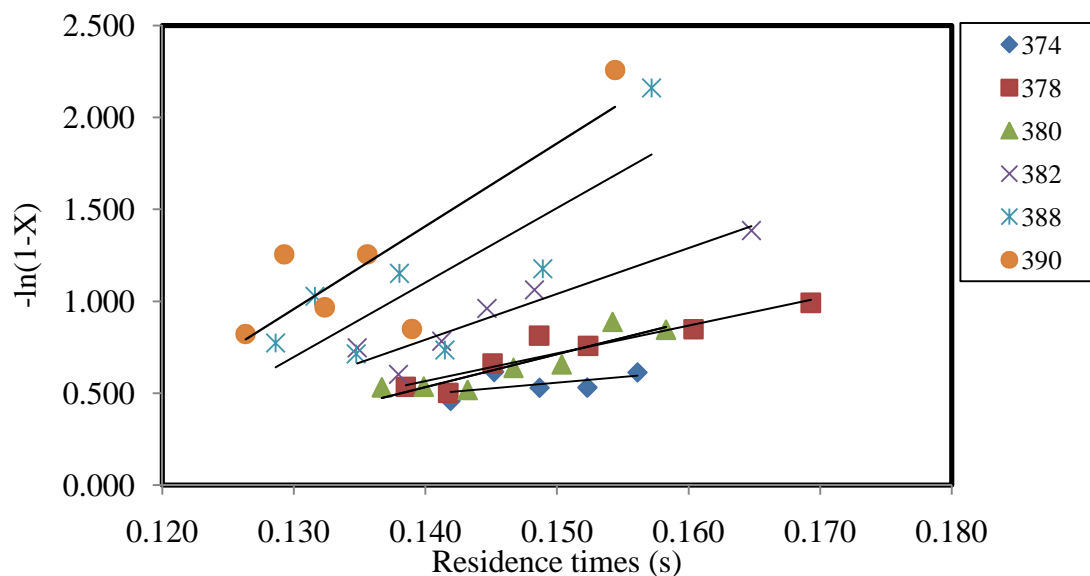
Figure 33. Conversion plot for the rate constant of cellulose reaction in supercritical water
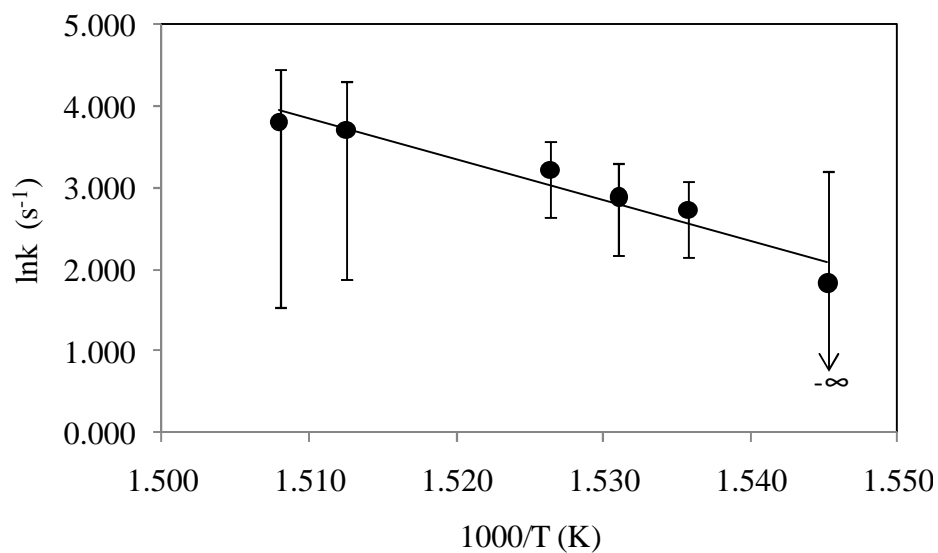
Figure 34. Arrhenius plot for the conversion of crystalline cellulose in supercritical water

The activation energy, E_a, and the pre-exponential or frequency factor, A, evaluated based on Figure 31 are 290 ± 160 kJ mol^{-1} and $10^{24\pm13}$ s^{-1}. The error values were estimated based on 95 % confidence intervals. From the activation energy obtained for

the conversion of cellulose in supercritical water (a mixture of hydroysis and dissolution) as compared with the activation energy obtained for the conversion in subcritical water, it seems that the conversion of cellulose has different rate-limiting steps under the two conditions.

4.3.4 Conclusions

Hydrolysates obtained as a result of dissolving crystalline cellulose in supercritical water contain unreacted cellulose. These hydrolysates were centrifuged to separate the water soluble part via decantation from the sample as a whole. Subsequently, the unreacted cellulose or cellulose residues were dried and analyzed gravimetrically. Conversion was calculated and the detail kinetics parameters based on a first order rate equation were evaluated. The activation energy (EA) and pre-exponential factor (A) obtained for the dissolution rate are 290 ± 160 kJmol^{-1} and $10^{24\pm13}$s^{-1} respectively. Comparatively, the activation energy obtained for the conversion of cellulose in supercritical water (dissolution/hydrolysis) is higher than the activation energy obtained when cellulose is reacted in subcritical water. Thus, it appears that conversion of cellulose in subcritical and supercritical water has different rate-limiting steps.

4.4 Kinetic Analysis of the Conversion of Crystalline Cellulose in Subcritical and Supercritical Water

In this section, the kinetic parameters obtained based on the two kinetic models adopted in this project for the conversion of cellulose in a hydrothermal system were compared. Arrhenius trends for the conversion of crystalline cellulose in subcritical and supercritical water based on first order and shrinking core models were compared with results of similar work by Sasaki et al. (2004). The conversion plots that result in the

Arrhenius plot of cellulose reaction in supercritical water for both the first order and shrinking core models were not allowed to go through the origin. The reason is because the intercepts of these plots are not anywhere near the origin. Error estimation in this study was based on a 95 % confidence interval and this perhaps may explain why the margin of error is quite significant relative to what was obtained in Sasaki et al's. It is not certain what level of confidence is the estimated error in Sasaki et al but is likely to be based on standard error estimation. Also, error estimation in the plots forced through the origin is less in value compared with the margin of error in the plots that are not forced through the origin and the reason is based on the degree of freedom. A critical review of this observation revealed that the former has more degrees of freedom than the latter. The values of the kinetics parameters and their errors from Sasaki et al. are left as they were reported while in this study, the kinetic values are rounded to 2 significant figures.

4.4.1 Shrinking Core Model

Figure 35 depicts the Arrhenius plots of cellulose conversion in subcritical and supercritical water obtained from this study and the study conducted by Sasaki et al. The trends for the two separate studies appear to closely follow each other in the supercritical region though at the high end they seems to widen while a clear difference in their trends was observed in the subcritical region. The kinetic parameters obtained in the supercritical region were found to be, $E_a = 290 \pm 160$ kJ mol^{-1} , $A = 10^{24 \pm 13}$ s^{-1} for this study, and $E_a = 547.9 \pm 27.8$ kJ mol^{-1} , $A = 10^{44.6 \pm 2.2}$ s^{-1} for Sasaki et al. respectively. In the subcritical region, the kinetic parameters obtained were found to be, $E_a = 99 \pm 29$ kJ mol^{-1}, $A = 10^{8.9 \pm 2.7}$ s^{-1} for this study, and $E_a = 145.9 \pm 4.6$ kJ mol^{-1} , $A = 10^{11.9 \pm 0.4}$ s^{-1} for Sasaki et al. Figure 36 seems to portray the same trend as observed in Figure 35 but the only exception is the difference in the error margin in the subcritical region. A larger error range in the subcritical region was observed in Figure 36 than in Figure 35. The

corresponding conversion plots upon which k-values in Figure 36 were estimated weren't forced through the origin. The kinetic parameters obtained in this case were found to be $E_a = 110 \pm 57$ kJ mol^{-1}, $A = 10^{9.5 \pm 5.3}$ s^{-1}. In Figure 37, the Arrhenius trend across the critical regions, i.e. the subcritical and supercritical regions, reflects a much better fit of the data in this study than in the study conducted by Sasaki et al. In Figure 37, the kinetic parameters obtained in this study across the critical region were found to be, $E_a = 92 \pm 13$ kJ mol^{-1}, $A = 10^{8.1 \pm 1.1}$ s^{-1} While in Sasaki's work, the kinetic parameters were found to be $E_a = 210 \pm 86$ kJ mol^{-1} and $A = 10^{11.9 \pm 0.4}$ s^{-1}. Thus, the kinetic parameters obtained for this study, in Figure 38, were estimated to be $E_a = 88 \pm 15$ kJmol^{-1}, $A = 10^{7.8 \pm 1.3}$ s^{-1}. There is no kinetic data trend for Sasaki et al in Figure 38 and the reason is because the conversion plots reported by Sasaki et al., only pass through the origin. Therefore, we were constrained to only estimate the kinetic parameters from Sasaki's work for plots passing through the origin.
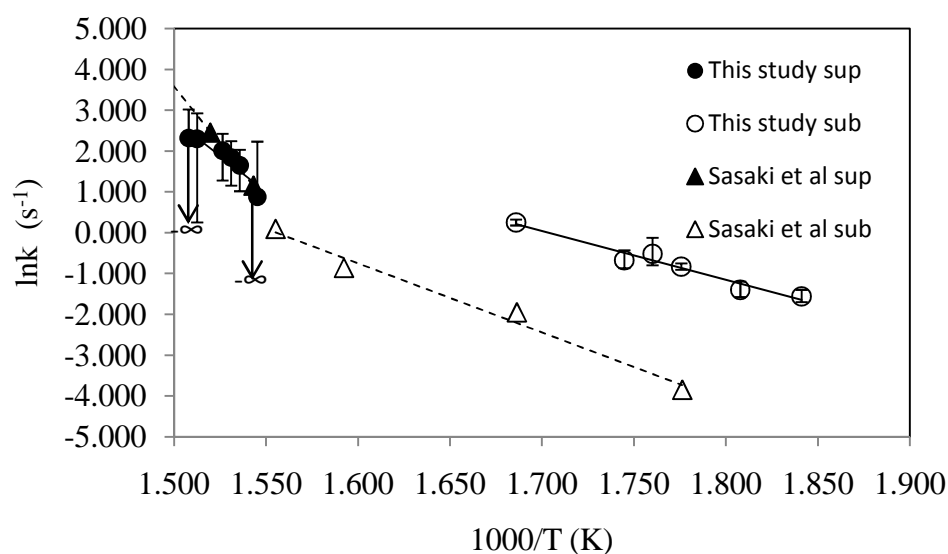
Figure 35. Shrinking Core Model: Separated Arrhenius plot for the conversion of crystalline cellulose in subcritical and supercritical water with conversion plot of cellulose reaction in subcritical water passing through the origin
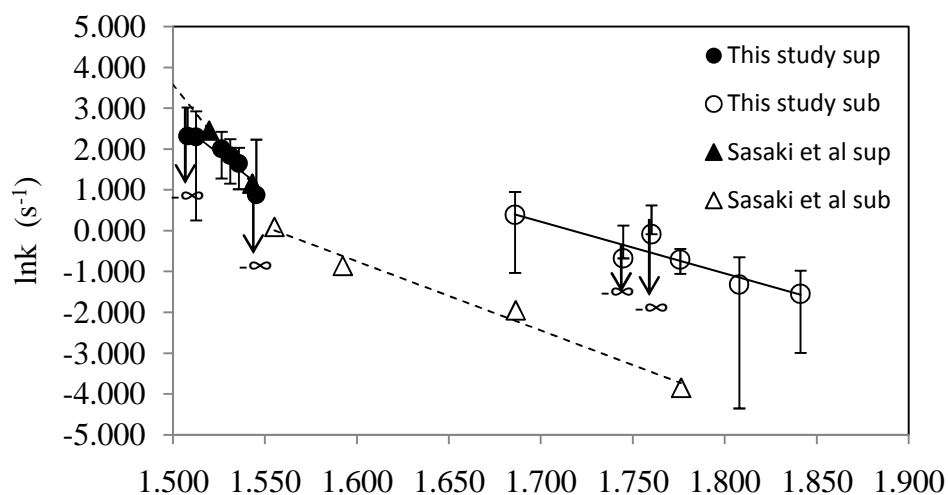
Figure 36. Shrinking Core Model: Separated Arrhenius plot for the conversion of crystalline cellulose in subcritical and supercritical water without forcing the conversion plot of cellulose reaction in subcritical to pass through the origin
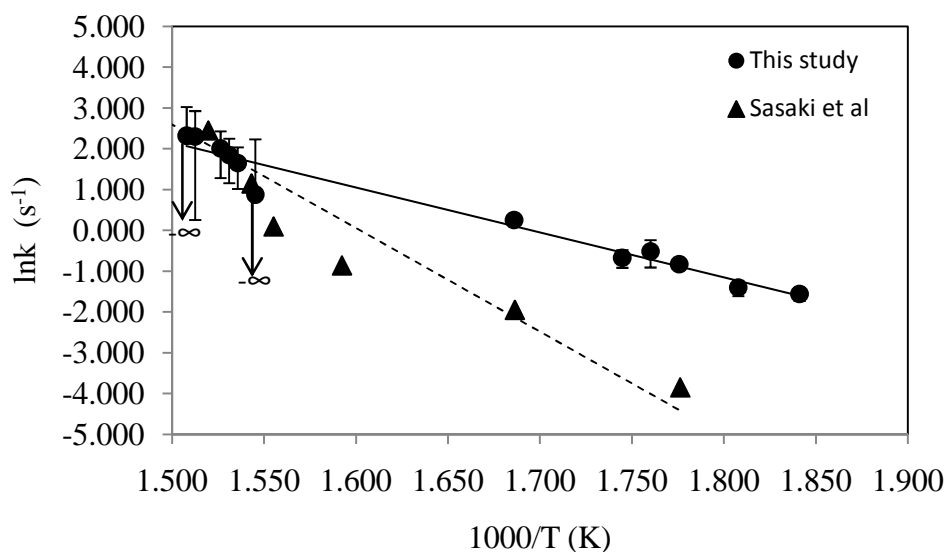
Figure 37. Shrinking Core Model: Combined Arrhenius plot for the conversion of crystalline cellulose in subcritical and supercritical water with conversion plot of cellulose reaction in subcritical water passing through the origin
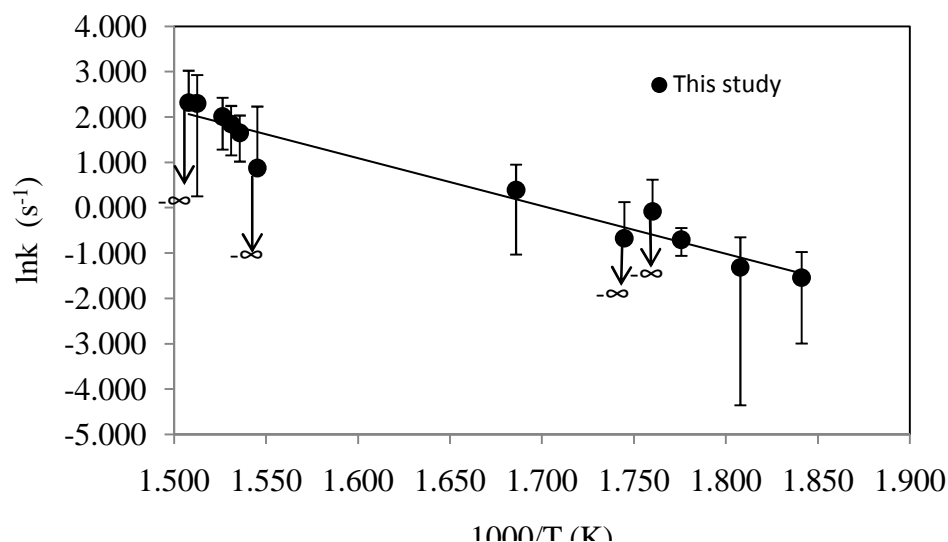
Figure 38. Shrinking Core Model: Combined Arrhenius plot for the conversion of crystalline cellulose in subcritical and supercritical water without forcing the conversion plot of cellulose reaction in subcritical water to pass through the origin

4.4.2 First Order and Shrinking Core Models

Figure 39 depicts the Arrhenius plots of cellulose conversion in subcritical and supercritical water obtained based on first order and shrinking core models. The trends for the two models appear to roughly parallel each other in both regions with lower k-values for the shrinking core model. The kinetic parameters obtained in the supercritical region were found to be E_a =420 $\pm$ 140 kJ mol^{-1}, A= $10^{34\pm11}$ s^{-1} for first order, and E_a=290 $\pm$ 160 kJ mol^{-1}, A=$10^{24\pm13}$s^{-1} for shrinking core. In the subcritical region, the kinetic parameters obtained for the first order and the shrinking core were found to be, E_a =150 $\pm$ 67 kJ mol^{-1}, A=$10^{15\pm6.2}$ s^{-1}, and E_a=99 $\pm$ 29 kJ mol^{-1}, A=$10^{8.9\pm2.7}$ s^{-1}, respectively. Similar trends as observed in Figure 39 were displayed in Figure 40 except that the k-values for the first order and shrinking core models do not parallel each other as much as in the former, and a slightly higher difference in the k-values was observed on the high side of both regions. A much wider error range in the subcritical region was observed in Figure 40 than in Figure 39. The corresponding conversion plots for which k-values in Figure 40

were estimated weren't forced through the origin. The kinetic parameters obtained for first order in this case were found to be $E_a = 120 \pm 39$ kJ mol^{-1}, $A = 10^{11 \pm 3.6}$ s^{-1} while corresponding kinetic parameters for the shrinking core model were estimated to be $E_a = 110 \pm 57$ kJ mol^{-1} and $A = 10^{9.5 \pm 5.3}$ s^{-1}.

In Figure 42, the corresponding conversion plot for the Arrhenius plots for either the subcritical or supercritical region per each of the models were not forced through the origin while opposite is the case in Figure 41. In Figure 41 and 42, the Arrhenius trend across the subcritical and supercritical regions display similar trends but with higher k-values for the first order than their corresponding shrinking core values. In Figure 41, the kinetics parameters obtained for first order across the critical region were found to be $E_a = 100 \pm 18$ kJ mol^{-1}, and $A = 10^{9.5 \pm 1.6}$ s^{-1} while in Figure 42, the kinetic parameters were found to be, $E_a = 94 \pm 23$ kJ mol^{-1}, and $A = 10^{8.9 \pm 2.0}$ s^{-1}. The kinetic parameter for shrinking core were found both in Figure 40 and 42 to be $E_a = 92 \pm 13$ kJ mol^{-1}, $A = 10^{8.1 \pm 1.1}$ s^{-1}, and $E_a = 88 \pm 15$ kJ mol^{-1}, $A = 10^{7.8 \pm 1.3}$ s^{-1}.
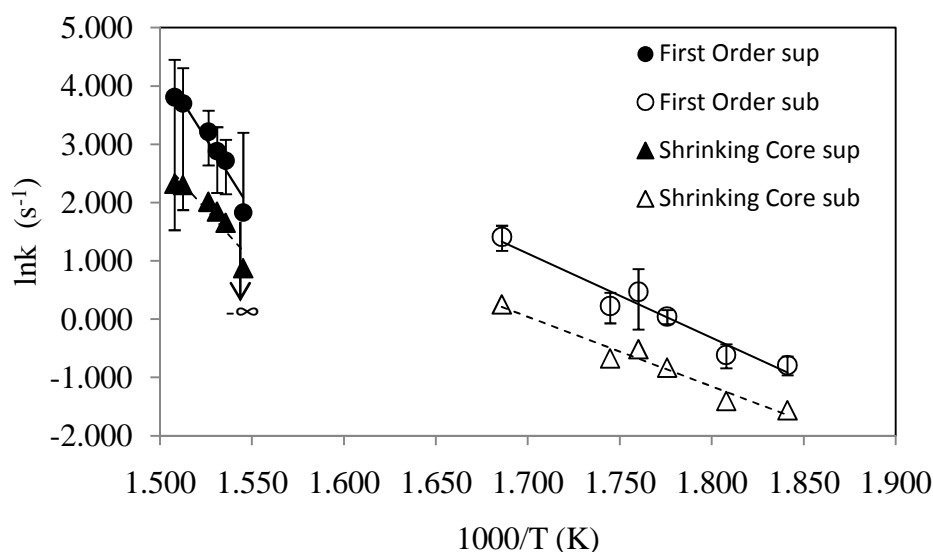
Figure 39. First Order Model: Separated Arrhenius plot for the conversion of crystalline cellulose in subcritical and supercritical water with conversion plot of cellulose reaction in subcritical water being forced through the origin
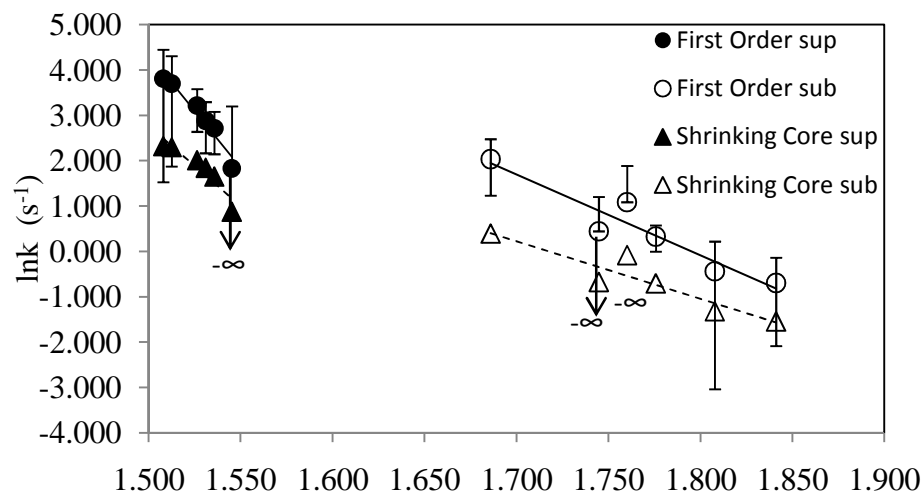
Figure 40. First Order Model: Separated Arrhenius plot for the conversion of crystalline cellulose in subcritical and supercritical water without allowing the conversion plot of cellulose reaction in subcritical water not being forced through the origin
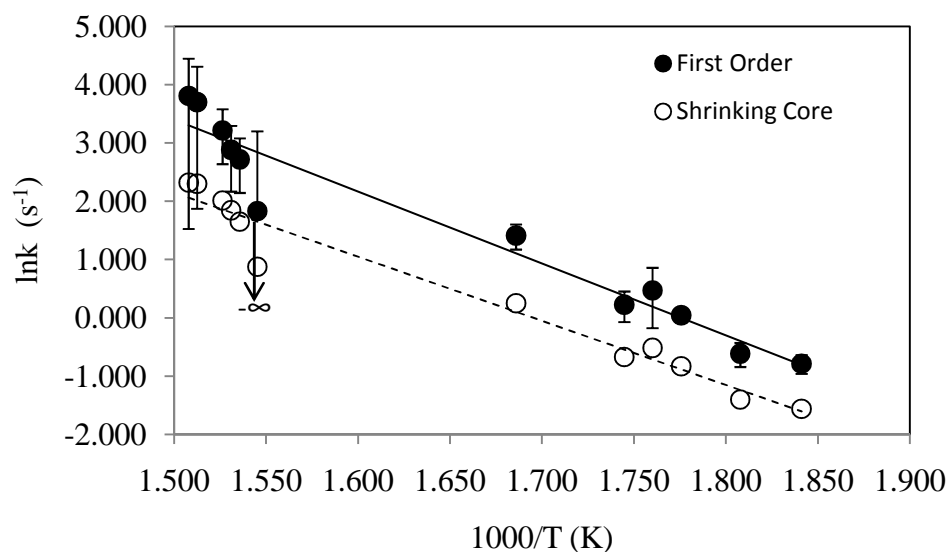
Figure 41.First Order Model: Combined Arrhenius plot for the conversion of crystalline cellulose in subcritical and supercritical water with conversion plot of cellulose reaction in subcritical being forced through the origin
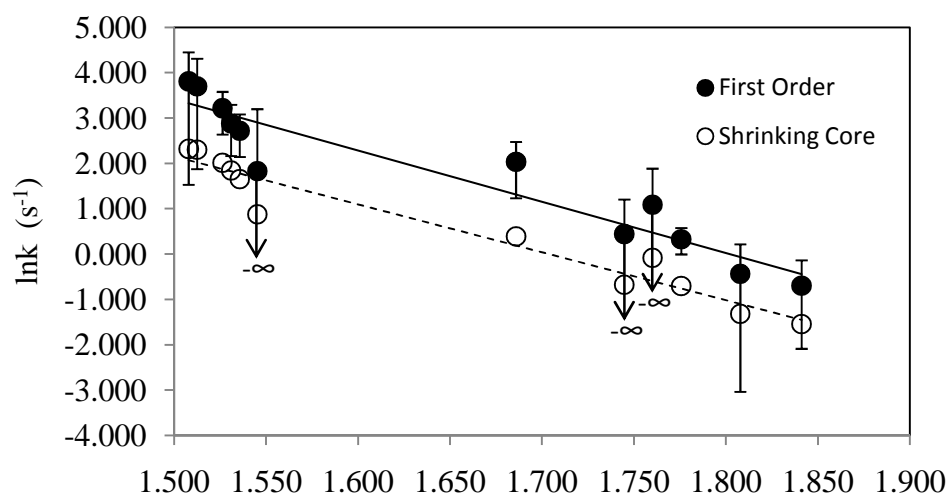
Figure 42. First Order Model: Combined Arrhenius plot for the conversion of crystalline cellulose in subcritical and supercritical water without allowing the conversion plot of cellulose reaction in subcritical not being forced through the origin

4.5 Summary of Experiments

In this chapter, a kinetics analysis describing the reactive behavior of cellulosic biomass in a hydrothermal microreactor has been discussed. The most important conclusions from the various experiments conducted can be summarized as the following:

1. The hydrolysis of crystalline cellulose in subcritical water is best explained by the low solubility level of cellulose in subcritical water resulting in heterogeneous reaction. The hydrolysis is surface based and its kinetics is modeled after the shrinking core or grain model. The solubilization or solvation effect of subcritical water on crystalline cellulose increases as the subcritical temperature increases. Kinetic parameters for the overall conversion of crystalline cellulose include the activation energy and the pre-

exponential factor and were evaluated respectively as 99 ± 29 kJ mol^{-1} and $10^{8.9\pm2.7}$ s^{-1}.

2. Dilute solution viscometry analysis was conducted to evaluate the DP of cellulose as received and cellulose residue obtained from hydrolysis. As the subcritical temperature increases at similar residence time, a decreasing trend of the DP of the cellulose chain is observed. The degree of polymerization (DP) is observed to drastically reduce from the initial DP of 228 to as low as 7.

3. Hydrolysis of cellulose in subcritical water was investigated. A first order bond concentration rate equation was employed in assessing the hydrolysis. The activation energy and the pre-exponential factor obtained for the hydrolysis of the glycosidic bonds evaluated from DP_v(s) obtained via DSV and SEC are 110 ± 89 kJ/mol, $10^{10\pm4.7}$ s^{-1} and 102 ± 35 kJ/mol, $10^{9.5\pm1.8}$ s^{-1}.

4. Conversion of crystalline cellulose in supercritical water proceeds in a two-steps reaction. In supercritical water, the reaction proceeds very fast and the liquefaction is so drastic that it gives little or no room for unreacted cellulose to survive after reaction. Maximum conversion of 89.5 % was obtained at supercritical temperature of 390 °C and residence time of 0.154 s. Minimum conversion of 36.8 % was obtained at supercritical temperature of 374 °C and residence time of 0.142 s. At supercritical conditions, the kinetic parameters for the conversion of crystalline cellulose in the microreactor were experimentally determined. Activation energy and pre-exponential factor obtained for the first order cellulose conversion in supercritical water are 290 ± 160 kJ mol^{-1} and $10^{24\pm13}$ s^{-1} respectively.

5. Arrhenius trend obtained based on shrinking core model from this study and Sasaki et al are quite similar in the supercritical region using rate plots going through the origin. While the trends for the two separate studies appear to

closely follow each other in the supercritical region, a clear difference in their trends was observed in the subcritical region. The trends for the first order and shrinking core models appear to parallel each other in both critical regions with lower k-values for the shrinking core model.

CHAPTER 5. INVESTIGATING YIELD OF WATER SOLUBLE HYDROLYSATE IN HYDROTHERMAL MEDIA

Previous studies showed a better monosaccharide yield from cellulose hydrolysis in subcritical water [14, 50] than in supercritical water. This trend is caused by the relatively higher hydrolysis rate of crystalline cellulose compared to the decomposition rate of the hydrolysate in subcritical water. But in supercritical water, the hydrolysis rate proceeds at a slower pace than the decomposition rate. This understanding is considered helpful in the design of a process path that can potentially improve the yield of fermentable sugars from crystalline cellulose. The process path entails setting up a reaction sequence intended to first dissolve cellulose and subsequently hydrolyze the dissolved cellulose in subcritical water.

Since dissolving cellulose is difficult, dissolved starch will be use as a surrogate for cellulose in the hydrolysis reaction in subcritical water. The rationale behind this approach is seen from the observation made from one of Taiying Zhang's works[14] (Figure 30) that hydrolysis of maltosaccharides and cellosaccharides in subcritical water are similar. Dissolved starch, at subcritical conditions of water, will be hydrolyzed within the reaction volume of the microreactor. The water soluble product (hydrolysate) obtained from the reaction will be analyzed with high performance liquid chromatography (HPLC).

Decoupling the dissolution of cellulose from its hydrolysis could be approached by dissolving cellulose under a very short time (0.01-0.2 s) in supercritical water and afterward, hydrolyze the dissolved cellulose in subcritical water at a relatively longer residence time. Before coming up with the idea of decoupling the reaction, the

conventional way has always been to dissolve and hydrolyze crystalline cellulose within the same hydrothermal reactor while allowing the reaction conditions to change from subcritical to supercritical phase. The notion of sequencing the two phases, subcritical and supercritical, per experimental degradation is similar to the study conducted by Ehara and Saka[11] on phase-separating the reaction media to improve yield and selectivity of target products.

Another approach is in-situ pretreatment of crystalline cellulose in an ionic liquid or non-derivatizing solvent.[71-73] As it has been discussed extensively,[74-76] ionic liquid will deconstruct the crystallinity of the cellulose to a far less crystalline structure. Dissolved cellulose in the ionic liquid will subsequentlybe precipitated at the introduction of an anti-solvent (water or aliphatic alcohol) via preferential solute-displacement mechanism.[74] Non-volatile ionic liquid is afterward recovered by stripping off the anti-solvent via flash distillation. Thereafter, decrystallized cellulose will be hydrolyzed in the hydrothermal (subcritical) reactor.

5.1 Experimental Methods

The experimental methods present a detailed description of the experimental setup and the processing steps, sample product analysis, and data analysis methods.

5.1.1 Experimental Setup and the Processing Steps

Hydrolysis of starch and cellulose were conducted both in the microreactor and the tubular reactor. Figure 14 depicts the experimental setup for the reaction of crystalline cellulose and dissolved starch in the microreactor. The same setup was used for the polysaccharide reactions in the tubular reactor but the only difference is the point at

which feedstock is fed into the process stream. With the microreactor, the feedstock is fed into the reactor positioned midway along the process flow path while for the tubular reactor, the feedstock solution is fed at the starting point of the process stream. A schematic chart of the process for the microreactor can be seen in Figure 15, while Figures 43 is a schematic diagram of the tubular reactor.
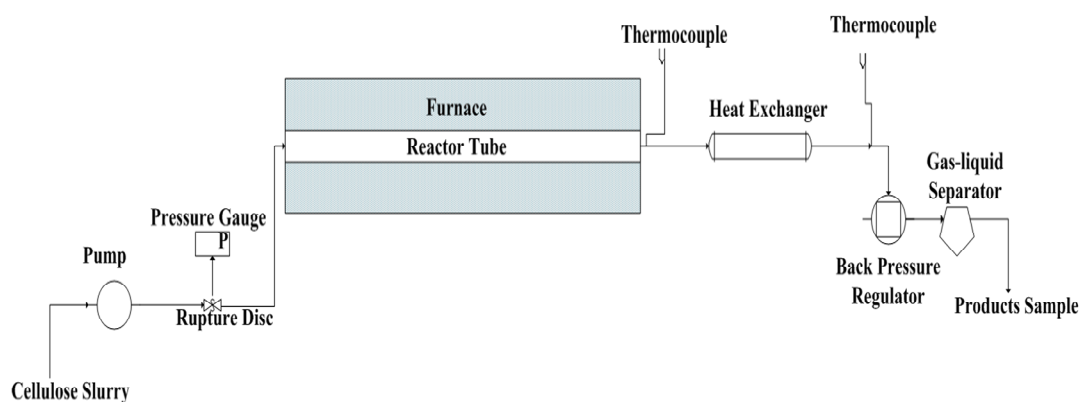
Figure 43. Schematic flow process for cellulose hydrolysis in hydrothermal tubular reactor

For microreactor experiments, deionized water obtained from a nanopure Infinity water purification system was fed into a tube enclosed within a tube furnace (Thermolyne79400) by Lab Alliance series II pump at flow rates ranging from 5 ml/min to 10 ml/min. Subsequently, the deionized water was heated to subcritical temperatures ranging from 280°C to 340°C for separate experimental runs. The pressure of the fluid was about 5,000 psig was set and control by a 15,000 psig capacity Tescom back pressure regulator downstream. The pressure gauge displays the operating pressure. Just after the pressure gauge is a rupture disc. This safety device, unlike the relief valve which opens when the maximum pressure is exceeded, is ruptured when the operating pressure

exceeds its limit. In this experimental setup, the rupture disc can support a maximum pressure of 9000 psi, so therefore, any pressure beyond this limit can lead to rupture of the disc.

The subcritical water exited into the microreactor insulated with fiber glass and served as both hydrolytic agent and the reaction medium for the 2 wt % polysaccharide solutions entering the upper inlet port of the microreactor just at the outlet of the tube furnace. The temperature the furnace can support range from room temperature to 1200 °C. The cellulose slurry/dissolved starch solutions was mixed with the subcritical water at equal volumetric flow rate, thereby diluting the cellulose slurry/dissolved starch concentration to 1 wt%. The reaction was quenched by the deionized water from the other upper inlet port of the microreactor and also by the shell and tube heat exchanger just at the outlet end of the microreactor. With the rapid heating and quick quenching of the polysaccharides reaction in the microreactor, the reacting volume within the microreactor is estimated to be 0.17ml. The schematic flow detail in the microreactor can be seen in Figure 16 of chapter 4.

For the tubular reactor, cellulose/starch slurry (2 wt %) solution was fed into the hydrothermal tubular reactor at temperatures ranging from 200 °C- 400 °C and pressure of about 5000 psig. The reactions were conducted at flow rates of 5 ml/min and 10 ml/min and were quenched by the heat exchanger downstream of the reactor. The reacting volume for the tubular reactor is 2.13 ml, while residence times due to temperature range span between 12 – 23 s for 5 ml/min and 6 – 11 s for 10 ml/min. The product samples which flow via the back-pressure regulator are collected downstream in the gas-liquid separator. The water soluble part of the hydrolysate was analyzed with

HPLC. The insoluble part obtained from the unreacted cellulose was either centrifuged or filtered and subsequently dried for further analysis.

5.1.2 Sample Product Analysis Method

5.1.2.1 Materials.

Cellulose suspensions and starch solutions in deionized water are the reactant mixture used in this section of the research project. The chemical compounds used for the experiments and the standard solutions for calibration curves were all obtained from Sigma-Aldrich and they are highlighted as follows: crystalline cellulose (sigmacell type 20), cellobiose (>98 %), maltose monohydrate (>98 %), glucose (>99.5 %), fructose (>98 %), 5-(hydroxymethyl)-2-furfural, and furfural .

5.1.2.2 Aqueous products (water soluble hydrolysate).

Water soluble hydrolysate was analyzed by ionic HPLC comprising: pump (LC-10ADvp), refractive index detector (RID-10A), SSI 505 LC column oven, Aminex HPX-87H & HPX-42A columns (300 x 7.8 mm), mobile phase (0.1 mmol/L H_2SO_4 & Water). A large percentage of the samples was analyzed with HPLC using auto sampler injection, but for the latter part of the project manual injection was used. The mobile phase flow rate was of 0.6 ml/min and the column oven temperature was 50 °C. Hydrolysate quantification and identification were obtained based on hydrolysate standard calibration and characteristics retention time respectively.

5.1.2.3 Water Insoluble Hydrolysate.

This is the solid portion of the product samples obtained from the hydrolysis reaction. These products were analyzed gravimetrically by filtering the hydrolysate via Stericup® 0.22 μm Millipore GV PVDF membrane. The solid residues left after filtration were dried at room temperature until the weight of the solid products remained constant. This method was used to find the mass of unreacted cellulose per volume of the product mixture solely for evaluating the conversion of crystalline cellulose under hydrothermal conditions.

5.1.3 Data Analysis Method

In the hydrothermal (micro and tubular) reactor, the average time the reactants spend in the reacting volume is refers to as the residence time (τ) and can be expressed mathematically as:

$$\tau = \rho_c V / \rho_r F_r \tag{47}$$

where ρ_c is the density of the reactant mixture at reactor conditions, V is the reacting volume of the hydrothermal reactor, and ρ_r is the density of the reactant mixture at room temperature. F_r is the volumetric flow rate of the reactant mixture being fed into the reactor. Other descriptive data analysis variables include conversion and yield. Conversion is denoted symbolically as X and is define as the amount of solute (in solution/suspension) reacted with respect to the initial amount. Yield is the amount of the product formed with respect to the initial amount of the reactant fed. The mathematical representation of both the conversion and yield are expressed as Equations 48 and 49 in chapter 4.

Products in this case could be glucose, cellobiose, maltose, fructose, 5-(hydroxymethyl)-2-furfural (HMF), furfural, and organic acids while reactants could be either cellulose suspension or starch solution. Cellulose and starch are polymers of glucose, and obtaining their concentration in mole/litre may prompt an initial line of thought of finding the DP to obtain the molecular weight so as to obtain the moles of the polymer. The approach is logical but not necessary because these polysaccharides are polymer of glucose and concentration can be based on the mass of glucose units in the polysaccharides. Approximating the density of the dilute aqueous solution at room conditions to be 1000g/L, the composition (mass ratio) of solute in terms of wt% was expressed in Equation 50.

5.2 Yield of Water Soluble Hydrolysates in the Hydrothermal Reactor

Hydrolysis of starch and crystalline cellulose were conducted in both tubular reactor and microreactor at subcritical and supercritical conditions of water. The yields of water soluble hydrolysates such as glucose, cellobiose, and furfural vary as the temperature and residence times are altered. The thing to look out for in this section is the residence time and the temperature at which optimum yield of fermentable sugars are attained. The reason is because some of the fermentable sugars formed during reaction degrade to other compounds that perhaps could serve as inhibitors in the fermentation stage of biofuel production. Thus, the yield of water soluble hydrolysates in both the tubular reactor and the microreactor will be investigated. Finally, a detailed comparison of the water soluble hydrolysate yields obtained at subcritical conditions for dissolved starch, a surrogate for the dissolved cellulose, will be compared with yields obtained

from the hydrolysis of crystalline cellulose in subcritical and supercritical water. This section of the project is largely driven by hypothesis No. 2 in Chapter 3 which propounds that: glucose formation from dissolved cellulose is better optimized in subcritical water than in supercritical water.

5.2.1 Yield of Water Soluble Hydrolysates in the Tubular Reactor

Hydrolysis of cellulose and starch in the hydrothermal tubular reactor results in the formation of water soluble and insoluble hydrolysates. Unreacted cellulose primarily constitutes the insoluble hydrolysates while soluble hydrolysates for both starch and cellulose include fermentable sugars and hydrolysate decomposition products. Cellulose slurry solution or starch solution were fed to the process unit, and products resulting from the reaction were collected downstream. The sampled hydrolysate products were analyzed with HPLC and the yield of the water soluble hydrolysates were evaluated.

5.2.1.1 Experimental Description

Figure 35 shows a schematic flow process of cellulose hydrolysis in the tubular reactor. Cellulose slurry (2 wt%) was fed into the hydrothermal tubular reactor at temperatures used ranged from 200 °C to 400 °C. The reactor pressure of about 5000 psig. The reactions were conducted at flow rates of 5 ml/min and 10 ml/min and were quenched by the heat exchanger after exiting the reactor. The sample products which flow via the back-pressure regulator were collected downstream in the gas-liquid separator.

5.2.1.2 Sample Analysis

Water soluble hydrolysates collected at the different subcritical temperatures and at different residence times were analyzed with HPLC. Hydrolysate quantification was based on hydrolysate standard calibration and species identification was determined by characteristic retention time. The quantification was established based on the peak areas of HPLC compared against a known standard.

5.2.1.3 Results and Discussions

Figure 44 depicts the fractional yield of water soluble hydrolysate obtained in the hydrothermal tubular reactor at a flow rate of 10 ml/min. Crystalline cellulose was reacted at subcritical and supercritical conditions of water, and yields of water soluble hydrolysates at temperature ranging from 300 °C to 400 °C were obtained. Glucose yield, showed a maximum of 15 % at the lowest subcritical temperature of 300 °C, and decreased appreciably as temperatures increased. The same trend was observed with cellobiose and fructose which peak at 2.5 % and 7 % yield and subsequently decreases as reaction temperature increased. While experiencing a drastic decrease in the percent yield of sugars, a net formation of 5-(hydroxymethyl)-2-furfural (HMF) and furfural were observed. Yield of HMF and furfural which peak at about 6.7 % and 8.6 % and at subcritical temperatures of 310 °C and 330 °C, respectively decrease subsequently as temperatures increase from subcritical to supercritical. However, the decomposition of HMF and furfural is not as pronounced as what was observed with the decomposition of monosaccharides and cellobiose as reaction temperature increased. The significant reduction in the quantity of sugars is strongly believed to have contributed relatively to a considerable amount of the furanic compounds at high temperature.
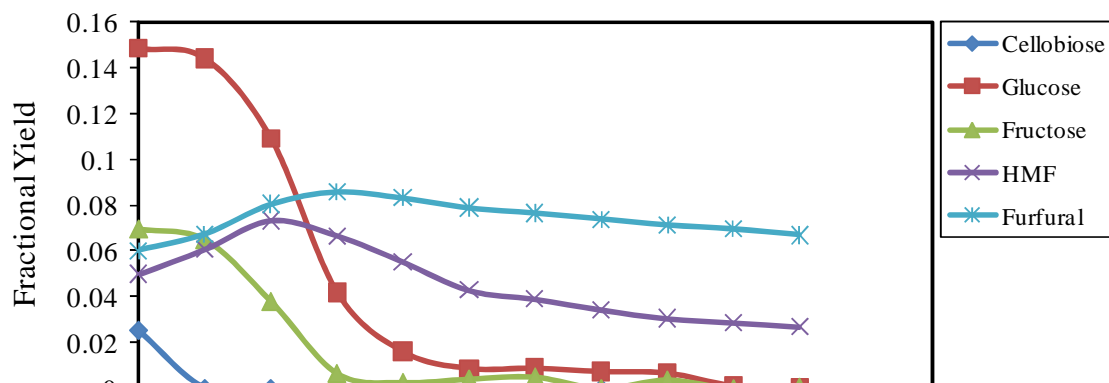
Figure 44. Fractional yield of water soluble hydrolysates in hydrothermal tubular reactor at 10 ml/min

Figures 45 and 46 portray fractional yield of water soluble hydrolysates obtained from starch and cellulose in the hydrothermal tubular reactor at 5 ml/min. Figure 45 reflects an increase in the yield of glucose and fructose as the exit temperature rises from 200 °C up until 250 °C, where yield for both monosaccharide peak at about 35% and 5.3% respectively. Monosaccharide yield decreases after the reactor exit temperature increases from subcritical temperature to supercritical temperature. While similar trend, though at a relatively lower yield when compared with glucose, was observed with maltose. Maximum yield for maltose was obtained at 7.6% and at subcritical temperature of 230 °C. Maltose yield subsequently decreased as temperature increased. However, the temperature at which maximum glucose yield was obtained is 20 °C lagging the temperature at which yield of maltose is at the maximum. This trend maybe indicative of the fact that some glucose was formed as result of the hydrolysis of maltose.
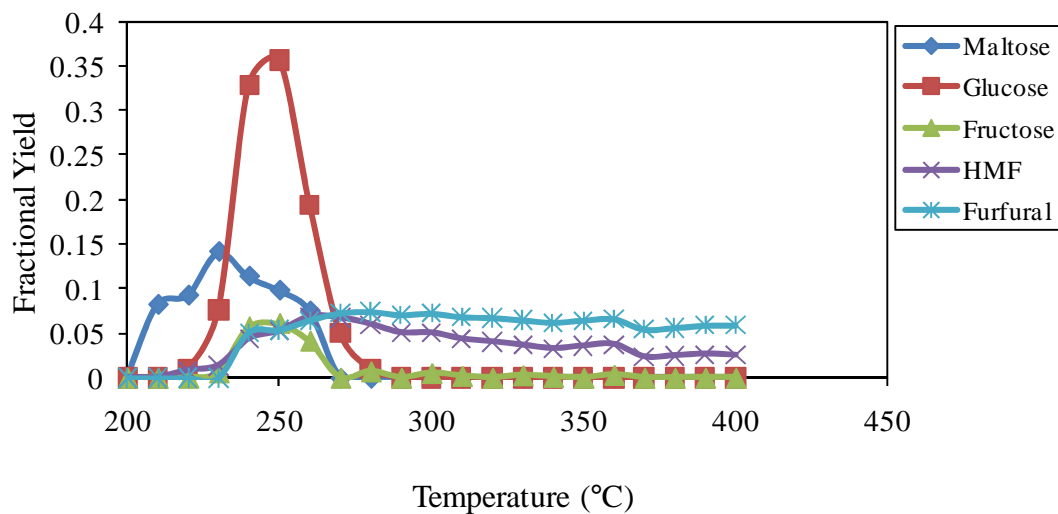
Figure 45. Fractional yield of water soluble hydrolysates obtained from starch in a hydrothermal tubular reactor at 5ml/min
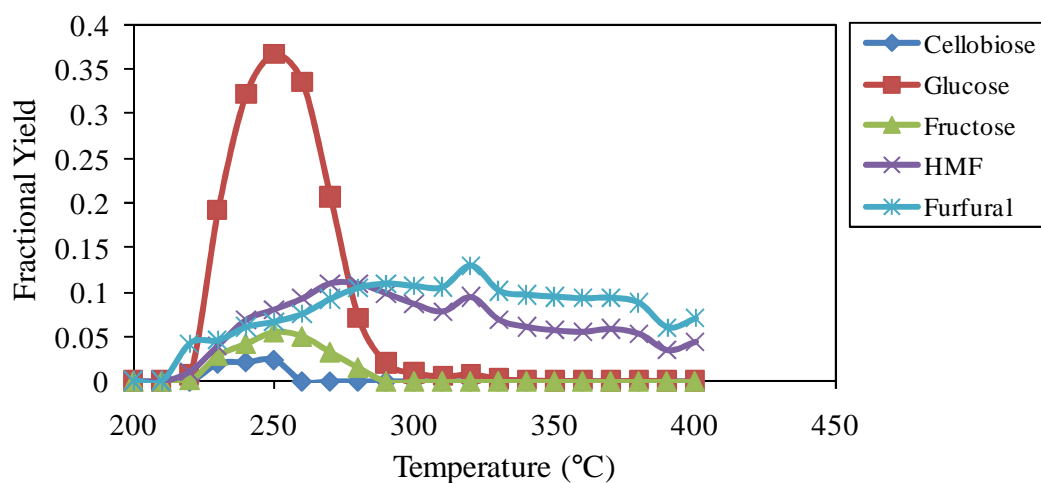
Figure 46.Fractional yield of water soluble hydrolysates obtained from cellulose in a hydrothermal tubular reactor at 5ml/min

While observing drastic decrease in the monosaccharide and disaccharide yield in the upper subcritical temperature and supercritical region, a net increase in the formation of

HMF and furfural was observed. Maximum HMF and furfural yield was observed at 7.2% and at 270 °C and subsequently remain constant for furfural as temperature increased while some of the HMF decomposes further perhaps to furfural and other compounds.

Yields evaluated for all the soluble hydrolysates portray on Figure 45, follow similar trend as delineated in Figure 44 with just two exceptions and they are 1) the temperature at which each hydrolysate yield peaks and 2) the percent yield. Both Glucose and fructose yields increase as the reactor exit temperature increases from 200 °C and peak at subcritical temperature of 250 °C and at percent yields of 36.7% and 6.7% respectively. Yields for the glucose and fructose (monosaccharides isomers) decreased after the reactor exit subcritical temperature increased past the 250 °C and approach temperature in the supercritical region. Cellobiose yields do follow similar trend with maximum percent yield of 2.9% obtained at subcritical temperature of 230 °C. As yields for simple sugars decreased with increasing temperature, a net formation of HMF and furfural were observed. The maximum yield obtained for HMF and furfural and at subcritical temperature of 320 °C are 9.4% and 12.9%. There is a substantial presence of HMF and furfural relative to simple sugars at supercritical condition of water. This trend is obviously connected to excessive net decomposition of the monosaccharide at high temperature to HMF, furfural and other compound such as organic acids.

5.2.1.4 Conclusions

Water soluble hydrolysates yield obtained while reacting crystalline cellulose and starch at 5 ml/min in the hydrothermal tubular reactor follow similar trend with the 10 ml/min flow rates. The only two features distinguishing each trend are the maximum

yields obtained for each hydrolysate and the temperature at which these maximum yields were obtained. For the 10 ml/min flow rates, more simple sugars were formed at subcritical temperature than at supercritical temperature. At high temperature, more of the simple sugars decompose into HMF, furfural and other compounds. An aggregated sum of maximum glucose (15%) and fructose (7%) yield obtained at 10 ml/min is 22%. However, at 5 ml/min, it is interesting to observe maximum glucose yield from starch (35% glucose) and cellulose (36.7% glucose) occurring at the same temperature and virtually exhibiting same maximum yields. Similar trend was observed for the temperature at which fructose, cellobiose and maltose peaked though with different yields. But with furanic compounds, the temperatures at which HMF and furfural peaked for the 5 ml/min flow rate are totally different. An aggregated sum of the maximum glucose and fructose yield obtained from the hydrothermolytic conversion of crystalline cellulose and starch at 5 ml/min are 43.4% and 40.3% respectively.

5.2.2. Hydrolysates Yield from Crystalline Cellulose Hydrolysis in the Microreactor at Subcritical Condition of water

Hydrolysis of cellulose in the hydrothermal microreactor results in the formation of water soluble and insoluble hydrolysates. Samples obtained from the reaction consist of unreacted cellulose and water soluble hydrolysates. Unreacted cellulose primarily constitutes the insoluble hydrolysates while soluble hydrolysates include fermentable sugars and hydrolysate decomposition products. Cellulose suspensions were fed to the process unit, and products resulting from the reaction were collected downstream. The

sampled hydrolysate products were analyzed with HPLC and the yield of the water soluble hydrolysates were evaluated.

5.2.2.1 Experimental Description

Cellulose suspension was fed into a tube enclosed within the tube furnace at flow rates ranging of 5 ml/min and 10 ml/min. Subsequently, the deionized water was heated to subcritical temperatures ranging from 280°C to 340°C. The pressure of the fluid was about 5000 psig was set and controlled by a back pressure regulator downstream. The subcritical water exit into the glass fiber insulated microreactor serving both as hydrolytic agents and reaction medium for the 2 wt % cellulose suspension entering from the upper inlet port of the reactor just at the tube furnace outlet. The 2 wt% cellulose suspension was mixed with the subcritical water at equal volumetric flow rate, thereby diluting it to 1 wt%. The reaction was quenched by the deionized water entering the other upper inlet port of the microreactor closer to the heat exchanger. The samples were collected in the gas-liquid separator and were analyzed.

5.2.2.2 Sample Analysis

Water soluble hydrolysates collected at the different subcritical temperatures and at different residence times were analyzed with HPLC. Hydrolysate quantification was based on hydrolysate standard calibration and species identification was determined by characteristic retention time. The quantification was established based on the peak areas of HPLC compared against a known standard.

5.2.2.3 Results and Discussions

Figures 47 – 51, depict yield of water soluble hydrolysate obtained along side the cellulose residue evaluated for conversion. Figure 47 shows apparently low yield in water soluble hydrolysate production at 280 °C. Fractional yields for each hydrolysate increases with residence time with maximum glucose yield of 2.2% at 0.83 s , while at the same residence time, fructose and cellobiose yield peak at about 2.0% and 4.4%. Figure 48 unfolds a slight increase in water soluble hydrolysate yield at 290 °C than at 280 °C. Maximum yields of glucose and fructose obtained under this condition and at residence time of 0.61 s are 3.1% and 1.9% respectively. Cellobiose displays better yield (with maximum yield of 5.2% at the same residence time) than the yield of the monosaccharides.

Figure 47. Fractional yield of water soluble hydrolysates obtained from cellulose at 280 °C in microreactor

Figure 48.Fractional yield of water soluble hydrolysates obtained from cellulose at 290 °C in microreactor

Figure 49. Fractional yield of water soluble hydrolysates obtained from cellulose at 300 °C in microreactor

Figure 50. Fractional yield of water soluble hydrolysates obtained from cellulose at 320 °C in microreactor
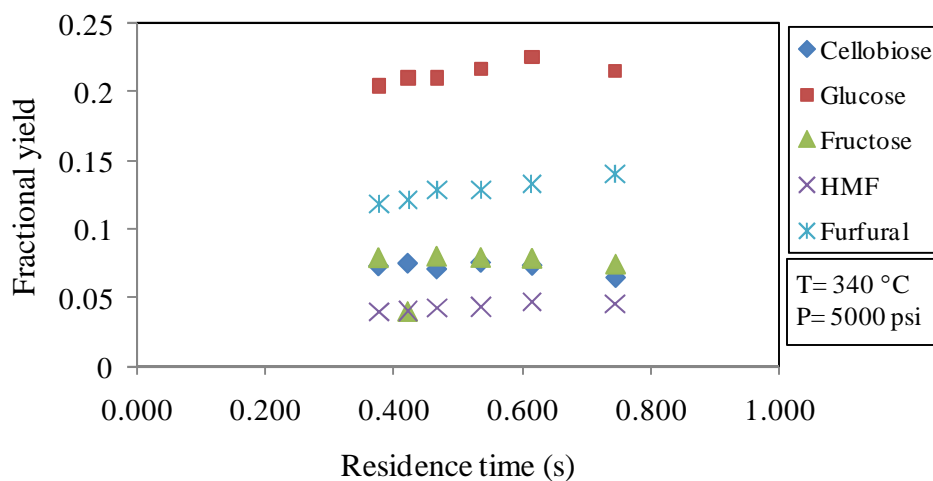
Figure 51. Fractional yield of water soluble hydrolysates obtained from cellulose at 340 °C in microreactor

However, formation of hydroxymethylfurfural (5-HMF), one of glucose decomposition products, started becoming apparent at 300 °C, while at 320 °C and 340 °C, a relatively higher HMF yields were observed. In Figure 49, yield of water soluble

hydrolysates obtained at 300 °C increased with residence times. More monosaccharide are generated at this temperature with almost 10% maximum glucose yield, 4% maximum fructose and HMF yields while cellobiose has a better yield of 11.1% . Figure 50 reflects at 320 °C an increase in glucose yield with residence time, while cellobiose decreased as residence time increased. It is most likely that some of the cellobiose are further hydrolyzed to form glucose. Amount of fructose and HMF formed remain relatively constant across the residence time. This contrasting variation of cellobiose and glucose yields with residence time, explains why their respective maximum yields of about 14.4% and 19% occur at the lowest and highest residence time. Figure 51, displays a steady but not apparent increasing trend in hydrolysates yield with residence time at 340 °C. This trend includes cellobiose yield which decreases as residence time increases. Reduction in the quantity of cellobiose, as stated earlier, is due to further hydrolysis to glucose and other simpler compounds. Quantity of furfural formed, which though becomes only measurable under this reaction condition, exceed the respective yields of HMF, fructose, and cellobiose. Overall maximum glucose yield of 22.5% was obtained at 340 °C which exceeded yields obtained at any of the operating temperature considered in this experiment. As temperatures increased within the subcritical phase (280 °C – 340 °C) more glucose are formed possibly from hydrolysis of soluble oligosaccharide such as cellobiose, cellotriose, and heterogeneous hydrolysis of insoluble cellulose.

5.2.2.4 Conclusions

Hydrolysis of crystalline cellulose was conducted in a hydrothermal microreactor at subcritical temperature ranging from 280 °C to 340 °C and at 5000 psig. Sample

contain water soluble hydrolysates were obtained and subsequently analyzed with HPLC. Water soluble hydrolysates analyzed consist of glucose, fructose, cellobiose, HMF, and furfural. More cellobiose yield relative to the yield of other hydrolysates were obtained at subcritical temperature ranging from 280 °C to 300 °C. But at 320 °C, the yield which is more than what was obtained at 280 °C to 300 °C, is relatively less than the glucose yield and decreased as the residence time increased. At 340 °C, cellobiose yields are almost equal with the yield obtained for fructose. Glucose yield at all subcritical temperature in question increased with residence times. In this experiment, maximum glucose yield of 22.5% was obtained at 340 °C and at residence time of 0.615 s, while in the case of fructose, maximum yield of 8.03% was obtained at 340 °C and at 0.468 s. The maximum aggregate sum of the monosaccharide yield which is 30.4% was obtained at 340 °C and at residence time of 0.615 s. Formation of HMF and furfural began formation at 300 °C with maximum HMF yield of 4.6% occurring at residence time of 0.615 s and at subcritical temperature of 340 °C. While maximum furfural yield of 14% was obtained at 340 °C and at 0.745 s. The maximum of the sum of the aggregate yields of the two furanic compounds at 340 °C and residence time of 0.745s is 18.4 %.

5.2.3. Hydrolysates Yield from Dissolved Starch Hydrolysis in the Microreactor at Subcritical Condition of Water

Hydrolysis of dissolved starch in the hydrothermal microreactor results in the formation of water soluble hydrolysates. These soluble hydrolysates from starch include fermentable sugars and hydrolysate decomposition products. Dissolved solution of starch was fed to the process unit, and products resulting from the reaction were collected

downstream. The sampled hydrolysate products were analyzed with HPLC and the yield of the water soluble hydrolysates obtained were evaluated.

5.2.3.1 Experimental Description

Dissolved starch solution was fed into a tube enclosed within the tube furnace at flow rates ranging of 5 ml/min and 10 ml/min. Subsequently, the deionized water was heated to subcritical temperatures ranging from 280°C to 340°C. The pressure of the fluid was about 5000 psig was set and controlled by a back pressure regulator downstream. The subcritical water exit into the glass fiber insulated microreactor serving both as hydrolytic agents and reaction medium for the 2 wt % starch solution entering from the upper inlet port of the reactor just at the tube furnace outlet. The starch solution was mixed with the subcritical water at equal volumetric flow rate, thereby diluting it to 1 wt%. The reaction was quenched by the deionized water entering the other upper inlet port of the microreactor closer to the heat exchanger. The samples were collected in the gas-liquid separator and were analyzed.

5.2.3.2 Sample Analysis

Water soluble hydrolysates collected at the different subcritical temperatures and at different residence times were analyzed with HPLC. Hydrolysate quantification was based on hydrolysate standard calibration and species identification was determined by characteristic retention time. The quantification was established based on the peak areas of HPLC compared against a known standard.

5.2.3.3 Results and Discussions

Figures 52 – 57 showed yields of water soluble hydrolysates obtained from the hydrolysis of dissolved starch in subcritical water. Maltose, as shown in Figure 52, displays a better yield at 270 °C than the yield obtained for glucose and fructose. Percent yields for each of the hydrolysates.i.e. maltose, glucose, and fructose decreased within the residence time range of 0.45s and 0.57s, and subsequently increased as the residence time increased. Maximum percent yield for maltose, glucose and fructose which occurred at residence times of 0.847s are 3.1%, 1.04% and 0.4% respectively. Though the percent yield for each hydrolysate are significantly small but the plots showing the variation of their respective yields with residence time follow the same trend. This similarity in trend could be indicative of the fact that glucose was formed from the hydrolysis of maltose and not directly from starch. In otherword, maltose was formed from starch hydrolysis before hydrolyzing into glucose. As glucose is formed, simultaneously, is also getting isomerized into fructose. Figure 53 displays a better yield performance for the hydrolysate than the yield portrayed in Figure 52. Therefore, at 280 °C which is the reaction temperature depicted in Figure 53, hydrolysates yield increased with residence time with maximum percent yield of 9.6% for maltose, 5.5% for glucose and 3.6% for fructose, occuring at 0.804 s. A similar trend is observed with the variation of the percent yields with residence time for each of the hydrolysate. This observation further confimed a direct connection between the amount of glucose formed in the course of the reaction and the quantity of maltose generated from the hydrolysis of starch. Hydrolysates yield obtained at this reaction condition increased with the residence time. Worthy of note, at these two subcritical temperatures, 270 °C and 280 °C, is the rate of

formation of maltose and glucose with regard to their rate of disppearance. The fact that maltose has a better yield thus far, clearly shows that rate of hydrolyzing maltose to glucose is lower than the rate at which maltose is being formed from the hydrothermal conversion of starch. Also noted is the isomerization of glucose to fructose which occurs at a slower pace than fructose isomerizing back to glucose.
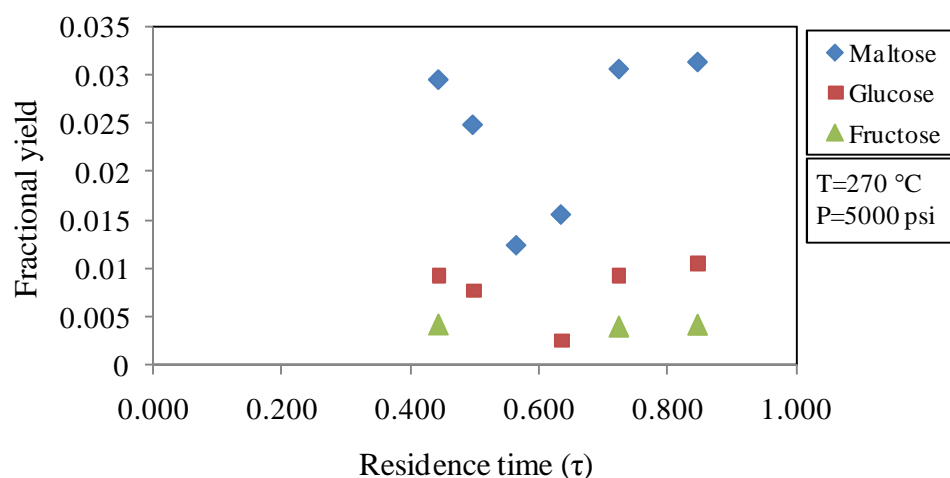
Figure 52.Fractional yield of water soluble hydrolysates obtained from starch at 270 °C in microreactor
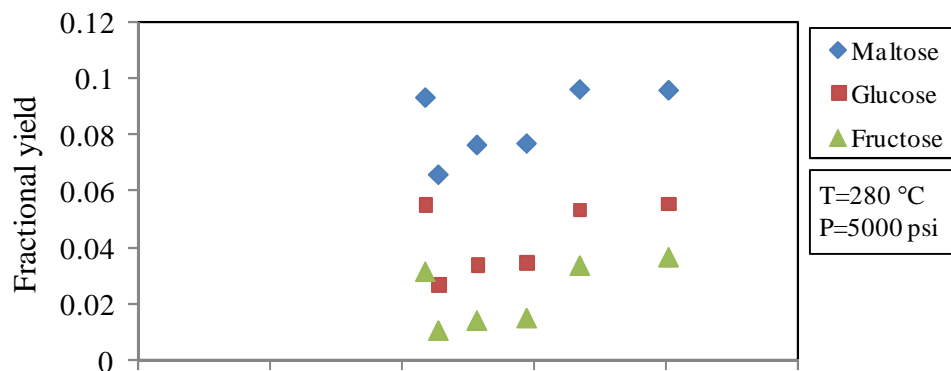
Figure 53. Fractional yield of water soluble hydrolysates obtained from starch at 280 °C in microreactor

The fractional yield as shown in Figure 54, displayed an improved yield as compare with the hydrolysates yield in Figures 52 and 53. At 290 °C, hydrolysates yield initially increase with residence times and subsequently decrease slightly after 0.505 s. Maximum percent yields obtained for maltose, glucose and fructose are 11.5%, 11.9% and 6.2% respectively and the residence times at which the optimum yields occurred are 0.505 s for the disaccharide and 0.563 s for the monosaccharides. In the two previous temperatures (270 °C and 280 °C), maltose yields are often significantly higher than glucose yields but at 290 °C, the yields appear very close. This strongly indicate that, as the temperature is increasing, the rate at which maltose hydrolyzes to glucose is increasing faster relative to the rate of its formation. Other reason could be that formation of glucose is not only limited to maltose hydrolysis but also from hydrolysis of some other oligomers formed during the reaction. Figure 55 unfolds a clear deviation from a better yield of maltose relative to other hydrolysate yields to a better yield of glucose. At

300 °C, HMF formation started becoming apparent and fractional yields of glucose and fructose including HMF are relatively constant over the residence times. However, maltose yields display some significant variation with residence time. In spite of the level of steadiness in the monosaccharide yield with residence times, maximum percent yield of 14.4%, 9.3%, and 1.5% respectively glucose, fructose, and HMF could still be identified at a residence time of 0.439s. Maximum percent yield of maltose which occurred at a residence time of 0.507 s is 10.9%. One thing to note in Figure 55 is that at 300 °C, yield of fructose is increasingly matching up to maltose yield, meaning that the rate of glucose-fructose isomerization which is often significantly slower than the fructose-glucose isomerization rate is occurring at a rate close in comparison with the net formation rate of maltose.
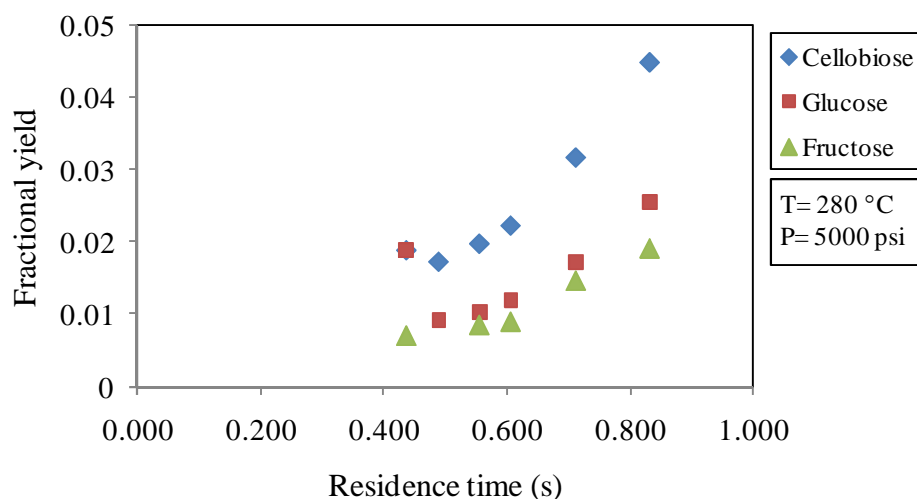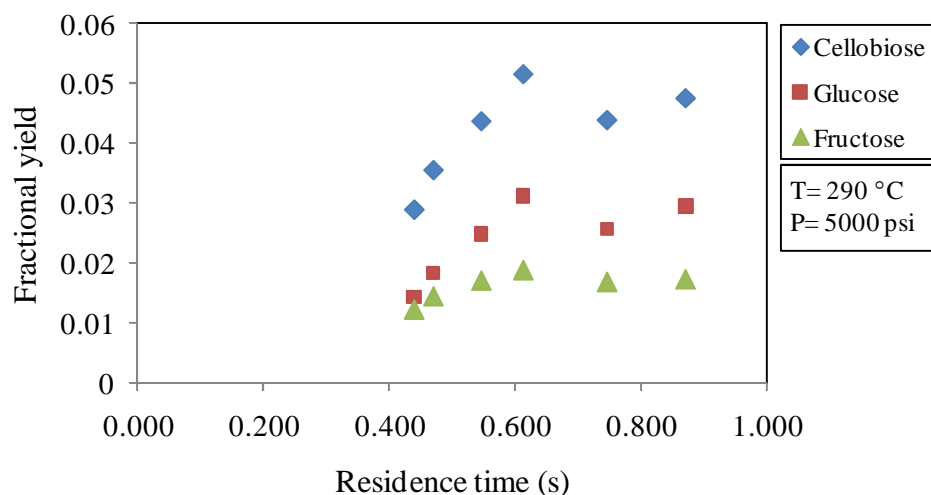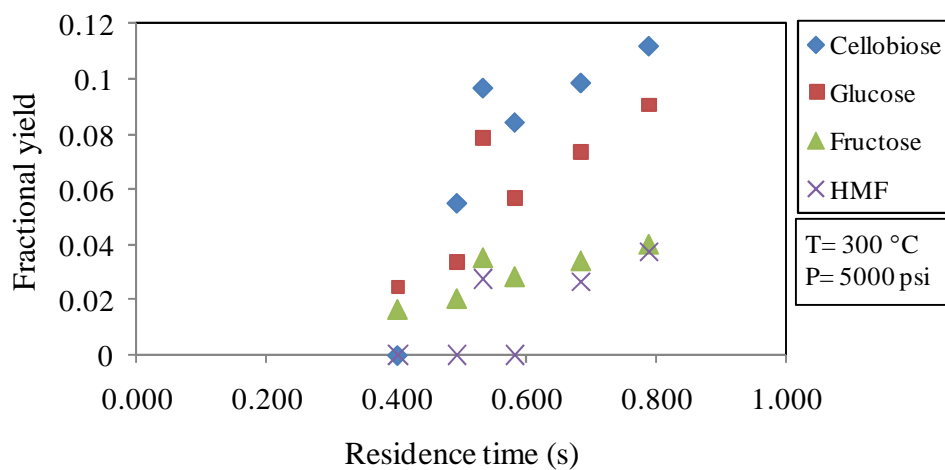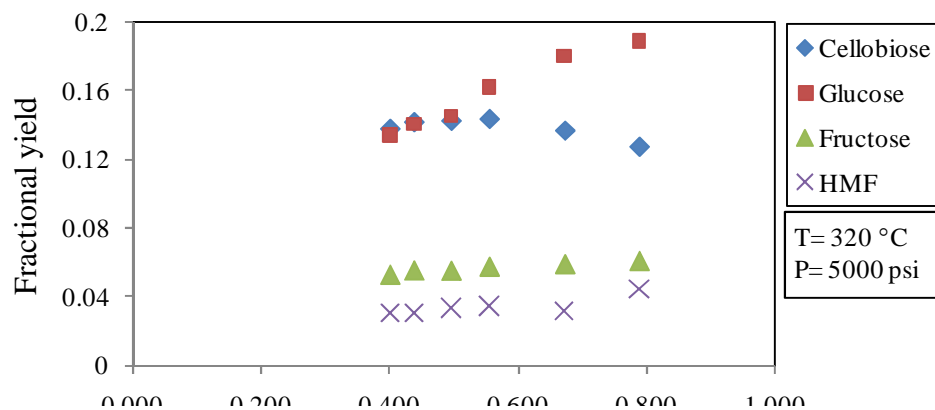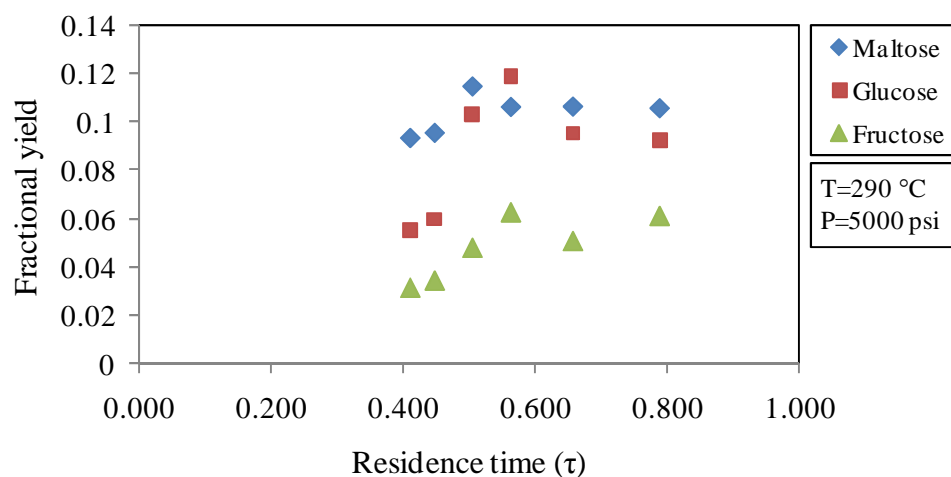

Figure 54.Fractional yield of water soluble hydrolysates obtained from starch at 290 °C in microreactor
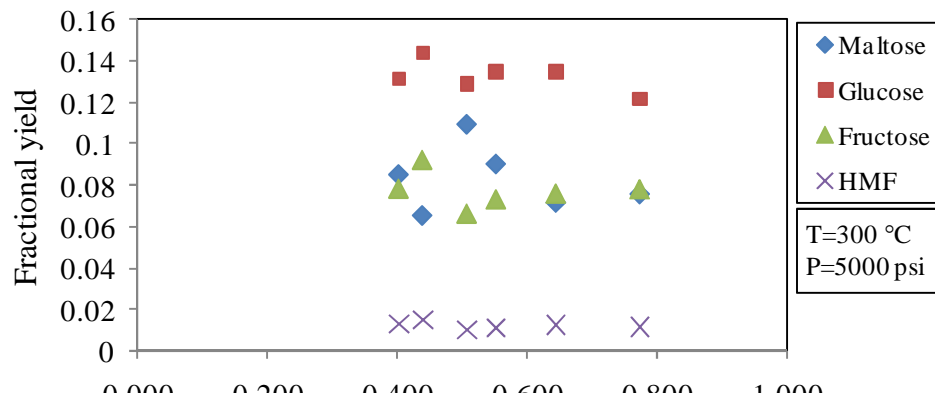
Figure 55.Fractional yield of water soluble hydrolysates obtained from starch at 300 °C in microreactor

Figure 56 depicts the plot of the hydrolysate yields with residence times at 320 °C. At residence time of 0.392s to 0.526s, glucose display better yield than the yields obtained for fructose and maltose but as the residence times increased, glucose and fructose yields equilibrate. These trends depicting the fractional yields of glucose and fructose with residence time reflect a decrease in the fractional yield of glucose with residence times until 0.526 s and subsequently remain constant. And with fructose yields, the reverse is the case but remain constant also after 0.526 s. However, fractional yields for maltose and HMF are constant over the residence times and their respective percent yields ranges from 6.3% to 7.4%, and 1.0% to 1.2 %. The equilibration of the fractional yield of glucose and fructose after 0.526 s tends to suggest that the rate of glucose to fructose isomerization and fructose to glucose isomerization is equal. Maximum percent yields of 13.7% and 12.5% were obtained at a residence time of 0.472 s for glucose and fructose respectively.

Figure 57 unveils the plots of the hydrolysate yields with residence times at 340 °C. A better and an improved yield was observed for fructose over the residence times

ranging from 0.370 s to 0.629 s but afterwards fructose yield decreases and equilibrates with the yield obtained for glucose. Invariably, yields of glucose increased with residence times but after 0.757 s it decreased. A more improved yield was seen with HMF over maltose from residence times ranging between 0.536 s to 0.948 s. The same reason cited earlier could be the cause of the equilibration of glucose yield with the yield obtained for fructose. Maximum yield obtained for fructose, glucose, HMF, and maltose are 13.4%, 10.3 %, 2.9% and 2.5 % respectively. While the residence times at which these respective percent yields were obtained are 0.629 s, 0.757 s, 0.757 s and 0.413 s.
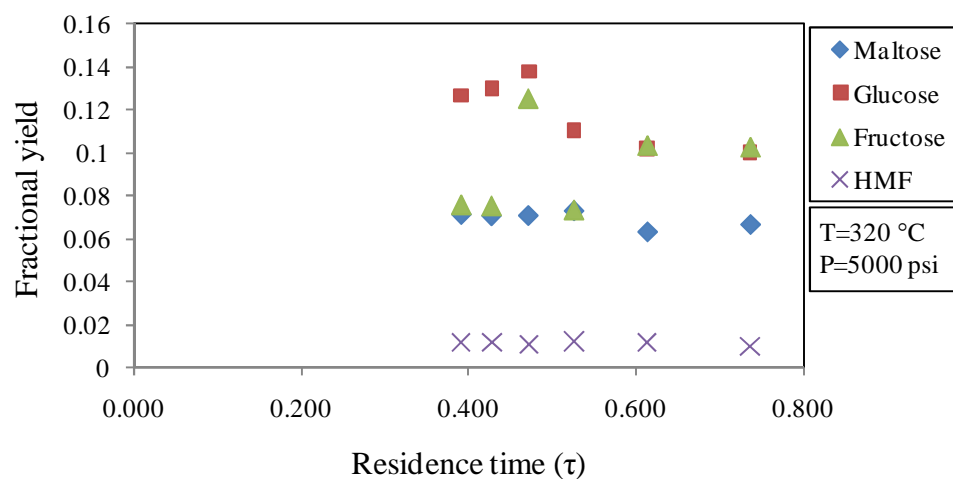
Figure 56.Fractional yield of water soluble hydrolysates obtained from starch at 320 °C in microreactor
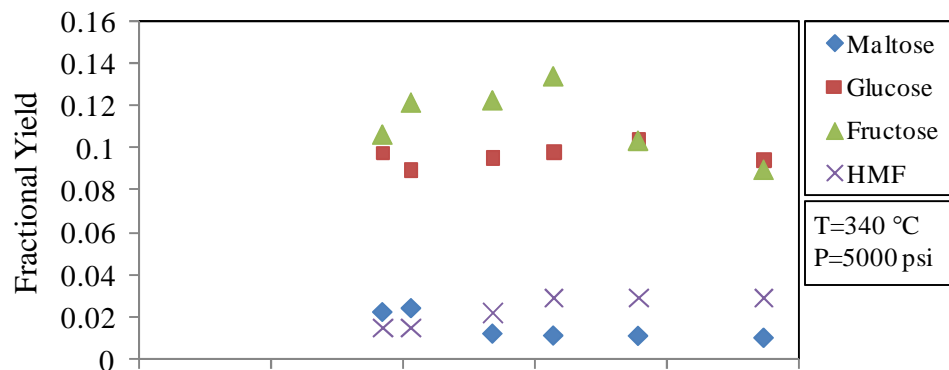
Figure 57.Fractional yield of water soluble hydrolysates obtained from starch at 340 °C in microreactor

Table 8. Summary of the Water Soluble Hydrolysates Yields obtained from Cellulose and Starch

Reaction in Microreactor	Starch Soluble Hydrolysates	Cellulose Soluble Hydrolysates
At 270 °C – 290 °C	Better yields of maltose than glucose	Better yields of cellobiose than glucose
Maximum glucose yield obtained at what temperature and residence time?	14.4 %, 300 °C, 0. 370 s	22.5 %, 340 °C, 0.615 s
Formation of furfural and HMF started becoming apparent	At 300 °C	At 300 °C
Glucose to fructose isomerization	Increasing rate when compare with cellulose	Relative slower rate when compare with starch
Maximum fructose yield obtained at what temperature and residence time?	13.4 %, 340 °C, 0.629 s	7.9 %, 340 °C, 0.539 s
Comparing yields of glucose with disaccharide above 300 °C	Better glucose yields	Better glucose yields

5.2.3.4 Conclusions

Hydrolysis of dissolved starch was conducted in a hydrothermal microreactor at the subcritical temperatures ranging from 270 °C to 340 °C and at 5000 psi. Samples containing water soluble hydrolysates were obtained and subsequently analyzed with HPLC. The hydrolysates in question consist of glucose, fructose, maltose, and HMF. Maltose yield exceeded the yield obtained for the other hydrolysates analyzed at the subcritical temperatures ranging from 270 °C to 290 °C. But at 300 °C, the disaccharide yield is relatively less than the glucose yield and decreases as the residence time increases. While at 320 °C, yield obtain for maltose is apparently constant but relatively less than the yield generated for the monosaccharides. At 340 °C, maltose yield is not only less than the monosaccharide yields but also less than the HMF yield. One interesting trend in this experiment is the isomeric behavior of glucose and fructose. Fructose yields improve significantly as temperature increases and this is largely due to an increase in the isomerization rate of glucose to fructose with temperature. The climax of increasing rate in glucose to fructose isomerization was made evident when fructose yield at 340 °C and residence times ranging between 0.370s and 0.629s exceeded glucose yield. In this experiment, maximum glucose yield of 14.4 % was obtained at 300 °C and residence time of 0.370 s while in the case of fructose, maximum yield of 13.4 % was obtained at 340 °C and at 0.629 s. The maximum aggregate sum of the monosaccharide yield which is 26.3 % was obtained at 320 °C and at residence times of 0.472s. Formation of HMF began manifesting at 300 °C with maximum HMF yield of 2.9 % occurring at residence time of 0.757 s and at subcritical temperature of 340 °C.

5.2.4 Hydrolysates Yield from Crystalline Cellulose Hydrolysis in the Microreactor at Supercritical Condition of Water

Hydrolysis of cellulose in a hydrothermal microreactor results in the formation of water soluble hydrolysates. Soluble hydrolysates include fermentable sugars and hydrolysate decomposition products. Cellulose suspensions were fed to the process unit and products resulting from the reaction were collected downstream. The sampled hydrolysate products were analyzed with HPLC and the yield of the water soluble hydrolysates obtained were evaluated.

5.2.4.1 Experimental Description

Cellulose suspension was fed into a tube enclosed within a tube furnace at flow rates ranging from 5 ml/min to 10 ml/min. Subsequently, the deionized water was heated to supercritical temperatures ranging from 375 °C to 395 °C per experimental run. The pressure of the fluid was 5000 psig and was set and controlled by a back pressure regulator downstream. The supercritical water exit into the glass fiber microreactor and serve as both hydrolytic agents and reaction medium for the 2 wt% cellulose suspension entering from the upper inlet port of the reactor closer to the tube furnace outlet. The 2 wt% cellulose suspension mixed with the supercritical water at constant volumetric flow rate of 10 ml/min thence diluting it to weight percent ranging from 0.67 to 1 wt%. The reaction is quenched by the deionized water entering from the other upper inlet port of the microreactor and also by the heat exchanger downstream. The samples were collected in the gas-liquid separator and were analyzed.

5.2.4.2 Sample Analysis

Water soluble hydrolysates collected at the different subcritical temperatures and at different residence times were analyzed with HPLC. Hydrolysate quantification was based on hydrolysate standard calibration and species identification was determined by characteristic retention time. The quantification was established based on the peak areas of HPLC compared against a known standard.

5.2.4.3 Results and Discussions

Figure 58 – 62 unveil the fractional yields of monosaccharide formed from the hydrolysis of crystalline cellulose in the hydrothermal microreactor at temperature ranging from 375°C to 395°C and 5000 psi. The reactions were conducted at supercritical condition and dissolution dominates the reaction of crystalline cellulose at this condition. The yield of the monosaccharides obtained at each supercritical temperature considered decreased with increasing residence time except at 395 °C. Decomposition products of glucose such as HMF and furfural were sampled but at a very negligible amount.

In Figure 58, Glucose yield decreased from 6.5% to 1.8% as residence time changes from 0.318 s to 0.442 s while fructose yields with the exception of percent yield at 0.347 s ranges between 2.5% and 2.8% over the residence times. Thus, fructose yield obtained at 0.347 s is 4.3%. Figure 59, reveal similar trend with the yield of glucose as depicted in Figure 58 with the residence time but the only difference is that glucose yield decreased from 5.0% to 1.5% as residence time changes from 0.308 s to 0.429 s . While Fructose yield ranges between 3.14 % and 1.38 % as over the residence time with maximum yield of 3.14 % occurring at 0.336 s.

Figure 60 unveils both yields of the monosaccharide decreasing as the residence times increases from 0.297 s to 0.413 s. However, it is interesting to observe glucose and fructose displaying about the same yields over the residence time. Maximum fructose yield of 5.3% was obtained at 0.297 s, while 1.2%, the minimum fructose yield, was obtained at 0.361 s. Maximum and minimum yields obtained for glucose are 5.0% and 1.4% and at the residence times of 0.297 s and 0.413 s respectively.
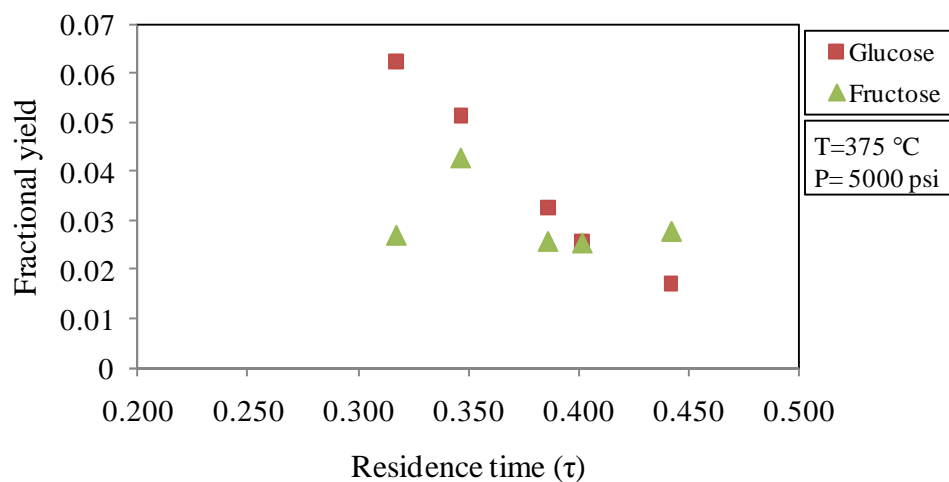
Figure 58. Fractional yield of monosacchride obtained at 375 °C in the microreactor
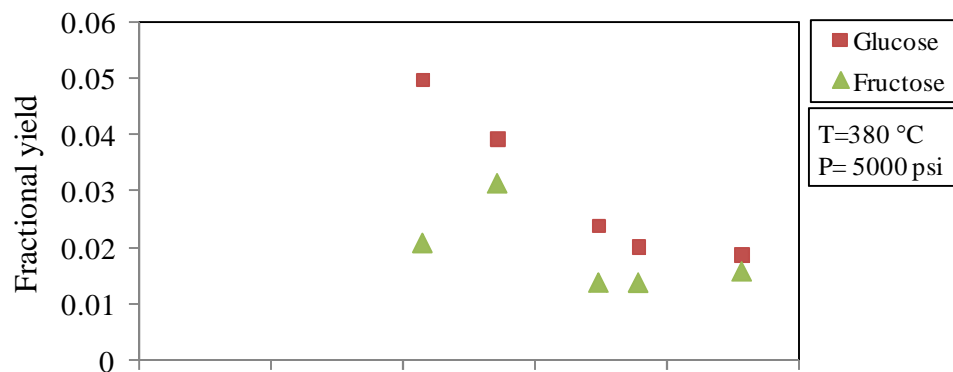
Figure 59. Fractional yield of monosaccharide obtained at 380 °C in the
  microreactor
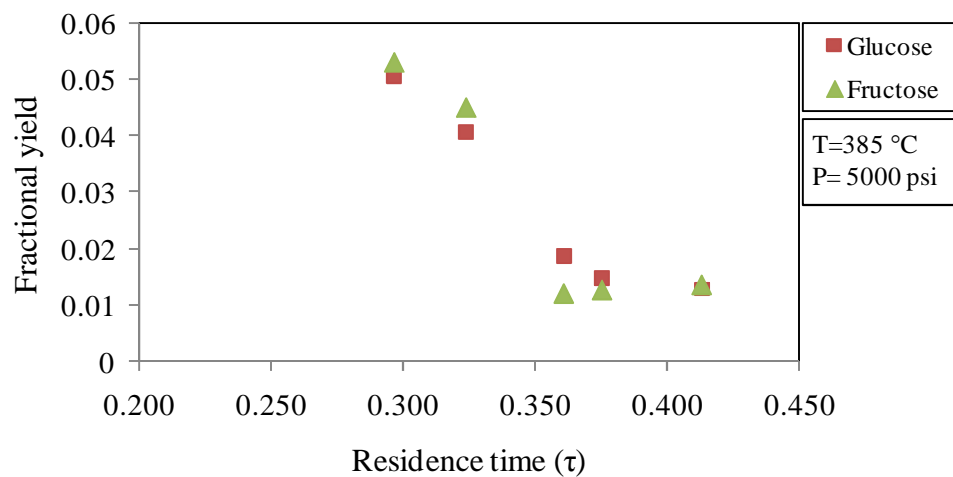
Figure 60. Fractional yield of monosaccharide obtained at 385 °C in the
  microreactor

Figure 61 displays yields of glucose and fructose with residence times at 390 °C.

Glucose yield decreased with increasing residence times (0.284 s to 0.398 s) while

fructose yield decreased with increased residence times. But after 0.346 s, the quantity of

fructose formed relative to the feed increased with the residence times. The minimum yield obtained for fructose at a residence time of 0.346 s is 1.3%, while maximum fructose yield of 2.7% was obtained at a residence of 0.284 s. For glucose, maximum and minimum yields of 3.9% and 1.4% were obtained at residence times of 0.284 s and 0.398 s respectively. Figure 51 portray yields of glucose and fructose with residence times at 395 °C. Glucose and fructose yields increased as residence time increased but decreased after 0.329 s. The minimum yield obtained for fructose at a residence time of 0.342 s is 1.2% while maximum fructose at a residence time of 0.329 s yield is 2.9%. Maximum and minimum glucose yields obtained at residence times of 0.329 s and 0.378 s are 3.3% and 1.6% respectively.
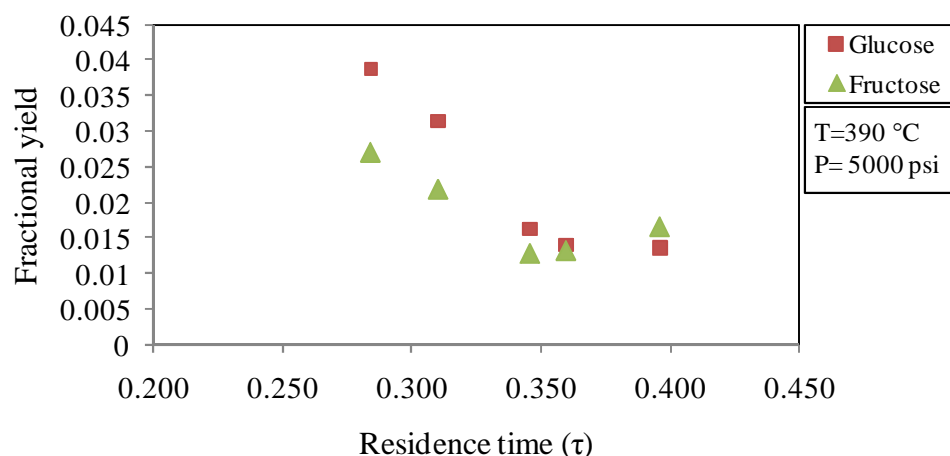
Figure 61. Fractional yield of monosaccharide obtained at 390 °C in the microreactor
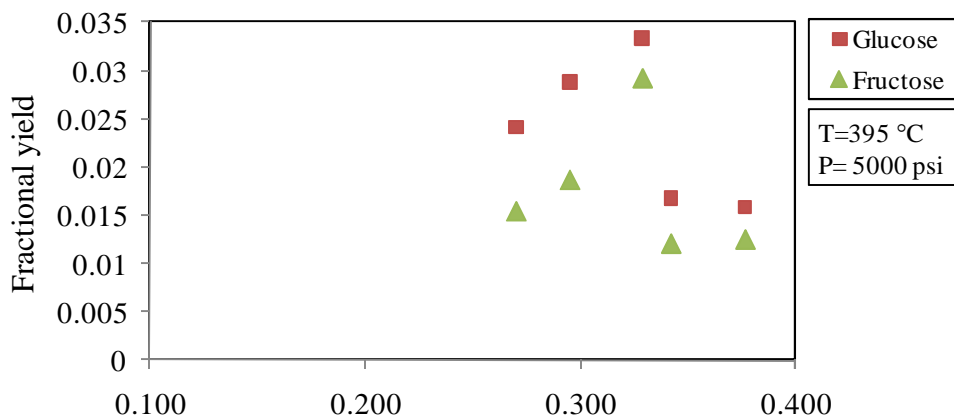
Figure 62. Fractional yield of monosaccharide obtained at 395 °C in the microreactor

5.2.4.4. Conclusions

The residence times depicted at the supercritical temperature appears lower and shorter in range than what was obtained at subcritical conditions. The reason is because of the density of the supercritical water which is lower than the subcritical water. Keeping all other variables in calculating residence time aside from density constant, density of the fluid at reaction condition is obviously going to alter the residence times evaluated at subcritical and supercritical conditions of water.

Unlike monosaccharide yield obtained at subcritical condition which increases relatively with residence times, the yield obtained for the monosaccharide at supercritical condition decreased with the residence time and with increasing temperatures. The Maximum glucose yield of 6.2% occurs at a residence time of 0.318 s while minimum glucose yield of 1.3% occurs at a residence time of 0.413 s. However, the maximum fructose yield of 5.2% occurs at a residence time of 0.297 s.

5.3. Summary of Experiments

This chapter explored yields obtained from the hydrothermal conversion of crystalline cellulose and starch in tubular and micro- reactors. The range of reaction was done under different reaction conditions and the yields generated as per the hydrolysate have been extensively discussed. The most important conclusions from the various experiments conducted can be summarized as the following:

1. In the tubular reactor and at subcritical temperature, hydrolysates such as glucose, fructose and cellobiose exhibit better product yield than decomposition products of the hydrolysates. But as temperature increased, hydrolysates including monosaccharide start experiencing net decomposition rate. For 10 ml/min, maximum glucose and fructose yields are 15% and 7% and are obtained at 300 °C. As temperature increased past 300 °C and began approaching supercritical condition, less monosaccharide were formed as a result of an increase in the net decomposition rate of glucose to HMF and furfural. In other word, more furanic compounds and other decomposition product were formed in the supercritical region. For 5 ml/min, maximum glucose and fructose yields obtained from hydrolysis of starch are 35% and 5.3% while maximum glucose and fructose yields obtained from hydrolysis of crystalline cellulose are 36.7% and 6.7%. These maximum yields were obtained at subcritical temperatures of 250 °C but as temperatures increased and approach supercritical region the same scenario that was observed for 10 ml/min also unfolded. That is, a net decomposition rate of the hydrolysate as against its formation occurred thus giving rise to more HMF, furfural and

array of other decomposition product. Better monosaccharide yields are observed for 5 ml/min than 10 ml/min.

2. Hydrolysis of crystalline cellulose in the microreactor revealed an increase in the monosaccharide yield relative to other hydrolysate and decomposition products present as temperature increased from a lower subcritical temperature (280 °C) to a higher subcritical temperature (340 °C). Maximum glucose and fructose yield in this experiment are 22.5% and 8.03% and both yields were obtained at 340 °C. As temperature move toward a higher subcritical temperature, to be precise 300 °C, HMF start becoming apparent while at 340 °C formations of HMF and furfural became visible. These trends further underscore this fact that, increasing temperature towards a near supercritical region will certainly increase the net decomposition rate of glucose and fructose via their formation rate to an array of decomposition products. Cellobiose yield, though increases as temperature increases, relatively decreases with the yield of other hydrolysates. The reason is due to an increase in its hydrolysis rate to glucose as temperature increases.

3. Hydrolysis of dissolved starch was aim at serving as surrogate for hydrolyzing dissolved cellulose. More formation of monosaccharide was observed as temperature increase from 270 °C to 340 °C. The same trend of increasing formation rate of the monosaccharide as observed in the hydrolysis of crystalline cellulose was also noticed in this experiment. One trend in this experiment is the increase in the isomerization rate of glucose to fructose as temperature increased. Thus, opening up opportunity for fructose at some

temperature to have a better yield than glucose. Maximum glucose and fructose yields are 14.4% and 13.4%; the former is quite lower than its counterpart obtained from cellulose hydrolysis while the latter is not. HMF also becomes apparent at 300 °C while no measurable furfural was obtained at any of the subcritical temperature. Maltose yield though increase as temperature increases but relatively decreases when compared with other hydrolysates. The reason is due to more of it hydrolyzing to glucose. The lowest array of maltose yield was obtained at 340 °C.

4. Due to the lower density characteristics of supercritical water, the average residence time in this experiment is than the average residence time observed at subcritical condition of water. The yield obtained for the monosaccharide decreased with residence time and with increasing supercritical temperature.

5.4. Comparison of the Monosaccharide Yields Obtained at Subcritical and Supercritical Conditions of Water in the Microreactor

To compare monosaccharide yield obtained at supercritical condition with the yield obtained at subcritical temperature will be relatively skewed except to look at the residence times that can be accommodated at the two conditions. Thus, at supercritical condition, maximum glucose yield obtained at 0.318 s is 6.2% while maximum fructose yield obtained at 0.297 s is 5.2%. Thus yield obtained within residence time ranging from 0.270 s to 0.442 s and at subcritical condition for dissolved starch is consider qualified for comparison. Maximum glucose yield obtained from the hydrolysis of dissolved starch within the ballpark residence times range is 14.4% and the residence

time is 0.439 s . While maximum fructose yield is 12.1 % and the residence times is 0.413 s. For the hydrolysis of crystalline cellulose, maximum glucose and fructose yields obtained within the stipulated ballpark residence times are 21 % and 7.9 %. The latter was at residence times of 0.378 s while the former was at residence times of 0.437 s. It is clear that a better glucose yield is highly plausible for the hydrolysis of dissolved starch and even crystalline cellulose than glucose yield from hydrolysis of cellulose in supercritical water.

CHAPTER 6. DEGRADATION PATTERN AND MODE OF SCISSION

OF CELLULOSE HYDROLYSIS IN HYDROTHERMAL SYSTEMS

Cellulose is a bioorganic polymer formed from condensation polymerization of glucose. Polymerization often commences by an initiator propelling the monomer to action and after the initiation, a chain reaction of monomers combining with one another will be invoked until terminated. The termination step is a pointer to the fact that there is no limit to the number of monomers that can get polymerized until reaction is terminated. Thus, a polymer can be formed from varying numbers of monomers as long as the chain reaction is still active. In a simpler term, a polymer is a compound which does exhibit the ability to be defined by a range of molecular weights and as a result, the need to express their weights in a distribution format is necessary. Thus, the distributive nature of the weights of the polymer molecule best explained why averaging the molecular weight is a reasonable step in ascribing one single molecular weight to the polymer. The molecular weight average can be depicted, as indicated in Chapter 2, as viscosity average molecular weight, number average molecular weight, or weight average molecular weight. Polymeric compounds can also be characterized by chemical structure, average molecular size, degree of branching, stereoregularity (tacticity) and crystallinity. To alter both the physical and chemical properties of a polymeric compound, reaction such as hydrolysis, ozonolysis, mechanical degradation, and hydrothermolysis need to be applied to it. The main effect of some of these processes on the array of polymer molecules is to scission or break their chains thereby altering the molecular weights distribution.

As explained in Chapter 2, continuous changes in the molecular weight distribution pattern due to scission or recombination of polymer molecules is referred to

as the degradation pattern. There are different modes of scissioning polymer chains and these include center scission, unzip scission, and random scission. Once the polymer molecules are scissioned, the molecular weight distribution changes. As for bioorganic polymer molecules such as cellulose and starch, hydrolysis is often the common way of scissioning the molecules. Characteristic features of cellulose such as molecular weight distribution, molecular weight average, and crystallinity are altered when its chains are scissioned. To assess these changes, characterization methods such as size exclusion chromatography, osmometry, ultracentrifugation, and mass assisted laser desorption and Ionization (MALDI) mass spectroscopy, and multiangle laser light scattering (MALLS) can be applied.

This section of the proposed research is focus at determining mode of scission (random or nonrandom) and the degradation pattern of cellulose in subcritical and supercritical phase. Till date, it is rare to see in the literature any work done on the study of molecular weight distribution pattern of cellulose residue obtained from hydrothermal reaction. And that explains the drive behind conducting a detail study on the changes in the molecular weight characterization of cellulose residue obtained from hydrothermal reaction. Size exclusion chromatography (SEC) method will be adopted to unveil the molecular weight distribution (MWD) pattern before and after stages of hydrolysis in the hydrothermal reactor. Subsequently, the degradation pattern currently being simulated based on different mode of scission such as random scission, unzip (end-wise) scission, and mid-point or center scission, will be used to fingerprint experimentally generated degradation patterns obtained from SEC.

6.1. Analysis of the Molecular Weight Distribution of Crystaline Cellulose

Molecular weight distribution analysis of crystalline cellulose as received and cellulose residue obtained from the hydrothermal reaction was conducted. The reaction entails the hydrolysis of crystalline cellulose at subcritical conditions of water in the microreactor. The characterization method used for the molecular weight distribution analysis is the size exclusion chromatography. The detail procedure of the hydrolysis experiment was well explained in section 4.1.1 of chapter 4 while the detail procedure for the SEC experiment will be presented in this chapter.

6.1.1. Materials.

Materials. Most of the chemical compounds used for the molecular weight distribution experiments were obtained from Sigma-Aldrich and are highlighted as follows: crystalline cellulose (sigmacell type 20), N,N-dimethylacetamide (99 %), lithium chloride. Pullulan standards with peak molecular weights (Mp), 180, 667, 5900, 11100, 21100, 47100, 107100, 200000, were purchased from Polymer Laboratories. These standards were used to generate the calibration curve for the molecular weight distribution. Lithium chloride (5g) was oven dried before being dissolved in 1 litre of N,N-dimethylacetamide (DMAc). The method involve in mixing the relative quantity of LiCl in DMAc (DMAc/0.5% LiCL) was stated in the procedure adopted in this project for the dissolution of the polysaccharides (cellulose and pullulan). This procedure was published in an article[73] written by Striege and Timpa.

6.1.2 Hydrolysates Analysis.

The sampled products from the hydrolysis reaction which includes water soluble and water insoluble (cellulose residue) were analyzed by different analytical instruments. The insoluble hydrolysate which is our main concern here is the unreacted cellulose generated after the hydrolysis reaction and can simply be refers to as the cellulose residue. They were not filtered but centrifuged and decanted to be set up for drying. The solid residues left after centrifugation and decantation are freeze dried with a 4.5 Labconco freeze dryer. The reason for freeze drying the cellulose residue needed for the SEC is to avoid caking of the cellulose residue which is common with drying maybe in an oven or desiccators. But in the case of freeze drying, the cellulose residue is obtained in powdery form which does allow for easy dissolution in DMAc/0.5%LiCl. The only disadvantage with freeze drying is the tendency of losing some residue in the process and after drying. But with conventional method of drying via oven or at room temperature the likelihood of losing any of the solid residues in the process and after drying is greatly reduced. After the freeze-dried cellulose residue is finally dissolved in DMAc/0.5%Licl, the next step is to perform the size-exclusion chromatography experiment. The chromatography set-up is not significantly different from HPLC's. The only unit in the two set-ups that is different is the column. Thus, the SEC used in this experiment consist of the pump (LC-10ADvp), Refractive index detector (RID-10A), SSI 505 LC column oven, PLgel 5μm MIIXED-D (300 x 7.5 mm); mobile phase (DMAC/0.1% Licl). The mobile phase operates at a flow rate of

1.0 ml/min and the oven temperature was set at 70 ^{o}C. The sample was manually injected and the chromatograms were analyzed and converted to molecular weight distribution plot with CIRRUS GPC Software. Detail of the software will be presented later.

6.1.3 SEC Calibration.

Different polymers of the same molecular weight will display unique hydrodynamic volume and conformation when dissolved in a given solvent. The hydrodynamic volume which is a measure of the intrinsic viscosity and molecular weight forms the basis of the universal calibration. Cellulose and pullulan are both polysaccharides but with different hydrodynamic behavior in DMAc/liCl. Pullulan is a polymer of maltotriose unit while cellulose is formed from glucose polymerization. To accurately assess the MW of cellulose based on calibration developed through pullulan standard, the following equation built on the premise of universal calibration is applied.

$$\log M_2 = \frac{1+a_1}{1+a_2}\log M_1 + \frac{1}{1+a_2}\log\left(\frac{K_1}{K_2}\right) \tag{53}$$

Where M_2 is the molecular weight of cellulose, M_1 is the molecular weight obtained based on pullulan standard calibration; a_1, K_1 and a_2, K_2 are Mark-Houwink constants for the two polymers in question.

6.2 Degradation Pattern

Degradation pattern, as defined earlier, describes continuous changing in the molecular weight distribution plots as a result of changes in the chain length of the

polymer molecules constituting the distribution. Changes in chain length are brought by either breaking the bonds binding the polymer chain or by recombination of the polymer molecules/monomers present in the distribution. In this study, we will only be looking at the former, i.e. breaking or scissioning of the bonds. Degradation pattern can be assessed by either conducting molecular weight distribution experiments on the size of the polymer at each stage of a reaction or by simulating these changes in chain length and re-making the distribution plots. In this chapter, degradation pattern of cellulose residue obtained from hydrolysis will be generated via SEC. Thereafter, degradation pattern generated from simulation will be explored. Finally, a detail comparison of the degradation pattern from experiment and simulation will be conducted. The comparison is necessitated because of the need to establish the scission mode that does transpire during hydrothermal reaction of crystalline cellulose.

6.2.1 Experimentally Generated Degradation Pattern

Hydrolysis of crystalline cellulose in the hydrothermal microreactor results in the formation of water soluble and insoluble hydrolysates. Unreacted cellulose which most often will be refers to as cellulose residue, constitutes the insoluble hydrolysates. Cellulose slurry solution was fed upstream the process unit and products resulting from the reaction were collected downstream. Cellulose as received and the cellulose residues from the samples were analyzed with high performance size exclusion chromatography (HPSEC) or simply size exclusion chromatography. The chromatograms obtained were analyzed and converted to molecular weight distribution plots.

6.2.2 Experimental Description

Hydrolysates samples were centrifuged and the supernatant decanted. After decantation, the cellulose residues after centrifugation were frozen and subsequently freeze dried in 4.5 labconco Freeze Dryer. Cellulose as received and dried cellulose residue were subsequently dissolved in DMAc. To prepare standard solution for calibration, 30 mg of the pullulan was dissolved in 5ml DMAc in 10 ml sample tube. The tube was seated in a heating block placed on magnetic stirrer plate and heated, after ensuring that the temperature of the sample is 150 °C, for 1 hr.   After an hour of heating and stirring with an egg-shaped magnetic stirrer expires, the sample temperature is allowed to cool to 100 °C and then, 0.250 g of LiCl was added. Subsequently, the sample is made to stay at 100 °C for the next 1 hr, and afterwards left overnight or for 6 to 7 hrs at 50 °C. The sample solution is finally emptied into a 50 ml volumetric flask and diluted with the DMAc solvent up to the 50 ml mark. The last step is done at room temperature and the final concentration is 0.6 mg/ml in DMAc/0.5% LiCl. The same procedure was followed for the dissolution of cellulose as received and cellulose residue in DMAc, but with different final concentrations. The starting masses use for the cellulose as received and cellulose residue ranges between 30 mg and 120 mg and 25 ml volumetric flask was used in lieu of the 50 ml volumetric flask. Major reasons for these differences are 1) a more final concentrated solution is desired and 2), the quantity of some of the residue obtained after hydrolysis is limited.

The sample solution of the polysaccharide is manually injected into the size exclusion chromatography unit and chromatogram were subsequently generated and reflected on the readout computer. The chromatograms were exported as a CDF

(common data format) file and imported into a GPC analytical software obtained from Polymer Laboratory now part of a larger company called Varian Inc. The software only support single channel chromatogram for conventional SEC/GPC analytical methods. It is designed to analyzed and processed data from a good numbers of chromatography system. Some of the major features of the Cirrus GPC software includes user interface, single analysis program, workbook, GPC calibration options, GPC analysis option, processed data, user definable MW range to mention a few. The Cirrus GPC software converts the CDF file back into chromatogram, and then analyzed the data by making a plot of the molecular weight distribution.

6.2.3 Sample Analysis

After exporting the chromatograms into Cirrus, a calibration curve was generated for the molecular weight distribution analysis. Subsequently chromatograms obtained for the cellulose as received and cellulose residue were imported and molecular weight distribution were generated for each chromatograms based on the calibration curve. The calibration curve can be seen in Appendix.

6.2.4 Results and Discussions

Figure 63-67 show the molecular weight distribution plots for the cellulose as received and cellulose residue obtained from the hydrothermal conversion. The number on the legend with a dash in between respectively depicts the temperature and flow rates at which the cellulose suspension is fed into the reactor. Table 9-13 unfold molecular weight averages and polydispersity index calculated by Cirrus GPC software while wt fraction was calculated with excel. The essence of showing the average on a table is to avoid crowding the plots with marks indictating these relevant molecular weight

averages. It also affords us the opportunity to compare these weight averages and also be able to compare the weight fraction alongside with the respective distribution after reaction.

A good number of the molecular weight (MW) distributions in Figure 63 appear changing from a monomodal distribution as displayed by the Initial MW distribution to biomodal distribution. Molecular weight distributions for cellulose residue obtained at 270 °C and flow rates at 5, 6,and 7 ml/min seem to follow a similar pattern but differ in their respective peak average molecular weight and differential weight fraction (y-axis). However, cellulose residue obtained at 270 °C and feed flow rate of 5 ml/min has the lowest peak avearge molecular weight but with the highest differential weight fraction. This is supportive of the fact that, more cellulose chain are broken to lower molecules at the lowest flow rate (5 ml/min) relative to other flow rates. The distribution with the maximum peak average molecular weight portrayed by MW distribution of cellulose before undergoing any reaction and its peak average molecular weight is approximately 49,987 Da. The MW distribution with the lesser number of smaller molecules but the highest peak average molecular weight has the widest distribution(PDI= 4.01) while MW distribution with narrowest distribution (PDI=2.86) has the highest number of smaller molecules though with the lowest peak average molecular weight of 2,675 Da. This maybe pointing to an increase in the hydrolysis rate of cellulose to forming molecules with lower degree of polymerization as flow rate reduces.
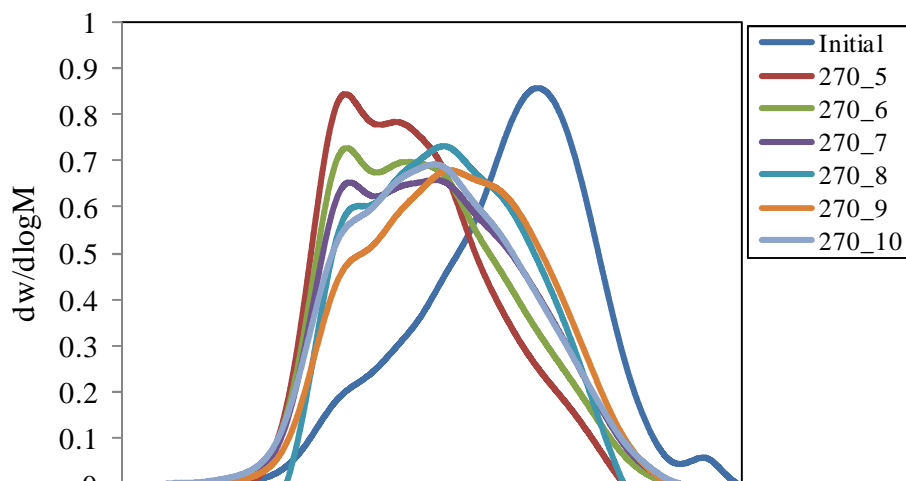
Figure 63. Molecular weight distribution for cellulose and residue obtained at 270 °C

Table 9. Molecular weight averages and wt fraction for cellulose residue obtained at 270 °C in the microreactor

Sample Name	Mp	Mn	Mw	Mv	PD	WT fraction
cellulose_residue270_5	2675	4702	14280	11915	2.86	0.658
cellulose_residue270_6	2895	5261	19835	16115	3.52	0.711
cellulose_residue270_7	11117	5788	23218	18916	3.75	0.798
cellulose_residue270_8	11371	7156	21667	18598	2.88	0.814
cellulose_residue270_9	13618	7199	27773	23214	3.63	0.743
cellulose_residue270_10	10468	5801	24252	19762	3.90	0.835
cellulose as received	49987	13660	58051	49032	4.01	1.000

Figure 64 and Table 10 unveil the molecular weight distribution and range of molecular weight averages obtained based on the chromatogram generated for cellulose residue sampled at 280 °C. As flow rates decreases, peak average molecular weight shifted from a higher value of 49,987 Da for cellulose as received to a lower value of 2,119 Da for cellulose residue obtained at 280 °C and 5 ml/min. A similar trend of an increased in the formation of smaller cellulose chain molecules could be observed as residence times increased. At this operating condition, the highest PDI was observed for 280_5 (i.e. the molecular weight distribution with the lowest peak average molecular weight), while MW distribution with the lowest PDI is displayed by cellulose residue obtained at 280 °C and 8 ml/min. As observed at 270 °C, where it is presumed that higher number of shorter cellulose chain is being formed, more smaller cellulose chains are seen emerging at 280 °C and 5 ml/min. The MW distribution patterns of cellulose residue obtained at 280 °C and at 9 and 10 ml/min are almost alike. This could be indicative of why the two distributions having almost equal PDI and a close peak average molecular weights of 13,116 Da and 12,491 Da.
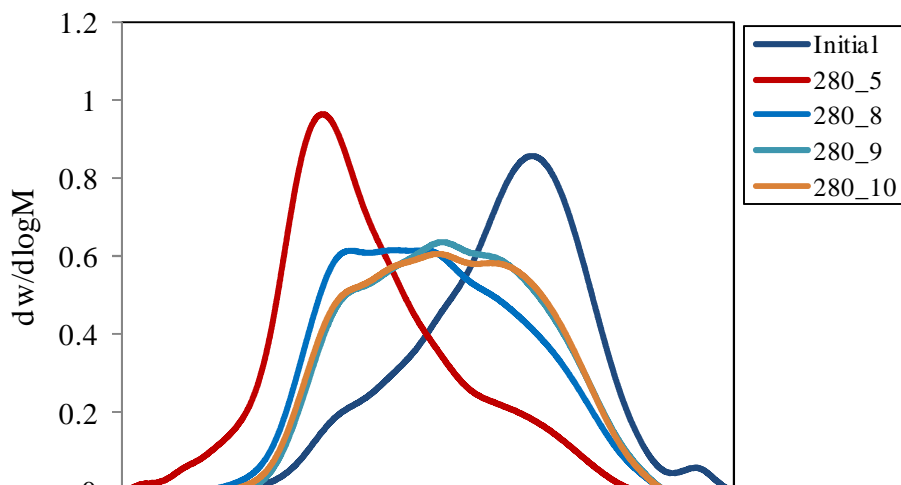
Figure 64.Molecular weight distribution for cellulose and residue obtained at 280 °C

Table 10.Molecular weight averages and wt fraction for cellulose residue obtained at 280 °C in the microreactor

Sample Name	Mp	Mn	Mw	Mv	PD	WT fraction
cellulose_residue280_5	2119	2136	10592	8048	4.54	0.598
cellulose_residue280_8	6495	5427	25151	20206	4.31	0.823
cellulose_residue280_9	13116	7155	29841	24663	3.91	0.738
cellulose_residue280_10	12491	6814	29702	24486	4.08	0.766
cellulose as received	49987	13660	58051	49032	4.01	1.000

Figure 65 depicts the molecular weight distribution for cellulose as received and cellulose residue obtained at 290 °C. While Table 10 reflects molecular weight averages, PDI, and weight percents for cellulose as received and cellulose residue. Almost all MW

distributions depicted for the cellulose residues seem to portray a mirror-like image of the MW distribution of the cellulose as received. A significant shift was observed for the peak average molecular weights of all the molecular weight distributions from initial distribution. The differential weight fraction increased as the flow rate decreased. Thus, there is an increase in the hydrolytic conversion of cellulose to lower molecules as flow rate reduces. Detail information on the values of the molecular weight averages such as number average molecular weight, weight average molecular weight, and viscosity average molecular weight can be seen on Table 10. About 73 % of cellulose as received were hydrolyzed at 290 °C and flow rate of 5 ml/min, 50 % more when compare with flow rates at 9 and 10 ml/min. But with that, the areas depicted by the 9 and 10 ml/min MW distribution do not reflect a significant difference in the area portrayed by the MW of the flow rate at 5 ml/min.
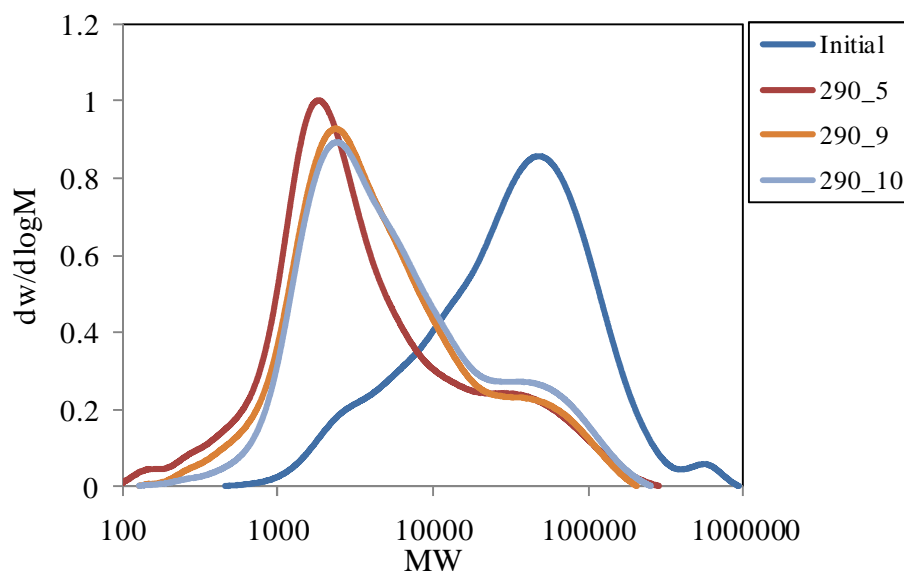
Figure 65.Molecular weight distribution for cellulose and residue obtained at 290 °C

Table 11. Molecular weight averages and wt fraction for cellulose residue obtained at 290 °C in the microreactor

Sample Name	Mp	Mn	Mw	Mv	PD	WT fraction
cellulose_residue290_5	1851	1812	12253	8909	6.09	0.369
cellulose_residue290_9	2381	2516	12214	9358	4.46	0.676
cellulose_residue290_10	2453	3025	14874	11405	4.51	0.670
cellulose as received	49987	13660	58051	49032	4.01	1.000

Figure 66 depicts the molecular weight distribution for cellulose as received and cellulose residue obtained at 295 °C. While Table 11 reflects molecular weight averages and weight percent for cellulose as received and cellulose residue. Molecular weight distributions depicted for the cellulose residues appear to portray images similar to what was obtained in Figure 65. In essence, similar trends with the molecular weight distribution shifting to a lower peak average molecular weight could also be observed. The differential weight fraction appear very close for 7, 8, and 9 ml/min though the lowest flow rate among these three still possesses more of smaller cellulose chain molecules. Hydrolytic conversion of cellulose to lower molecules at the three penultimate flow rate does not present a significant change relative to one another. One interesting observation is that, there is an increase in the number of oligomers and some measurable amount of glucose at this temperature. This observation could also be supported by the sizes of the PDIs obtained at this temperature. The bigger the PDI the more variable the sizes of the molecules represented in the distribution. Detail information on the values of

the molecular weight averages such as number average molecular weight, weight average

molecular weight, and viscosity average molecular weight can be seen on Table 11.
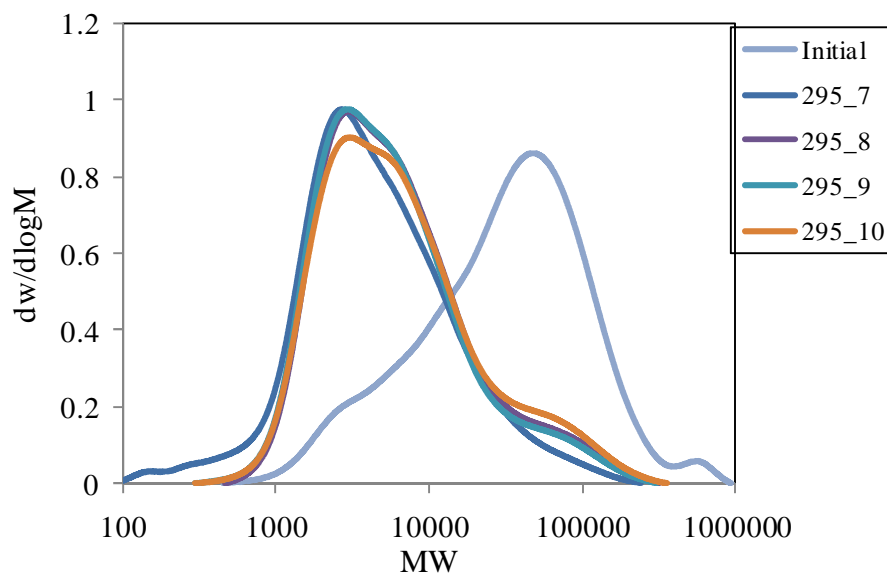
Figure 66. Molecular weight distribution for cellulose and residue obtained at 295 °C

Table 12. Molecular weight averages and wt fraction for cellulose residue obtained at 295 °C in the microreactor

Sample Name	Mp	Mn	Mw	Mv	PD	WT fraction
cellulose_residue295_7	2675	2501	9223	7506	3.45	0.419
cellulose_residue295_8	3017	3872	12800	10154	3.07	0.623
cellulose_residue295_9	3051	3716	12081	9608	3.02	0.569
cellulose_residue295_10	3028	3893	14428	11293	3.42	0.684
cellulose as received	49987	13660	58051	49032	4.01	1.000

Figure 67 depicts the molecular weight distribution for cellulose as received and cellulose residue obtained at 300 °C. While Table 13 reflects molecular weight averages and weight percent for cellulose as received and cellulose residue. A significant shift was observed in the peak average molecular weights of the distribution of the unreacted cellulose to the MW distributions of the cellulose residue with lower peaks average molecular weight. The differential weight fraction increases with decreases in the flow rates. Increase in the differential weight fraction at lower peak average molecular weight indicates an increase in the hydrolytic conversion of cellulose chain to molecules with smaller chain length such as oligomers. The small spikes at molecular weight slightly higher than 100 Da perhaps between 100 and 300 Da, reflect a measurable formation of glucose as oppose to what was obtain at other temperatures.
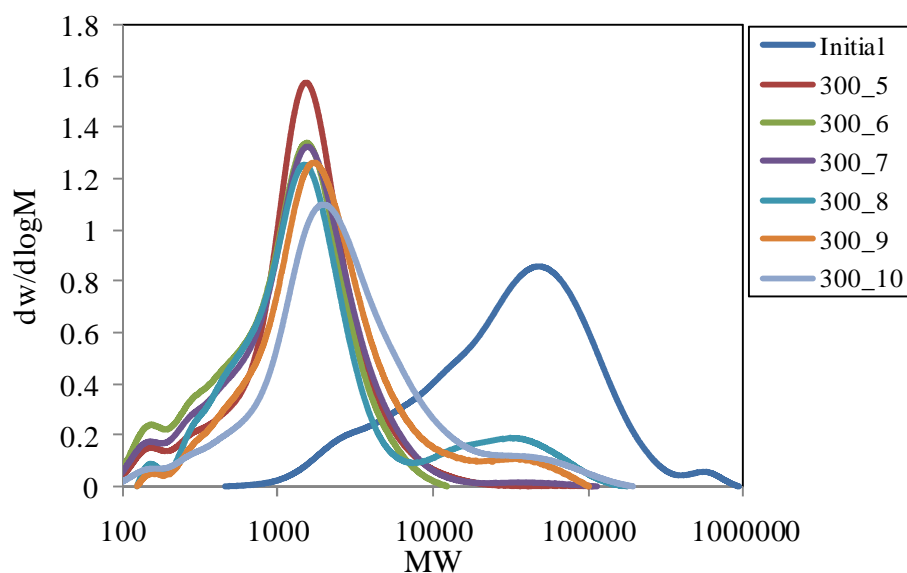
Figure 67. Molecular weight distribution for cellulose and residue obtained at 300 °C

Table 13. Molecular weight averages and wt fraction for cellulose residue obtained at 300 °C in the microreactor

Sample Name	Mp	Mn	Mw	Mv	PD	WT fraction
cellulose_residue300_5	1528	926	1971	1783	2.06	0.302
cellulose_residue300_6	1557	712	1574	1440	2.14	0.435
cellulose_residue300_7	1575	834	2179	1869	2.48	0.536
cellulose_residue300_8	1483	1107	6796	4716	5.47	0.694
cellulose_residue300_9	1749	1301	4591	3568	3.25	0.513
cellulose_residue300_10	1987	1443	6801	5127	4.30	0.535
cellulose as received	49987	13660	58051	49032	4.01	1.000

6.2.5 Conclusion

Changes in the molecular weight distribution pattern for cellulose residue relative to the initial distribution of cellulose as received have been explored. The shift in the peak average molecular weight of the initial MW distribution to a lower peak average molecular weight increases as temperature increases and flow rate are reduced. An increasing trend is observed with differential weight fraction at the lower end of the peak average molecular weight spectrum. This is suggestive of an increase in the formation of lower sized molecules such as oligomers and monomer precisely glucose. One last thing that was hardly mention in the result and discussion section is the mode at which cellulose chain scissioned. It is almost impossible to ordinarily look at experimentally generated molecular weight distribution and be able to predict the scission mode. To perform this task, a simulated molecular weight distribution modeled after a scission mode will be needed. This is why in the next section, scission mode and simulated degradation pattern will be addressed extensively.

6.3 Simulation of the Different Mode of Scission

Mode of scissions describe the different ways by which a polymer chain is broken or the bonds binding the monomers together are disengaged. It can occur at the center or

at the end of the chain or at any point along the polymeric chain. To determine the mode of scission by mere observing experimentally generated MW distribution looks highly uncertain. However, modeling the MW distribution based on different modes of scission and then compare it with the experimentally generated distribution is perceived to be highly feasible and doable. Detail reviewed on theories and concepts describing the different mode of scission have been performed in Section 2.4.2 of Chapter 2. Therefore, in this Section, we shall be applying one of the major concepts elucidated in Chapter 2 and that is the Algebraic Exact Statistical Formulations. It is based on binary tree chain cleavage model which depicts chain rupturing as sequence of probabilistic events and as a non-linear function of time. It assumes that one bond is broken at each step of degradation. The latter algorithm, which is the algebraic exact statistical formulation, is adopted and served as the mathematical formulation basis for the simulation in this research project. This approach utilizes an algebraic equation to express the expected fragmentation outcome of finite sets of chains from a large population. The equations are formulated from a list of logically defined degradation schemes that are specific to a particular mode of scission. Under this formulation, two probability-based criteria of selecting the affected polymer chain were considered: 1) chain length frequency, and 2) bond density. The probability-based mathematical models describing each criterion and the different modes of scission (random, center, and unzip) are expressed in Equation 38-46. These equations will be incorporated into the simulation, and it will be coded in MATLAB. Monte Carlo simulation was also adopted as an alternative to the algebraic exact statistical simulation. The problem with the Monte Carlo is the time it takes for the simulation to converge specifically for the random scission which is set to randomly select a bond for example from several tens of thousands of bonds within a matrix of 5902 by 5624. The column and row of the bond matrix are number of bonds per size of molecule (DP) and number of molecules per DP respectively. For instance, it takes roughly 7 hours for 0.2 % of the bonds to be broken from a population size of 1175

molecules with 41,953 bonds. The simulation was run on one of the Hewlett-Packard personal computers (PC) in the engineering computer laboratory. The components of the computer include an intel(R) Core(TM) i7 CPU 860 @ 2.80GHz processor, a memory ram of 8.00 GB and a 64-bit operating system. The rating of the computer was in the range of 7.5 to 5.9.

Therefore, due to time constraint, Monte Carlo simulation will be put on hold for future work. The Matlab codes for the algebraic exact statistical formulation and Monte Carlo method for the simulation of the scission modes can be seen in Appendices C and D respectively.

6.3.1 Importation and Analysis of Experimental Data in the Simulation Environment

The simulation environment is the MATLAB code written and run within the MATLAB environment. Experimental data is the data based on the chromatogram generated in the high performance size exclusion chromatography. The chromatogram was exported from HPSEC as CDF file format into Cirrus. The CDF format is converted within Cirrus software environment back into chromatogram with Response (mV) on the y-axis and retention time (min) on the x-axis. The chromatogram is further processed and re-modified into molecular weight distribution plots. Re-modification of the chromatogram is done based on the calibration curve generated from the pullulan standard. The curve can be seen in appendix B. Y-axis on the calibration curve reads MW while RT which means retention times is the x-axis.

There are different ways of representing the y-axis and x-axis of a molecular weight distribution. It can be by dw/dlogM vs MW mostly on a semilog plot or by weight fraction or number fraction vs DP or MW on a normal plot. However, representation of the molecular weight distribution with dw/dlogM vs MW on a semilog plot is often preferred and Cirrus GPC software is no exception. The dw/dlogM simply mean the

differential weight fraction of the polymer with respect to change in natural log of the mass of the polymer.

To generate the MW distribution from chromatogram and depict it using dw/dlogM as the y-axis and MW as the x-axis, the reciprocal of the gradient of the calibration must be multiplied with the normalized height of the chromatogram. This is simply the height of the chromatogram response (mV) at each RT divided by the sum of the heights at all the RTs. The reason is because each chromatogram response (mV) per RT represents the refractive index detector effect on the concentration of a definite molecular weight. Thus, the normalized height can also be seen as the change in weight fraction of the polymer per retention volume (dw/dv). Meanwhile the calibration equation for the molecular distribution weight can be expressed in the format as follows:

$$\text{Log } M = A + BX \tag{54}$$

Where M is the mass of the polymer, A is the intercept, B is the gradient and X can either be retention time or retention volume. Let assume X is retention volume, v, differentiating Equation 54 with respect to X will result in:

$$\frac{d \log M}{dv} = B \tag{55}$$

To obtain dw/dlogM, normalized height or change in differential weight fraction per the retention volume, v, is multiplied with the reciprocal of the gradient of Equation 55. Therefore, dw/dlogM is thus evaluated as follows in Equation 56.

$$\frac{dw}{d \log M} = \frac{dw}{dv} \times \frac{dv}{d \log M} \tag{56}$$

The reason for going through the task of explaining the connection between these variables is because of their significance in evaluating the various calculations performed in the simulation.

Once Cirrus GPC software finished analyzing the chromatogram, the data are extracted into ten columns which include retention time (RT), chromatogram response, normalized height, MW, dw/dlogM and some other columns of variables not particularly needed in the simulation. Cirrus does not calculate the number of molecules but from the data we were able to generate the number of molecules by dividing the dw/dlogM with the corresponding molecular weight (MW). The dw/dlogM which depicts mathematically the differential of weight fraction per differential of the logarithms of molecular weight is a product of the number of molecules and molecular weight. In other words, it typifies the total mass of each molecule size present in the distribution. Below is the equation reflecting the description.

$$\frac{dw}{d \log M} = NM \tag{57}$$

Where N is the number of molecules and M is the molecular weight.

The initial molecular weight distribution was developed based on raw data obtained from the experiment with DP ranging from 2.7003 to 5721.6436 as opposed to a unit increase stepsize integer DP. Problem of establishing the correctness of the algebraic exact statistical equation as per each mode of scission was encountered due to uneven distribution in the stepsize increase of DP and the real number format of the DP obtained from raw experimental data and. For every run, one bond must be broken and the number of molecules in the whole population must be increase by one. Thus, with the raw DP data, instead of breaking one bond for very run, roughly 14 bonds were recorded broken and tens of molecules were added. A critical evaluation of this anomaly shows a cumulative effect of the fractional part of the real number DP on the number of bond broken and the increment in the number of molecules. But when the DP was normalized into an integer with a uniform stepsize increase of 1, this anomaly was corrected especially with random scission. Though for center and unzip scission, increase in the

number of molecules was not exactly 1. Increase in the number of molecules for center scission was 1.025 as opposed to 1. The 0.025 may account for a fractional part of the molecule while breaking the polymer chain with even number of bonds at the center.

To normalized the real number DP into integer, the initial dw/dlogM per MW generated based on the raw data was fitted with a smoothing spline function. The function evaluated from curve fitting tool box with a command function of "cftool.m" is a piecewise polynomial computed from *p*. It is thus represented mathematically in Equation 58 as follows: .

$$f(x) = piecewise\ polynomial\ computed\ from\ p \qquad (58)$$

Where the smoothing parameter *p* equals 0.000798699 and the details of the goodness fit is presented as: R-square =1; Adjusted R-square = 1; Summation of Square Error(SSE) = 7.305e-5;and Root Mean Square Error (RMSE)=0.0003112. While *f(x)* is dw/dlogM and the piecewise polynomial is varing polynomial equations with MW as the independent variable. The DP obtained from the MW ranges from 1 to 5636 with a stepsize increase of 1.

Relevant data from Cirrus were manually exported into Excel. But for the simulation, Matlab code was written to export these data from excel.

6.3.2 A Step-by-Step Algorithm for the Matlab Code

Below are the highlighted steps of the matlab-based computer code for simulating the different mode of scission and subsequently generating the degradation pattern:

1. Import molecular weight of the polymer, normalized height, chromatogram response from excel files

2. Divide the molecular weight of the polymer (cellulose) with the molecular weight of the monomer (anhydroglucose) to obtain the degree of polymerization

3. Set the counter for number of scission.

4. Set another counter for when to make the distribution plot. It may be at every 10 multiples for the number of scission or any other multiple convenient for the person running the script.

5. Set the options for the mode of scissions.

6. Generate the Chromatogram plot.

7. Calculate the initial total number of molecules

8. Generate the initial distribution from the experiment

9. Generate a semilog plot for the initial distribution with dw/dlogM on the y-axis and MW on the x-axis

10. Store initial DP values in an array tag " iDP".

11. Import number of molecules from excel files

12. Set-up series of mathematical models (Algebraic Exact Statistical Algorithm Scheme) or develop a Monte Carlo scheme for the scissioning of the polymer chain based on different modes of scission highlighted below:

    a. Random scission model

    b. Center scission model

    c. Unzipping scission model

13. After ensuring the above steps are successful, the next line of action is to conduct series of calculations as expressed in the governing equations (38-46) for the

breaking of the polymer chain based on the scission mode in question and afterwards generate a new DP or MW distribution (dw/dlogM vs MW).

14. After each counter for the number of scission, the number of molecule is increase by one. This is because for each counter in the number of scission one new molecule is expected to be formed and one scission is expected to take place.

15. Calculate the new total number of molecules and re-introduce the array of the number of molecule back into the module section of the scission mode in question and let another scission take place.

16. The next step is to generate a new molecular weight distribution.

17. This cycle maybe repeated as many times as possible in order to evaluate pattern of degradation and be able to connect these patterns with mode of scission.

18. Series of calculation conducted in the simulation is based on the Algebraic exact statistical method and according to Bose and Grit[61] it *"introduces a totally new approach to mathematically modeling of the degradation process with statistically perfect expected instant calculation of MWD without error or approximation"*.

The molecular weight distribution pattern obtain after a predetermine time interval for each cycle of degradation as coded in the simulation will be utilized as a fingerprint for the mode of scission displayed by the experimentally generated molecular weight distribution of hydrolyzed cellulose in the reactor.

6.3.3 Simulation Results and Discussion

Figure 68 unveils changing in the molecular weight distribution based on random scission. The counter for number of scission was set to 1000 and at every multiple of 100

a new molecular weight distribution emerges. As the number of scission increases, the peak average molecular weight decreases with increasing dw/dlogMW. The molecular weight distribution get narrower as more bonds are broken which then results in shifting the peak average molecular weight from an approximately value of 39000 Da to roughly 6336 Da. Simultaneously, a net increase in the number of polymer chains with molecular weight lower than 6336 Da was observed relative to initial distribution.

Figure 69 unveils changing in the molecular weight distribution based on random scission. The counter for number of scission was set to 500 and at every multiple of 50 a new molecular weight distribution emerges. The peak average molecular weight decreases as the number of scissions and dw/dlogMW increases. A lower amount of glucose and oligosaccharides relatively to what was produced in Figure 68 was observed. The molecular weight distribution pattern was similar to the distribution depicted in Figure 68 but the only difference is the resultant peak average molecular weights and their corresponding total mass (dw/dlogMW) which are observed to be respectively 100 % higher and 50 % lower than its counterpart in Figure 68.
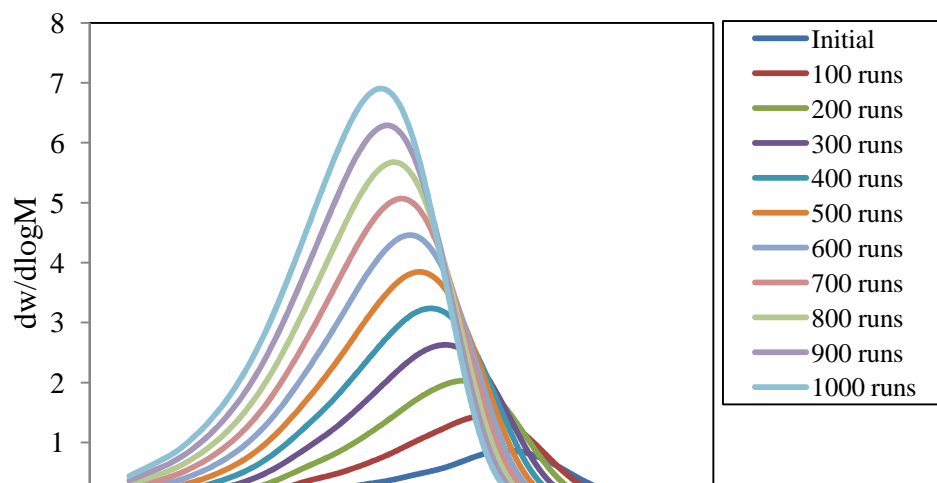
Figure 68. Random Scission -1000 simulated number of scissions
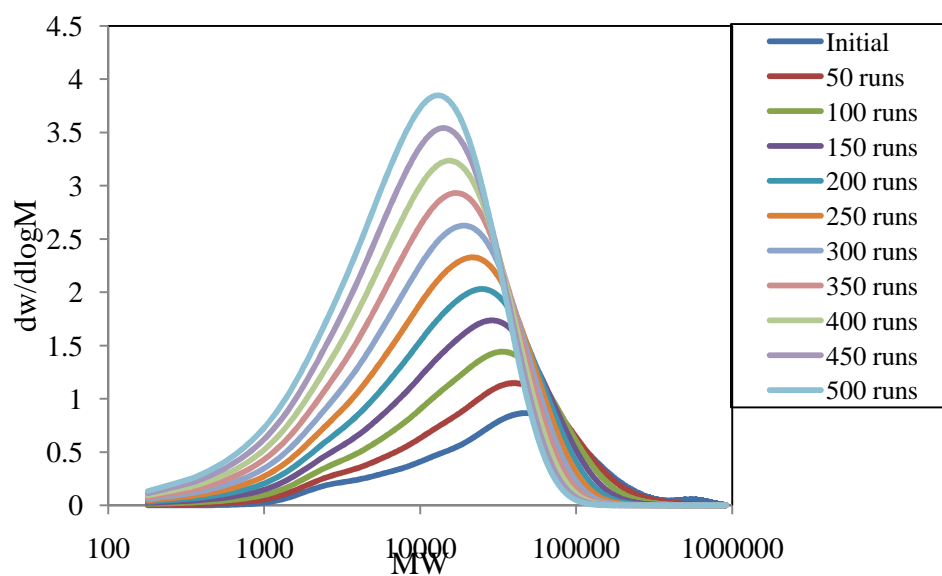
Figure 69. Random Scission -500 simulated number of scissions

Figure 70 unveils changing in the molecular weight distribution based on center scission. The counter for number of scission was set to 1000 and at every multiple of 100;

a new molecular weight distribution emerges. As the number of scissions increases, the distribution changes from a broader monomodal distribution to a bimodal distribution. The shape of the initial distribution started out with a monomodal distribution and as scission increases, the effect of the bimodality shape of the distribution becomes more apparent. The emerging peak averages MW on the medium end of the distribution decreases with increasing number of scissions while on the lower end, a constant peak average MW was observed at 180 Da (glucose). The differential weight fraction with respect to log of MW (dw/dlogMW) or the total mass increases with increasing scission number for both peaks, with maximum dw/dlogMW occurring at the peak average of roughly 1800 Da. Similar trend regarding the shape of the molecular weight distribution; variation of peak average molecular weight and dw/dlogMW with number of scission or runs was also observed in Figure 71. The only exception is the point at which peak average MW emerges on the distribution and the peak average at which maximum dw/dlogMW was obtained. The final bimodal peak average MW in Figure 71 occurs at 4554 Da and 180 Da.
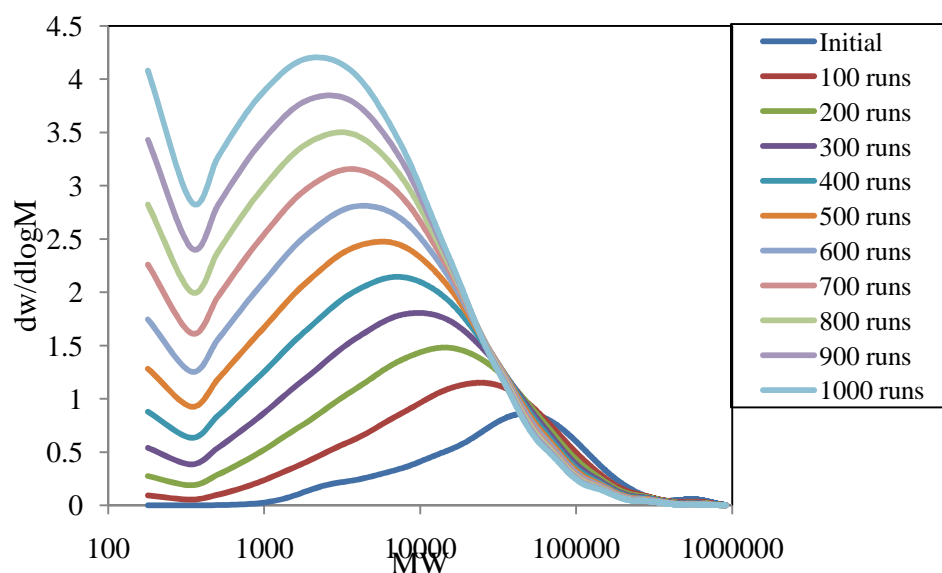
Figure 70. Center Scission -1000 simulated number of scissions
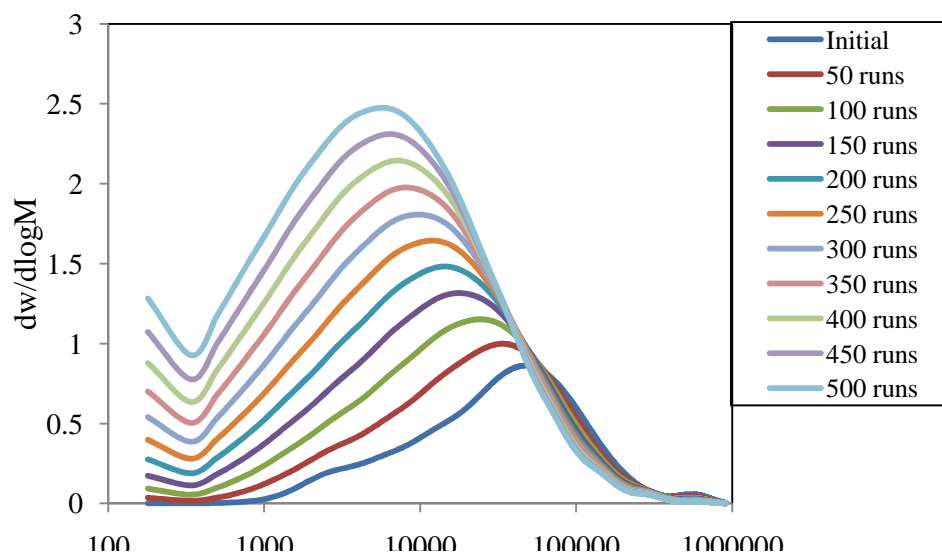
Figure 71. Center Scission- 500 simulated number of scissions

Figure 72 and 73 unveil changing in the molecular weight distribution based on unzip scission. The counter for number of scission was set to 1000 and 500 respectively and at every multiple of 100 and 50 a new molecular weight distribution emerges. As number of scission increases in Figures 72 and 73, a very slight change was observed in the MW distributions. The slight variation in the distribution is indicative of why the peak average molecular weight for the entire runs does change appreciably. One significant observation in the two distributions is the sizeable increase in the number of monomer molecules. Monomer generation is more pronounce for the 1000 scissions than the 500 scission and the reason is clear; more scissions more unzipping at the reducing ends for the former than the latter. The maximum dw/dlogMW obtain in Figure 72 is 0.83 at peak average molecular weight of roughly 44730 Da while maximum dw/dlogMW for the 500 simulated scissions is also 0.62 with peak average molecular weight of 38898 Da.
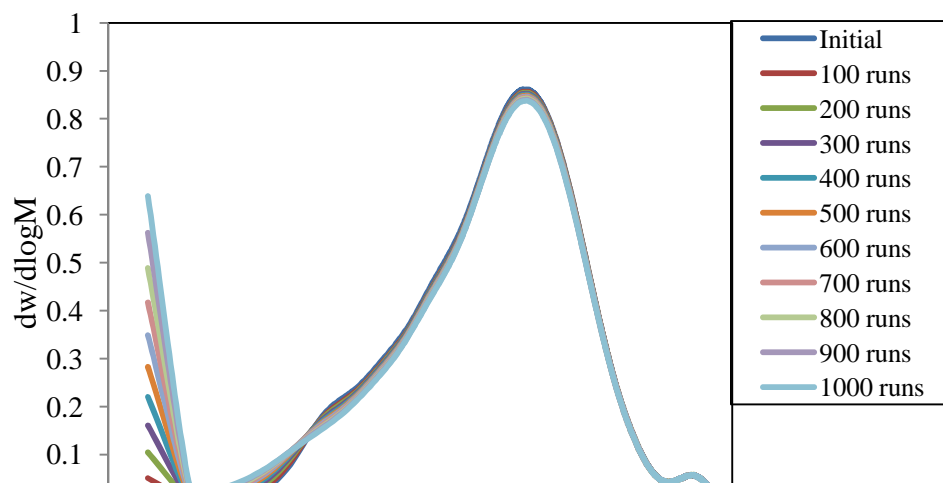
Figure 72. Unzip Scission- 1000 simulated number of scissions
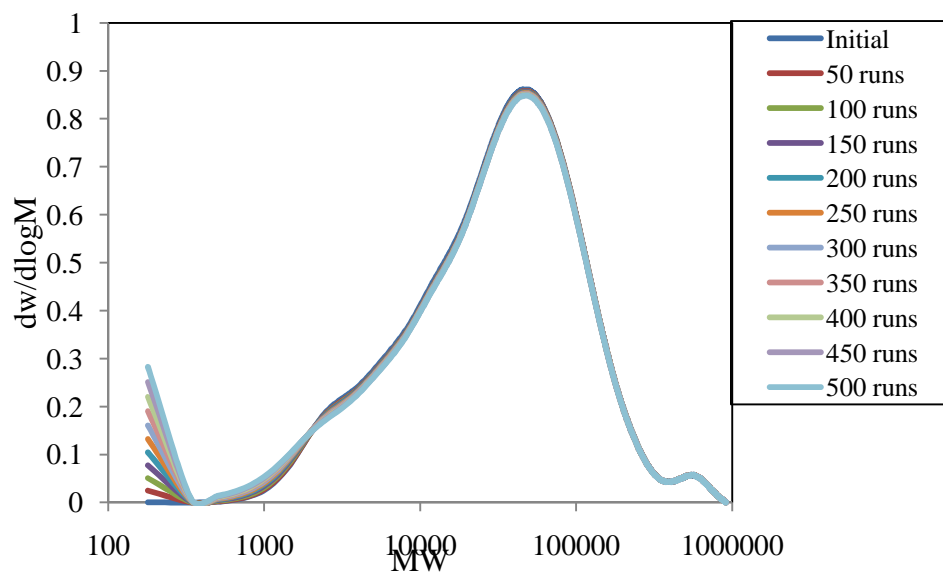
Figure 73. Unzip Scission- 500 simulated number of scissions

6.4 Comparison of the Degradation Pattern from Experiment and Simulation

This section compares the degradation pattern obtained from simulation with pattern generated from experiment. Since simulated pattern are based on a specific mode of scission, the goal is to see the possibility of fingerprinting the degradation pattern from experiment with the pattern generated from simulation. This approach is designed to establish the mode of scission characteristic of cellulose reaction in the hydrothermal system. Changes in the molecular weight distribution are largely due to alteration in the chain length of the various molecules in the distribution. The alteration can be by breaking the bonds or recombination of the bonds. In other words, changes in the number of bonds could be seen as directly related to changes in the molecular weight distribution. In view of this understanding, it is logical to use percent change in the number of bonds broken as a common criterion for comparison between simulated and experimentally generated pattern. Before finally delving into the comparison, some key observations in the course of the simulation need be stated to better understand why visually, the area of the simulated distribution appears bigger than the distributions from experiment.

a. The total mass (dw/dlogM) of the distribution from experiment is 643.31986 with an irregular stepsize increase in the MW of the polymer. The irregular stepsize differences in the MW or DP across the size range prohibit the simulation from breaking one single bond per run. Thus, for each scission, the number of molecule and the number of bonds are expected to increase and decrease by 1 respetively. But under this scenario, it is a different ball game as noted above in section 6.3.2.1.

b. To avoid the issue raised above, a smooth spline function was used to fit the initial distribution plot (MW vs dw/dlogM) so as to have a regular stepsize of 1 in the case of the DP and 162 in the case of MW. A perfect fit was generated with $R^2 = 1$. Thus, the number of molecule and the number of bonds, as expected, increases and decreases by 1 as noted in section 6.3.2.1. However, while trying to

resolve this problem, it is observed that extra DP or MW sizes of about 3600 were added which meant more masses to the whole distribution as a whole. The total mass (dw/dlogM) obtained from the fitted curve with DP ranging from 1 to 5636 and stepsize increase of 1 is 866.3658 Da. The difference in the total mass of the experimental distribution and the fitted distribution is 223.0459 Da. Worthy of note, is that, in the simulation, mass of water molecules which was inherently accounted for, was deducted from the total mass by the Matlab code shown below per scission or run:

```
dMH2O=(t*18/Mf)*(dw_dlogMW/sum(dw_dlogMW));
```

Where dMH2O is the accumulated mass of H2O per run; t is the number of run, Mf is the multiplication factor used for the number of molecules while dw_dlogMW is the same as dw/dlogM.

c. After addressing accumulated mass of water molecule, the sum total mass for each run which was 866.3658 Da, was observed constant throughout the simulation. After thorough review of the distribution pattern obtain from simulation vis-avis the distribution pattern from experiment, the relative larger plot from simulation is caused by the mass generated from the extra 3600 DPs obtained from the fitted distribution. Attempt was made to weightedly reduce the total mass of the fitted distribution from 866.36583 Da to 643.31986 Da but the plot obtained no longer reflects the same peak height and as such result in an R^2 of about 0.6. The plots of the experimental, fitted with total of 866.3658 Da and fitted with total mass of 643.31986 Da is shown in Figure 74.
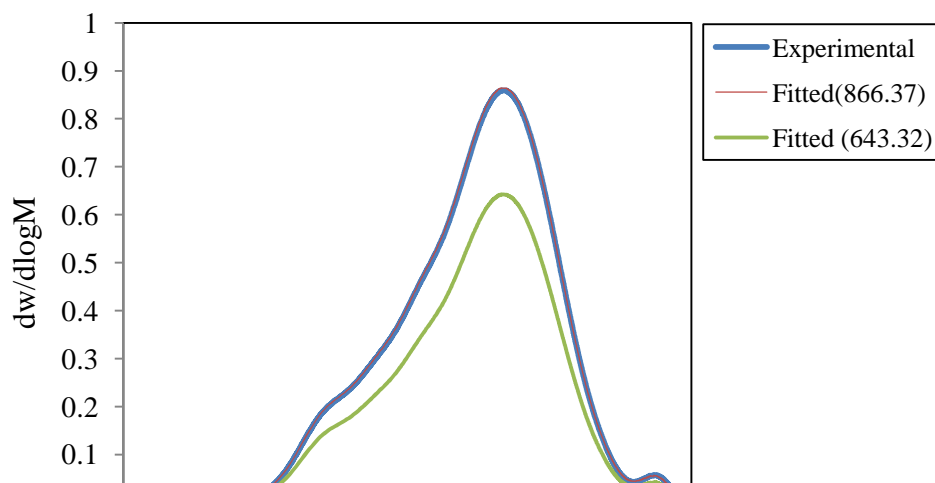
Figure 74. Plot of experimental, fitted (866.37), and fitted (643.32) distributions

d. Percentage bond broken was estimated based on Equation 59

$$Percent\ bond\ broken = \left(1 - \frac{N_{bt}}{N_{bi}}\right) * 100 \qquad (59)$$

Where N_{bt} is the number of bonds at run cycle t and N_{bi} is the initial total number of bonds.

Figure 75 depicts the molecular weight distributions for cellulose as received and cellulose residue obtained at 270 °C. The simulated pattern reflected on this same plot was generated based on random scission. The total number of bonds in the simulation is 53314 bonds and a bond is broken per run.The legend for the experimental distribution show the temperature, flow rates, and percent bonds broken as one word with dash in between. But for the simulation, it shows number of runs and percent bonds broken as one word with a dash in between also. The molecular weight distribution for the same percent bond broken on both sides of the aisles .i.e., experiment and simulation, were compare to observe their level of matchness in terms of shapes and pattern. Experimental distribution start off with the monomodal curve but as flow rates decreases and residence

time increases, more scission occur which thus lead to the shifting of the distribution to the lower end of the MW. However, as the scission increases, the shapes of the initial momodal distribution changes to a not-too visible bimodal distributions. On the simulation end, the initial monomodal distribution which gets narrower as the scission increases maintains it modality throughout the simulation. There is hardly any correlation in the molecular weight distribution pattern for the same percent bond broken with regards to the simulated and the experimentally pattern. The simulated patterns portray a higher differential weight fraction with respect to the molecular weight and a higher peak average MW than the experimentally generated pattern. This significant difference is as a result of the accumulation of more molecules generated based on DP accounted for in the simulation and not in the experiment. The DP considers in the simulation ranges from 1 to 5636 with one step increase while DP from the experiment ranges from 2.7 to 5721.6 with an irregular step-size increase and a size bins of about 2027. Thus, roughly 3600 more DPs were accounted for in the simulation than in the experiment. Based on these observations, simulated pattern obtained on the premise of random scission is far from modeling well the MW distribution pattern obtained from experiment.
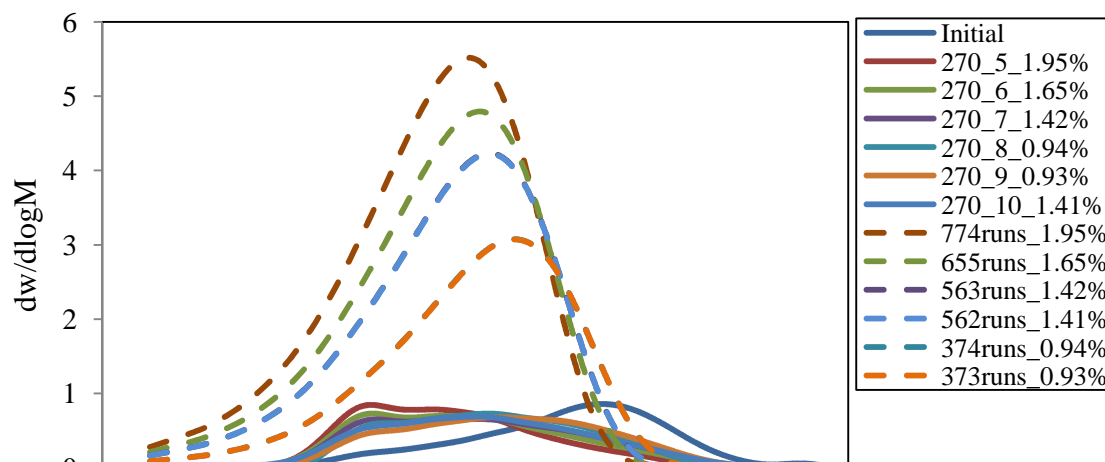
Figure 75. Experimental degradation pattern and simulated pattern based on random scission

Figure 76 depicts the molecular weight distributions for cellulose as received and cellulose residue obtained at 270 °C. The simulated pattern reflected on this same plot was generated based on center scission. One common observation is the shifting of the peak average molecular weight of the distribution to a much lower end of the MW. But one major difference is the difference in the differential weight fraction per MW (dw_dlogMW) and the peak average MW. The simulated pattern display a higher dw/dlogMW and peak average MW when compare with the distribution pattern obtain from experiment. This significant difference could be attributed to the same scenario observed under random scission. The shapes of the experimentally determined and simulated distributions differs with the former displaying a not-too apparent bimodal distribution as scission increases while the latter clearly show the emergence of bimodal type MW distributions as simulation runs proceed. With these changes in the shape and modality of the distribution for the same percent bond broken on the simulation and

experimental end, center scission also fail the test of fingerprinting the degradation pattern obtained from the experiment.
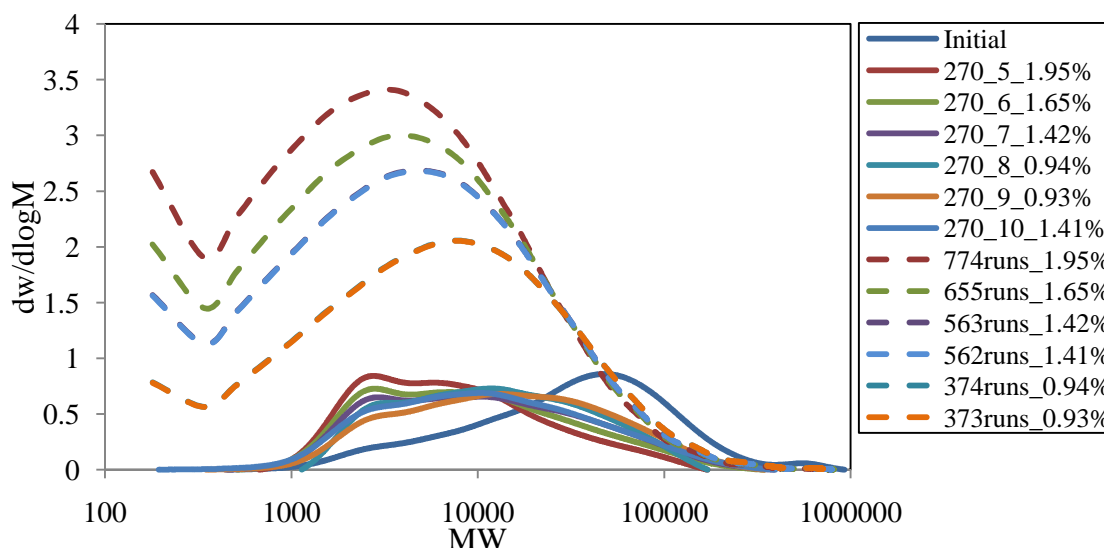
Figure 76. Experimental degradation pattern and simulated pattern based on center scission

Figure 77 depicts the molecular weight distributions for cellulose as received and cellulose residue obtained at 270 °C. The simulated pattern reflected on this same plot was generated based on unzip scission. As the scission increases (i.e increase in residence times), peak average MW in the distribution obtained from experiment shifted towards a lower MW end. However, the peak average MW on the simulation front virtually remains unchanged but with a very quasi-decrease in the height (dw/dlogM) of the plot as simulation runs progress. More so, monomer (glucose) concentration increases as scission increases. The shape of the experimentally determined distribution changes from unimodal distribution to bimodal distribution especially at 5 ml/min, 6 ml/min, and 7 ml/min but for the other flow rates, a slight multimodal curve appears emerging. The distribution evolving as simulation runs increase virtually remains the same though with

increasing glucose molecules spike. With these observations, unzip scission could also be seen as not helping the matter of establishing what scission is largely taking place in the hydrothermal reaction of cellulose.
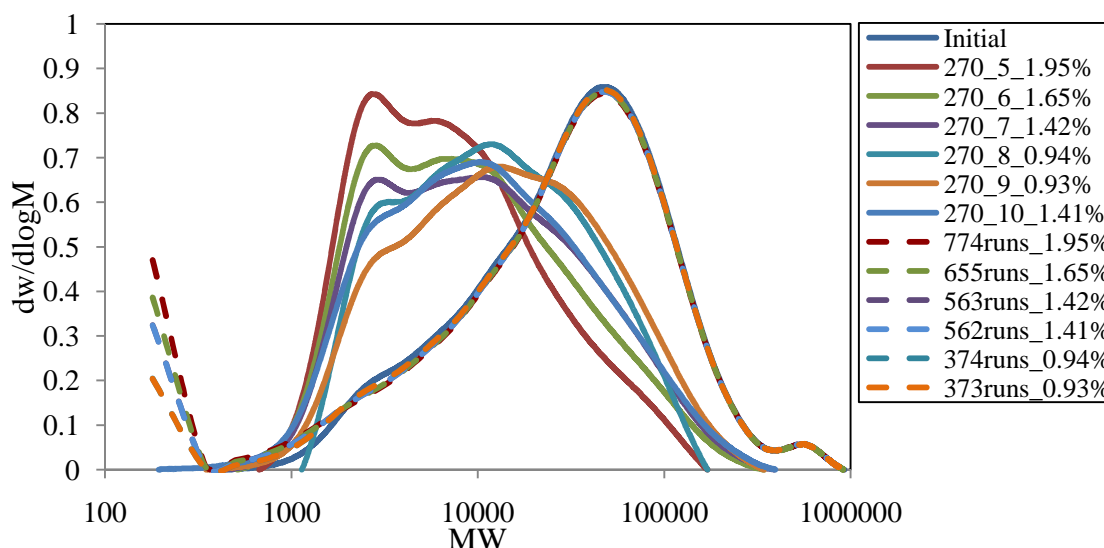
Figure 77.Experimental degradation pattern and simulated pattern based on unzip scission

6.5 Conclusions

Molecular weight distribution changes when bonds are broken. In this study, SEC was used to analyze the molecular weight distribution obtained from hydrolysis of crystalline cellulose in the hydrothermal system at temperatures ranging from 270 °C to 300 °C and at a pressure 5000 psig. The flow rates consider in this analysis range from 5 ml/min to 10 ml/min. Divers molecular weight distribution patterns emerge as operating conditions such as residence time and temperature change. On the other hand, raw molecular weight distribution data obtained from experiment was fed into a simulation environment to evaluate the effect of random, center and unzip scission on the distribution. The simulation were coded in Matlab and algebraic statistical formulations

were used to evaluate the different mode of scissions (random, center, unzip). Unique molecular distribution patterns were displayed by the different mode of scissions. It is observed that none of the molecular weight distributions obtained based on the different modes of scission was able to fingerprint the corresponding MW distributions obtained from the experiment. The shrinking effect of crystalline cellulose in subcritical water may affect proper representation of the different sizes of the cellulose chains in the molecular weight distribution from experiment. As a result, molecular weight distribution from experiment may be at a disadvantage for reasonable correlation with molecular weight distributions from simulation.

CHAPTER 7. IMPACT AND FUTURE WORK

The enormous availability of cellulosic biomass is increasingly gaining interest from both public and private organizations as a viable alternative to the current biofuel feedstocks. Government and private sectors are putting initiatives and programs in place to investigate ways of utilizing this rife organic matter with a view to promoting economic growth. One of such is the advanced biofuel initiative which is focus at exploring range of technologies for converting cellulosic biomass to fuel and chemicals. But the major reason why some are still skeptical of its potential to compete in a hydrocarbon-based economy is due to its recalcitrant nature which still remains an issue that must be thoroughly addressed. To address it will mean to come up with an effective pretreatment method, plausible degradation techniques and understanding its reactive mechanism at the morphologic level. The latter reason seems to be the most interesting and the most important of the three and why? It addresses the root cause of the problem: cellulose recalcitrance.

This work emphasizes the reaction kinetics of cellulose conversion which is very critical in designing a reaction pathway that can better optimized glucose production. Conventional method has been to thermally pretreat cellulosic biomass before hydrolytic degradation in enzymes[10]. In a complete thermo-transformation process, with subcritical and supercritical as reacting media, dissolution and hydrolysis of cellulosic biomass could be achieve under a very short time window unlike enzymatic degradation. Moreover, decomposition of hydrolysate is less pronounced than its formation in subcritical water, therefore dissolved cellulose in subcritical water gives a better glucose selectivity and yield than in supercritical water[14]. Two steps were involved in the

homogeneous conversion of crystalline cellulose to fermentable sugars. The steps are dissolution and hydrolysis. In this work, it has been established that the conversion of cellulose both in subcritical and supercritical water is limited by the concurrent reactions of hydrolysis and dissolution. This understanding is very useful in the optimization of target products such as glucose and also providing better control over product that may be inhibitory to the production of biofuel feedstock.

However, mode of scission of cellulose in a hydrothermal reactor unlike any other reacting media such as enzymatic and acidic media still appear complicated without a modeling tool that will predict its pattern of degradation within high temperature and high pressure environment. As a macromolecule compound, cellulose is better characterized by its molecular weight distribution. Therefore degradation of cellulose in any media is depicted strongly by pattern with which its molecular weight is being distributed at the different time interval. Range of molecular weight distribution pattern of cellulose residue obtained in a hydrothermal system has been conducted. Also addressed is the simulation of the changes in the molecular weight distribution due to the different mode of scission. There has not been any extensive work perform on this subject matter until now. This research project will remain one of its kinds and can also be consider a very good resource for any further work on the degradation pattern of cellulose in a hydrothermal system.

Detail work was conducted on the simulation aspect of the degradation pattern of bioorganic polymer such as cellulose in hydrothermal media. This facilitate our understanding of the degradation of cellulose in a hydrothermal media and invariably offers us pattern that can be utilized as tools to fingerprint[61] mode of scission in this

environment. It was established that none of the mode of scissions (random, center, unzip) was able to fingerprint the degradation pattern obtained from the experiment. The shrinking effect of crystalline cellulose in subcritical water may affect proper representation of the different sizes of the cellulose chains in the molecular weight distribution from experiment. Thus, further studies should be conducted to investigate the effect of shrinking core model on the molecular weight distribution of crystalline cellulose after hydrolysis.

Finally, Hydrothermolytic degradation of cellulose in subcritical and supercritical is energy intensive. Thus, improved understanding of the reaction kinetics, products distribution at the different critical temperatures, degradation pattern and mode of scission will aid the development of a comprehensive kinetics model and also help in designing an efficient reactor system that minimize cost (energy) and maximize yield of target product such as glucose and other valuable precursors in the emerging bioeconomy.

APPENDIX A: RATE CONSTANTS FOR THE ARRHENIUS PLOTS

SURFACE HYDROLYSIS IN SUBCRITICAL WATER	
Temperature(K)	Rate Constants (s^{-1})
543.150	0.210
553.150	0.246
563.150	0.436
568.150	0.597
573.150	0.510
593.150	1.285
GLYCOSIDIC BONDS HYDROLYSIS IN SUBCRITICAL WATER	
DP_v from Dilute Solution Viscometry	
Temperature(K)	Rate Constants (s^{-1})
543.150	0.450
553.150	0.555
563.150	1.060
568.150	1.708
573.150	1.174
GLYCOSIDIC BONDS HYDROLYSIS IN SUBCRITICAL WATER	
DP_v from Size Exclusion Chromatography	
Temperature(K)	Rate Constants (s^{-1})
543.150	0.449
553.150	0.571
563.150	1.069
568.150	1.176
573.150	1.324
CONVERSION OF CELLULOSE IN SUPERCRITICAL WATER	
Temperature(K)	Rate Constants (s^{-1})
647.150	11.010
651.150	14.318
653.150	14.352
655.150	20.483
661.150	28.147
663.150	34.451

APPENDIX B. CALIBRATION CURVE FOR THE PULLULAN

STANDARD

Retention time	Peak Average Molecular Weight of
	Pullulan
5.596	200000
5.833	107000
6.198	47100
6.248	36000
6.571	21100
6.874	11100
7.138	5900
8.185	667
8.822	180
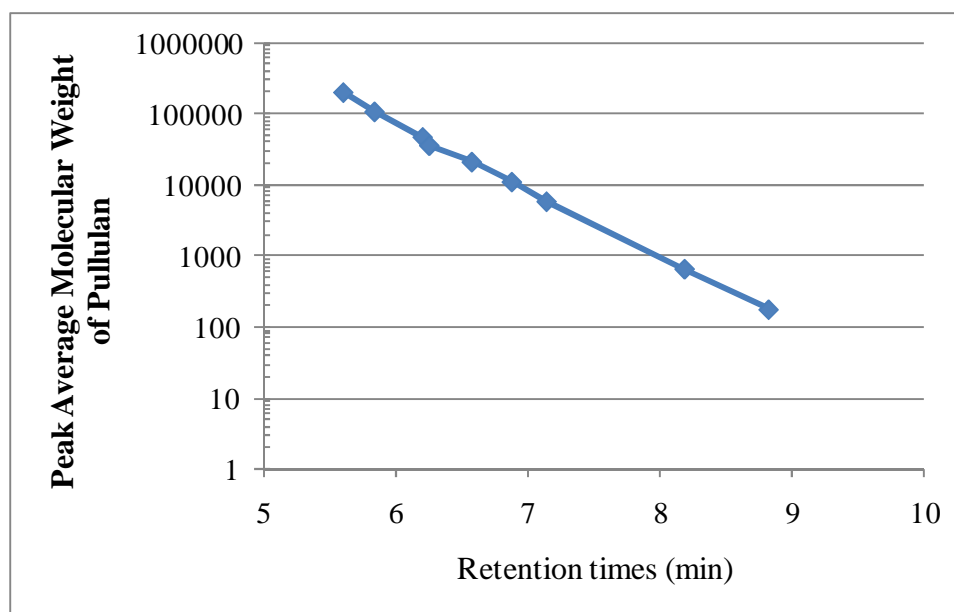
APPENDIX C: MATLAB CODE FOR THE ALGEBRAIC EXACT

STATISTICAL SIMULATION

```
close all
clear all




% Importing data from Excel file: DP_cellulose_from_experiment.xlsx
%=======================================================================
====
% Molecular weight :
 MW=
xlsread('C:\MATLAB\DP_cellulose_from_experiment','sheet3','BE127:BE5762
'); %sheet 1

%Normalized height: Weight fraction of each MW in the distribution
NH =
xlsread('C:\MATLAB\DP_cellulose_from_experiment','sheet3','AX127:AX5751
');% sheet 1

% Sum of all Molecular Weight
SWM = sum(MW);

%Chromotogram
%========================
Chromresp=xlsread('C:\MATLAB\DP_cellulose_from_experiment','sheet3','AW
127:AW5762');% sheet1

Mf=1E4;

% Simulated Data
%===========================
% Number of molecules for each Molecular Weight in the Distribution
d
=xlsread('C:\MATLAB\DP_cellulose_from_experiment','sheet3','BG127:BG576
2')*Mf;


%initial_d
initial_d=d;


% Array of DP generated from Experiments
%=====================================
DP = ((MW)-18)/162;
x=DP;
```

```
testDP=DP;
pause on
warning off

%Counter for number of runs: scissions
%======================================
dc=1E4; % dcc is dc counter
cystp=1E3; % cycle step ( for the mod function) for plotting every
"cystp"


iDP=DP;
plotlabel={'-r' '-b' '-r' '--r' '--k' '-k' '-g' '--g' '-m' '-y' '--y'};
plotlabel_run={'Initial' 'plot1' 'plot2' 'plot3' 'plot4' 'plot5'
'plot6'...
    'plot7' 'plot8' 'plot9' 'Final'};
lg=1; % legend indices for plotlabel
lw=1;
lk=1;
lh=1;




%Mode of scission options:
random_scission=0;
center_scission=1;
unzip_scission=0;
percent_cut_scission=0;

%Plotting chromatogram
%=========================================
figure(1)
semilogx(MW,Chromresp);
title('Chromatogram response vs MW');
xlabel('MW');
ylabel('mV');


%pause
%TN1=sum(d); % Affirming the Total number of molecules
TN=sum(d);
%pause


 % Initial total number of bonds
 inumbond=sum((DP-1).*d);

figure(2)
semilogx(MW,d);
title('Experimental MW Distribution ');
xlabel('MW');
ylabel('# of Molecules');
%hold on
```

```matlab
%number average degree polymerization or average bond length
n_average(1)=(sum(DP.*d)/sum(d));




% Calibration equation from experiment is of the form logMW = A + Bv;
% where: A and B are intercept and gradient respectively; v is elution
volume;
% dv/dlogMW equals the reciprocal of the gradient (constant- linear)
% therefore to obtain dw/dlogMW, we multiply dw/dv with dv/dlogMW
% dw/dlogMW = dw/dv * dv/dlogMW
%dv_dlogMW = 643;

%dw_dlogMW = dw_dv*dv_dlogMW;
dw_dlogMW =
xlsread('C:\MATLAB\DP_cellulose_from_experiment','sheet3','BF127:BF5762
'); %sheet 1;
ini_dw_dlogMW=dw_dlogMW;

ChromrespE=flipud(xlsread('C:\MATLAB\DP_cellulose_from_experiment','she
et4','C101:C2333'));
MWE=
flipud(xlsread('C:\MATLAB\DP_cellulose_from_experiment','sheet4','F101:
F2333'));
dw_dlogMWE=
flipud(xlsread('C:\MATLAB\DP_cellulose_from_experiment','sheet4','G101:
G2333'));

figure(3)
semilogx(MW,dw_dlogMW,'--b')%,plotlabel{lh})%'-g')%,DP,d,'-b');
%title(strcat('DP Distribution after Scission (random)',numberm_str));
xlabel('MW');
ylabel('dw/dlogMW');
hold on



%initial_d
initial_d=d;

% Number average MW:
iMn=sum(d/Mf.*MW)/sum(d/Mf);

% DPn
iDPn = (iMn-18)/162;

dw_dlogMWA=dw_dlogMW;
countd=d;
% Percentage number of bonds broken
Theoreticalpercent_bond_broken=(dc/inumbond)*100;

imassmonomer=sum((DP).*d);

%d=Sd;
```

```
m=1;
% DP with number of molecules > zero
%DP=[DP(6:end)];
%MW=MW-18;

% POLYMER DEGRADATION SECTION
%==========================================

%(1) Random scission:
%*****************************************
% dc : degradation cycle
if random_scission ==1
%dc=1;
fprintf('=================================');
fprintf('\nRunning random scissioning');
fprintf('\n=================================\n');
% DP is the degree of polymerization

mkdir('C:\MATLAB','Random_scission');
randomscission_files=('C:\MATLAB\Random_scission');

mkdir('C:\MATLAB','Random_scission_rawdata');
randomscission_rawdata=('C:\MATLAB\Random_scission_rawdata');


% DP=M/162;
to=0; % to : initial t
% step1 : randomly select a polymer chain for scissioning:
for t=1:dc

    % Calculating total number of bonds
    sTb=sum((DP-1).*d);



    % Checking number of bonds at every cycle
    CsTb(t)=sum((DP-1).*d);

    percentscissioned(t)=((inumbond-CsTb(t))/inumbond)*100;
    %sTb=sum(d)-d(1);
    clear r;

    %pause on

    % Probability based on number of bonds
    % Solving for probability for all DP sizes
    P=((DP-1).*d)/sTb; % Probability , P



    %Pini=initial_d./sum(initial_d);
    %P= d./sum(d);
```

```matlab
        % number of bonds as degradation progresses
        numbond=sum((DP-1).*d);
        massmonomer=sum((DP).*d);


        CP=vertcat(Chromresp,d,DP);



        for n=1:length(DP) %2<n<N



            if n==1
                sTbK=sum((DP(2:end)-1).*d(2:end));

                % Solving for P(k,t)
                Pk=((DP(2:end)-1).*d(2:end))/sTb;

                % Solving for sum of 2P(k,t)/k-1, range k=2 to N --Max(DP)
                Sk=sum(2*Pk./(DP(2:end)-1));

                % Equation for when n=1
                dt(n)= d(n) + Sk;


            elseif n==max(DP)

                 % Equation for when n=N
                dt(n)= d(n)-P(n);

            elseif n~=1 && n~=max(DP)


                %P(n) =((n-1)*d(n))/(sTb)  %P(n,t);
                k=n+1;

                %P=((DP-1).*d)/sTb; % Probability ,P
                sTbk=sum((DP(k:end)-1).*d(k:end));

                % Solving for P(k,t)
                pk=((DP(k:end)-1).*d(k:end))/sTb;

                % Solving for sum of 2P(k,t)/k-1, range k=n+1 to N --
Max(DP)

                sk=sum(2*pk./(DP(k:end)-1));

                % Equation for when 1<=n<=N
                dt(n)= d(n)-P(n) + sk;


            end
```

```
end
m=m+1;


d=dt'; % array of new values for the number of molecules
Number_m1(:,t)=d;

% Solving MW based response and number of molecules
%MW=Chromresp/d;

%MW=MW-18;

 %Number average MW:
Mn(t)=sum((d/Mf).*MW)/sum(d/Mf);

%Weight average MW:
Mw(t)=sum(d/Mf.*MW.^2)/sum(d/Mf.*MW);

% DPn
DPn(t) = (Mn(t)-18)/162;

% Percentage of average bonds broken
Percent_bond_broken(t) = ((iMn-Mn(t))/iMn)*100;

fracbondbroken(t)=((inumbond-CsTb(t))/inumbond)*100;


%Weight fraction in Dp
wt_frac=(DP.*d/Mf)/sum(DP.*d/Mf);


%Weight fraction in Mw
Mwt_frac=((DP*162+180).*d)/sum((DP*162+180).*d);

% Normalized height h/total_h also refers to dw/dv
dw_dv=(d.*MW)/sum(d.*MW);

%dw_dv=(NMW)/sum(NMW);
%dw_dv=Mwt_frac;

% Calibration equation from experiment is of the form logMW = A +
Bv;
% where: A and B are intercept and gradient respectively; v is
elution volume;
% dv/dlogMW equals the reciprocal of the gradient (constant-
linear)
% therefore to obtain dw/dlogMW, we multiply dw/dv with dv/dlogMW
% dw/dlogMW = dw/dv * dv/dlogMW


%
dw_dlogMW = MW.*(d/Mf);
```

```matlab
% Mass of accumulated water molecules
%=========================================================
dMH20=(t*18/Mf)*(dw_dlogMW/sum(dw_dlogMW));


%Deducting mass of accumulated water molecules from the total mass in
%the distribution as scission increases
%================================================================
dw_dlogMW=dw_dlogMW-dMH20;

%dw_dlogMW=dw_dlogMW-dSEM;

dw_dlogMWA(1:end,t)=dw_dlogMW;
countd(1:end,t)=d;




xlcol={'B' 'C' 'D' 'E' 'F' 'G' 'H' 'I' 'J' 'K' 'L' 'M' 'N' 'O' 'P' 'Q'};
xlcol_num=2:5636;

if mod(t,cystp)==0 %|| %t==1


    figure(3)
    %semilogx(MW,wt_frac,plotlabel{lh})%'-g')%,DP,d,'-b');
    semilogx(MW,dw_dlogMW,plotlabel{lh})%'-g')%,DP,d,'-b');
    %title(strcat('DP Distribution after Scission
(random)',numberm_str));
    xlabel('MW');
    ylabel('dw/dlogMW');
    legend(plotlabel_run);
    hold on
    %figname=strcat('random',numberm_str);
    cd(randomscission_files);
%       saveas(gcf, figname, 'pdf');
%       saveas(gcf, figname, 'fig');
%       saveas(gcf, figname, 'jpeg');
   % MW
    % Storing data in Excel
    %==============================
    %dw_dlogMW_SUCCESS =
xlswrite('C:\MATLAB\Random_scission_rawdata\Randomscissiondata.xlsx',dw
_dlogMW,'dw_dlogMW5000_500AA',...
    %
strcat(xlcol{lh},num2str(xlcol_num(1)),:,xlcol{lh},num2str(xlcol_num(56
24))));
    %MW_SUCCESS =
xlswrite('C:\MATLAB\Random_scission_rawdata\Randomscissiondata.xlsx',MW
,'dw_dlogMW5000_500AA','A2:A5625');
```

```matlab
        %=================================================
        lh=lh+1;
        %hold off


%
        figure(4)
        semilogx(DP,wt_frac,plotlabel{lg})%'-g')%,DP,d,'-b');
        %title(strcat('DP Distribution after Scission
(random)',numberm_str));
        xlabel('DP');
        ylabel('Weight Fraction');
        legend(plotlabel_run);
        hold on
        %figname=strcat('random',numberm_str);
        cd(randomscission_files);
%         saveas(gcf, figname, 'pdf');
%         saveas(gcf, figname, 'fig');
%         saveas(gcf, figname, 'jpeg');

%         %Storing data in Excel
%         ==============================
%         WTFRAC_SUCCESS = xlswrite('C:\Users\Kazeem\Documents\My
Documents\MATLAB\Random_scission_rawdata\Randomscissiondata.xls',wt_fra
c','weightfraction',...
%
strcat(xlcol{lg},num2str(xlcol_num(1)),:,xlcol{lg},num2str(xlcol_num(en
d))));
%         DP_SUCCESS = xlswrite('C:\Users\Kazeem\Documents\My
Documents\MATLAB\Random_scission_rawdata\Randomscissiondata.xls',DP,'w
eightfraction','A2:A454');
%         %=================================================
         lg=lg+1;
        %hold off



%
    end

    %MW=NMW;

    TN(t)=sum(d); % Caculating the new total number of molecues after
each cycle
    %d=TN*Probdf;
    %pause(4)

end



cd('..');

% clear i j
```

```
end

%% center scission session
%=========================================
%%(2)center scission:
%*****************************************
%polymer chain to be scissioned at the center
%%====================================================================
=====

% dc : degradation cycle
if center_scission==1
%dc=1;
% DP is the degree of polymerization
%dc=1;
fprintf('==================================');
fprintf('\nRunning center scissioning');
fprintf('\n==================================\n');
% DP is the degree of polymerization

mkdir('C:\MATLAB','Center_scission');
centerscission_files='C:\MATLAB\Center_scission';

mkdir('C:\MATLAB','Center_scission_rawdata');
randomscission_rawdata=('C:\MATLAB\Center_scission_rawdata');


% DP=M/162;
to=0 % to : initial t
% step1 : randomly select a polymer chain for scissioning:
for t=1:dc

    % Calculating total number of bonds
    sTb=sum((DP-1).*d);



    % Checking number of bonds at every cycle
    CsTb(t)=sum((DP-1).*d);
    %sTb=sum(d)-d(1);
    clear r;

     % Average bond length per cycle: DP(1:10) are molecules assume to
be
     % soluble in solvent(water) at room condition

    n_average(t+1)=(sum(DP.*d)/sum(d))-(sum((DP(1:10)-
1).*d(1:10)))/sum(d(1:10));


    % Probability based on number of molecules of a particular size(DP)
    % over total number of molecules
    %P= d./(TN1-d(1));
```

```
pause off

% Probability based on number of bonds
% Solving for probability for all DP sizes
%P=((DP-1).*d)/sTb; % Probability , P

% Probability based on chain length
%P=d/(TN-d(1));
%P(n) =((n-1)*d(n))/(sTb)  %P(n,t);

% number of bonds as degradation progresses
numbond=sum((DP-1).*d);

%P=((DP-1).*d)/sTb; % Probability , P


%CP=vertcat(Chromresp,P,d,DP);


for n=1:length(DP) %2<n<N


    if n==1
        sTbK=sum((DP(2:end)-1).*d(2:end));

        % Solving for P(k,t)
        %Pk=((DP(2:end)-1).*d(2:end))/sTb;

        % Solving for P(k,t)
        Pk=d(2:end)/(TN-d(1));

        % Solving for sum of 2P(k,t)/k-1, range k=2 to N --Max(DP)
        Sk=sum(2*Pk./(DP(2:end)-1));

        % Equation for when n=1
        dt(n)= d(n) + Sk;


    elseif n==max(DP)

         % Equation for when n=N
        dt(n)= d(n)-P(n);

    elseif n~=1 && n~=max(DP)

        %P(n) =((n-1)*d(n))/(sTb)  %P(n,t);
        k=n;

        sTbk=sum((DP(k:end)-1).*d(k:end));

        %P=((DP-1).*d)/sTb; % Probability , P
```

```
        P=d/(TN-d(1)); % Probability , P

        % Solving for P(2n-1,t)
        if k<=median(DP)
            %p2n11(n)=(((((2*n)-1)-1)*d((2*k)-1))/sTb;
            p2n11(n)=d((2*k)-1)/(TN-d(1));
        else
            p2n11(n)=0;
        end

        % Solving for P(2n,t)
        if k<=median(DP)-1
            %p2n12(n)=(((2*n)-1)*d(2*k))/sTb;
            p2n12(n)=d(2*k)/(TN-d(1));
        else
            p2n12(n)=0;
        end


        % Solving for P(2n+1,t)
        if k<=median(DP)-1
            %p2n13(n)=(((((2*n)+1)-1)*d((2*k)+1))/sTb;
            p2n13(n)=d((2*k)+1)/(TN-d(1));
        else
            p2n13(n)=0;
        end

        % Equation for when 1<=n<=N
        dt(n)= d(n)-P(n) + p2n11(n) + 2*p2n12(n) + p2n13(n);

    end



end

d=dt'; % array of new values for the number of molecules
Number_m1=d;

% Solving MW based response and number of molecules
%MW=Chromresp/d;

%Number average MW:
Mn(t)=sum(d/Mf.*MW)/sum(d/Mf);

% DPn
DPn(t) = (Mn(t)-18)/162;

% Percentage of average bonds broken
Percent_bond_broken(t) = ((iMn-Mn(t))/iMn)*100;
```

```matlab
        fracbondbroken(t)=((inumbond-CsTb(t))/inumbond)*100;




        %Weight fraction
        wt_frac=(DP.*d)/sum(DP.*d);

        % Normalized height h/total_h also refers to dw/dv
        dw_dv=(d.*MW)/sum(d.*MW);

        %dw_dv=Mwt_frac;

        % Calibration equation from experiment is of the form logMW = A +
Bv;
        % where: A and B are intercept and gradient respectively; v is
elution volume;
        % dv/dlogMW equals the reciprocal of the gradient (constant-
linear)
        % therefore to obtain dw/dlogMW, we multiply dw/dv with dv/dlogMW
        % dw/dlogMW = dw/dv * dv/dlogMW
 %
        dw_dlogMW = MW.*(d/Mf);


        % Mass of accumulated water molecules
        %==========================================================
        dMH20=(t*18/Mf)*(dw_dlogMW/sum(dw_dlogMW));


        %Deducting mass of accumulated water molecules from the total mass
in
        %the distribution as scission increases
        %===========================================================
        dw_dlogMW=dw_dlogMW-dMH20;

        %dw_dlogMW=dw_dlogMW-dSEM;

        dw_dlogMWA(1:end,t)=dw_dlogMW;
        countd(1:end,t)=d;

    xlcol={'B' 'C' 'D' 'E' 'F' 'G' 'H' 'I' 'J' 'K' 'L' 'M' 'N' 'O' 'P'
'Q'};
    xlcol_num=2:5636;

    if mod(t,cystp)==0 || t==1
        figure(3)
        semilogx(MW,dw_dlogMW,plotlabel{lh})%'-g')%,DP,d,'-b');
        %title(strcat('DP Distribution after Scission
(random)',numberm_str));
        xlabel('MW');
        ylabel('dw/dlogMW');
        legend(plotlabel_run);
        hold on
```

```
%           figname=strcat('center',numberm_str);
            cd(centerscission_files);
%           saveas(gcf, figname, 'pdf');
%           saveas(gcf, figname, 'fig');
%           saveas(gcf, figname, 'jpeg');
%
          % Storing data in Excel
          %==============================
          dw_dlogMW_SUCCESS =
xlswrite('C:\MATLAB\Center_scission_rawdata\Centerscissiondata.xlsx',dw
_dlogMW,'dw_dlogMW5000_500',...

strcat(xlcol{lh},num2str(xlcol_num(1)),:,xlcol{lh},num2str(xlcol_num(56
24)))));
          MW_SUCCESS =
xlswrite('C:\MATLAB\Center_scission_rawdata\Centerscissiondata.xlsx',MW
,'dw_dlogMW5000_500A','A2:A5625');
          %===============================================
          lh=lh+1;
          %hold off

%

    end


    %TN(dc)=sum(d); % Caculating the new total number of molecues after
each cycle
    TN=sum(d);
    TN1(t)=sum(d);
    %d=TN*Probdf;
    %pause(4)

end



cd('..');

% clear i j

end

%% unzip scission session
%=========================================
%%(2)unzip scission:
%*****************************************
%polymer chain to be scissioned at the end (reducing end)
%%=======================================================================
=====

% dc : degradation cycle
if unzip_scission==1
```

```
%dc=1;
% DP is the degree of polymerization
%dc=1;
fprintf('==================================');
fprintf('\nRunning unzip scissioning');
fprintf('\n==================================\n');
% DP is the degree of polymerization
mkdir('C:\MATLAB','Unzip_scission')
unzipscission_files='C:\MATLAB\Unzip_scission';

mkdir('C:\MATLAB','Unzip_scission_rawdata');
randomscission_rawdata=('C:\MATLAB\Unzip_scission_rawdata');




% DP=M/162;
to=0 % to : initial t
% step1 : randomly select a polymer chain for scissioning:
for t=1:dc

    % Calculating total number of bonds
    sTb=sum((DP-1).*d);



    % Checking number of bonds at every cycle
    CsTb(t)=sum((DP-1).*d);
    %sTb=sum(d)-d(1);
    clear r;

     % Average bond length per cycle: DP(1:10) are molecules assume to
be
     % soluble in solvent(water) at room condition

    n_average(t+1)=(sum(DP.*d)/sum(d))-(sum((DP(1:10)-
1).*d(1:10)))/sum(d(1:10));


    % Probability based on number of molecules of a particular size(DP)
    % over total number of molecules
    %P= d./(TN1-d(1));

    pause off

    % Probability based on number of bonds
    % Solving for probability for all DP sizes
    %P=((DP-1).*d)/sTb; % Probability , P

    %P=d/(TN-d(1)); % Probability based on chain length , P


    % number of bonds as degradation progresses
```

```
    numbond=sum((DP-1).*d);


    % unzipping involves scissioning of  z-mer(s) such as monomer,
dimers,etc
    % at either end of the polymer chain
    % selection of arbitrary z-mers that one desire to scission at
either
    % end of the polymer chain
    z=1;
    az=num2str(z);
    %CP=vertcat(Probdf,P,d,DP);
    %CP=vertcat(Chromresp,P,d,DP);

    for n=1:length(DP) %2<n<N

        if n==1
            sTbK=sum((DP(2:end)-1).*d(2:end));

            % Solving for P(k,t)
            %Pk=((DP(2:end)-1).*d(2:end))/sTb;

            % Solving for P(k,t)
            Pk=d(2:end)/(TN-d(1));

            % Solving for sum of 2P(k,t)/k-1, range k=2 to N --Max(DP)
            Sk=sum(2*Pk./(DP(2:end)-1));

            % Equation for when n=1
            dt(n)= d(n) + Sk;

        elseif n==max(DP)

             % Equation for when n=N
            dt(n)= d(n)-P(n);

        elseif n~=1 && n~=max(DP)


            %P(n) =((n-1)*d(n))/(sTb)  %P(n,t);
            k=n;

            sTbk=sum((DP(k:end)-1).*d(k:end));

            %P=((DP-1).*d)/sTb; % Probability , P
            P=d/(TN-d(1)); % Probability , P


            % Solving for P(n+z,t)
            if k<=max(DP)-z && k>z
                %pnz(n)=(((n+z)-1)*d(n+z))/sTb;
                pnz(n)=d(n+z)/(TN-d(1));
            else
```

```matlab
                    pnz(n)=0;
                end


                % Equation for when 1<=n<=N
                dt(n)= d(n)-P(n) + pnz(n);

            end




    end

    d=dt'; % array of new values for the number of molecules
    Number_m1=d;

    % Solving MW based response and number of molecules
    %MW=Chromresp./d;

    %Weight fraction
    wt_frac=(DP.*d)/sum(DP.*d);

     %Number average MW:
    Mn(t)=sum(d/Mf.*MW)/sum(d/Mf);

    % DPn
    DPn(t) = (Mn(t)-18)/162;

    % Percentage of average bonds broken
    Percent_bond_broken(t) = ((iMn-Mn(t))/iMn)*100;

    fracbondbroken(t)=((inumbond-CsTb(t))/inumbond)*100;




    % Normalized height h/total_h also refers to dw/dv
    dw_dv=(d.*MW)/sum(d.*MW);


    %dw_dv=Mwt_frac;

    % Calibration equation from experiment is of the form logMW = A +
Bv;
    % where: A and B are intercept and gradient respectively; v is
elution volume;
    % dv/dlogMW equals the reciprocal of the gradient (constant-
linear)
    % therefore to obtain dw/dlogMW, we multiply dw/dv with dv/dlogMW
    % dw/dlogMW = dw/dv * dv/dlogMW
%       %
     dw_dlogMW = MW.*(d/Mf);
```

```matlab
        % Mass of accumulated water molecules
        %===========================================================
        dMH20=(t*18/Mf)*(dw_dlogMW/sum(dw_dlogMW));


        %Deducting mass of accumulated water molecules from the total mass
in
        %the distribution as scission increases
        %===============================================================
        dw_dlogMW=dw_dlogMW-dMH20;

        %dw_dlogMW=dw_dlogMW-dSEM;

        dw_dlogMWA(1:end,t)=dw_dlogMW;
        countd(1:end,t)=d;

    xlcol={'B' 'C' 'D' 'E' 'F' 'G' 'H' 'I' 'J' 'K' 'L' 'M' 'N' 'O' 'P'
'Q'};
    xlcol_num=2:5636;



    if mod(t,cystp)==0 || t==1
%


        figure(3)
        semilogx(MW,dw_dlogMW,plotlabel{lg})%'-g')%,DP,d,'-b');
        %title(strcat('DP Distribution after
Scission(unzip',az,'mer)',numberm_str));
        xlabel('MW');
        ylabel('dw/dlogMW');
        legend(plotlabel_run);
        hold on
        %figname=strcat('unzip_',az,'mers',numberm_str);
        cd(unzipscission_files);
%         saveas(gcf, figname, 'pdf');
%         saveas(gcf, figname, 'fig');
%         saveas(gcf, figname, 'jpeg');

         % Storing data in Excel
        %===============================
        WTFRAC_SUCCESS =
xlswrite('C:\MATLAB\Unzip_scission_rawdata\Unzipscissiondata.xlsx',dw_d
logMW,'dw_dlogMW2000_200',...

strcat(xlcol{lg},num2str(xlcol_num(1)),:,xlcol{lg},num2str(xlcol_num(56
24)))));
        DP_SUCCESS =
xlswrite('C:\MATLAB\Unzip_scission_rawdata\Unzipscissiondata.xlsx',MW,'
dw_dlogMW2000_200','A2:A2050');
        %================================================

        lg=lg+1;
```

```
%
%

    end


    %TN(dc)=sum(d); % Caculating the new total number of molecues after
each cycle
    TN=sum(d); %
    TN1(t)=sum(d);
    %d=TN*Probdf;
    %pause(4)

end


% figure(3)
% %plot(x,fracpdfNormal2);
% plot(DP,d,'-r')%,DP,d,'-b');
% title('DP Distribution after Scission');
% xlabel('DP');
% ylabel('# of Molecules and Probability');
% hold on


cd('..');
% clear i j

end


% Percentage number of bonds broken
percent_bond_broken=((inumbond-numbond)/inumbond)*100;


% LIBRARY OF CODE
% =================================================
% histc(testDP,unique(testDP(1:end)))';
% unique(testDP(1:end))';
```

APPENDIX D: MATLAB CODE FOR THE MONTE CARLO

SIMULATION

```
close all
clear all




% Importing data from Excel file: DP_cellulose_from_experiment.xlsx
%====================================================================
====
% Molecular weight :
 MW=
xlsread('C:\MATLAB\DP_cellulose_from_experiment','sheet3','AZ127:AZ5751
'); %sheet 1

%Normalized height: Weight fraction of each MW in the distribution
NH =
xlsread('C:\MATLAB\DP_cellulose_from_experiment','sheet3','AX127:AX5751
');% sheet 1

% Sum of all Molecular Weight
SWM = sum(MW);

%Chromotogram
%=======================
Chromresp=xlsread('C:\MATLAB\DP_cellulose_from_experiment','sheet3','AW
127:AW5751');% sheet1


Mf=1E5; % Mf : multiplication factor
% Simulated Data
%===========================
% Number of molecules for each Molecular Weight in the Distribution
d
=xlsread('C:\MATLAB\DP_cellulose_from_experiment','sheet3','BA127:BA575
1')*Mf;%%.*((0.003)./(MW*1.66053886e-27*1000));      %*100000; % sheet
3


%initial_d
initial_d=d;


% Array of DP generated from Experiments
%======================================
DP =((MW)-18)/162;
x=DP;
testDP=DP;
pause on
```

```
warning off




%==========================================


%Counter for number of runs: scissions
%==========================================
% dc=1000; % dcc is dc counter
% cystp=100; % cycle step ( for the mod function) for plotting every
"cystp"


%Counter for number of runs: scissions
%==========================================
dc=Mf;%sum(d); % dcc is dc counter
cystp=dc/10;% cycle step ( for the mod function) for plotting every
"cystp"


%Mode of scission options:
random_scission=1;
center_scission=0;
unzip_scission=0;


%Plotting chromatogram
%============================================
figure(1)
semilogx(MW,Chromresp);
title('Chromatogram response vs MW');
xlabel('MW');
ylabel('mV');


%pause
%TN1=sum(d); % Affirming the Total number of molecules
TN=sum(d);
%pause


 % Initial total number of bonds
 inumbond=sum((DP-1).*d);

figure(2)
semilogx(MW,d);
title('Experimental MW Distribution ');
xlabel('MW');
ylabel('# of Molecules');

%number average degree polymerization or average bond length
```

```matlab
n_average(1)=(sum(DP.*d)/sum(d));


%Weight fraction in Mw
%Mwt_frac=((DP*162+180).*d)/sum((DP*162+180).*d);


% Normalized height h/total_h also refers to dw/dv
%dw_dv=(d.*MW)/sum(d.*MW);
dw_dv=NH;


% Calibration equation from experiment is of the form logMW = A + Bv;
% where: A and B are intercept and gradient respectively; v is elution
volume;
% dv/dlogMW equals the reciprocal of the gradient (constant- linear)
% therefore to obtain dw/dlogMW, we multiply dw/dv with dv/dlogMW
% dw/dlogMW = dw/dv * dv/dlogMW
dv_dlogMW = 643;


dw_dlogMW = dw_dv*dv_dlogMW;
ini_dw_dlogMW=dw_dlogMW;


figure(3)
semilogx(MW,dw_dlogMW)%'-g')%,DP,d,'-b');
%title(strcat('DP Distribution after Scission (random)',numberm_str));
xlabel('MW');
ylabel('dw/dlogMW');
hold on
% figname=strcat('random',numberm_str);
% cd(randomscission_files);
% saveas(gcf, figname, 'pdf');
% saveas(gcf, figname, 'fig');
% saveas(gcf, figname, 'jpeg');


iDP=DP;
plotlabel={'-r' '-b' '-r' '--r' '--k' '-k' '-g' '--g' '-m' '-y' '--y'};
plotlabel_run={'Initial' 'plot1' 'plot2' 'plot3' 'plot4' 'plot5'
'plot6'...
    'plot7' 'plot8' 'plot9' 'Final'};
lg=1; % legend indices for plotlabel
lw=1;
lk=1;
lh=1;
dw_dlogMWA=dw_dlogMW;




% Number of molecules for each Molecular Weight in the Distribution
%d =flipud(xlsread('C:\Users\Kazeem\Documents\My
Documents\MATLAB\DP_cellulose_from_experiment','sheet3','O130:O2152'))*
100000; % sheet 3

%initial_d
initial_d=d;
```

```matlab
% % Number average MW:
 iMn=sum(d/Mf.*MW)/sum(d/Mf);
%
% % DPn
 iDPn = (iMn-18)/162;




% Percentage number of bonds broken
Theoreticalpercent_bond_broken=(dc/inumbond)*100;

imassmonomer=sum((DP).*d);

%d=Sd;

% DP with number of molecules > zero
%DP=[DP(6:end)];

% POLYMER DEGRADATION SECTION
%=========================================

%(1) Random scission:
%*****************************************
% dc : degradation cycle
if random_scission ==1
%dc=1;
fprintf('==================================');
fprintf('\nRunning random scissioning');
fprintf('\n==================================\n');
% DP is the degree of polymerization

mkdir('C:\MATLAB','Random_scission');
randomscission_files=('C:\MATLAB\Random_scission');

mkdir('C:\MATLAB','Random_scission_rawdata');
randomscission_rawdata=('C:\MATLAB\Random_scission_rawdata');



% DP=M/162;
to=0; % to : initial t
% step1 : randomly select a polymer chain for scissioning:
for t=1:dc

    % Calculating total number of bonds
    sTb=sum((DP-1).*d);



    % book keeping number of bonds at every cycle
    CsTb(t)=sum((DP-1).*d);
    %sTb=sum(d)-d(1);
    clear r;
```

```
        CP=vertcat(Chromresp,d,DP);


    DP=DP';
%       % randomly selecting chain length for scission
%       SDP=DP(1,ceil(length(DP)*rand));
%       CSDP(t)=SDP;

    %Extracting the nonzeros elements.i.e. molecules with bonds
    [rDPb cDPb]=size(nonzeros(DPb));


    % randomly selecting bond to break from the whole molecules
     Pb=[ceil(rand*rDPb) ceil(cDPb*rand)];
     [i j]=find(DPb==Pb(1));% noting bond point within the matrix

     SDPb=DPb(i,j);
     CSDPb(t)=SDPb;

     % A(ceil(rand*4),ceil(5*rand))  ; A is a matrix of 4 by 5
     %=========================================================

    if SDPb==0
        d=d;
        DP=DP';

    else

%           %Randomly selecting bond from the bondmatrix
%           Pb=DPb(1,ceil([rDPb,cDPb]*rand));

        %To know the randomly selected bond
        %SDPb=DPb(Pb(1),Pb(2));

        % To know all the bonds in the array where the bond is selected
        LDPb=nonzeros(DPb(i,1:end));

        %The corresponding chain length from where the bond was
randomly
        %selecetd within bondmatrix
        SDP=length(LDPb)+1;

        % finding the spot at which the randomly selected bond is
broken
        SB=find(LDPb==SDPb);


        % Two different chains from scission
        SB1=SDP-SB;
        CDP=[SB SB1];
        DP1=CDP(1); DP2=CDP(2);
```

```
            % Adding one more molecule to the number of molecules
corresponding to DP with equal size to the two
            % new DPs formed
            d=d';
            dp=find(DP==SDP);
            dp1=find(DP==DP1);
            dp2=find(DP==DP2);

            %increasing number of molecules by 1 for each new chain
            %length formed which

            if DP1==DP2 || d(dp1)+2<d(dp1+1)

                d(dp1)=d(dp1)+2;
            elseif DP1~=DP2 || d(dp1)+1<d(dp1+1)

                d(dp1)=d(dp1)+1;

            elseif DP1~=DP2 && d(dp2)+1<d(dp2+1);

                d(dp2)=d(dp2)+1;
            else

            end

            MW=MW';
            % decreasing number of molecules by 1 from the chain length
            % selected scissioned and if a polymer chain has one molecule
and
            % is scissioned removed from the distribution to avoid
            % spikes between DP
            if isempty(dp)==1


            elseif d(dp)>=1 && d(dp)-1<1
                %d(dp)=0;
                %DP(dp)=0;
                %MW(dp)=0;
                %dw_dlogMWA(dp,t)=[];
                d(dp)=d(dp);

            elseif d(dp)<1
                d(dp)=d(dp);
            else
               d(dp)=d(dp)-1;

            end


            if SB==1 || SB==length(LDPb)
                ntzero=SDP-1;
                DPb(i,1:ntzero)=0;
                DPb(i,1:ntzero-1)=LDPb(1:length(LDPb)-1)';
```

```
        DPbr=DPb(DPb>max(LDPb))-1;
        DPb(DPb>max(LDPb))=DPbr;



    else
        ntzero=SDP-1;
        [ii jj]=size(DPb);
        DPb(i,1:ntzero)=0;
        DPb(i,1:SB-1)=LDPb(1:SB-1)';
        DPb(ii+1,1:DP2-1)=LDPb(SB:length(LDPb)-1);
        DPbr=DPb(DPb>max(LDPb))-1;
        DPb(DPb>max(LDPb))=DPbr;
        %maxnzero=max(nonzeros(DPb));
        %maxnzero:maxnzero+DP1-2;
        %DPb(ii+2,1:DP2-1)=maxnzero+DP1-1:(maxnzero+DP1-1)+DP2-2;

    end



    DP=DP';
    d=d';
    MW=MW'



 end



d=d; % array of new values for the number of molecules
%Number_m1(:,t)=d;



%Weight fraction in Dp
wt_frac=(DP.*d)/sum(DP.*d);


%Weight fraction in Mw
Mwt_frac=((DP*162+180).*d)/sum((DP*162+180).*d);

% Normalized height h/total_h also refers to dw/dv
dw_dv=(d.*MW)/sum(d.*MW);

%Number average MW:
Mn(t)=sum(d/Mf.*MW)/sum(d/Mf);

% DPn
DPn(t) = (Mn(t)-18)/162;
```

```matlab
    % Percentage of average bonds broken
    Percent_bond_broken(t) = ((iMn-Mn(t))/iMn)*100;


    %dw_dv=(NMW)/sum(NMW);
    %dw_dv=Mwt_frac;


    % Calibration equation from experiment is of the form logMW = A +
Bv;
    % where: A and B are intercept and gradient respectively; v is
elution volume;
    % dv/dlogMW equals the reciprocal of the gradient (constant-
linear)
    % therefore to obtain dw/dlogMW, we multiply dw/dv with dv/dlogMW
    % dw/dlogMW = dw/dv * dv/dlogMW
    %dv_dlogMW = 643.3198705;


    %dw_dlogMW = dw_dv*dv_dlogMW;


    %dw_dlogMWA(1:end,t)=dw_dlogMW;


    dw_dlogMW = MW.*(d/Mf);


    %Differential fraction
    dw_frac=(log(10))*(DP).*Mwt_frac;


    lgMw=log10(DP*162);


    %MW=MW;


    xlcol={'B' 'C' 'D' 'E' 'F' 'G' 'H' 'I' 'J' 'K' 'L' 'M' 'N' 'O' 'P'
'Q'};
    xlcol_num=2:2050;


    if mod(t,cystp)==0 || t==1


        figure(3)
        %semilogx(MW,wt_frac,plotlabel{lh})%'-g')%,DP,d,'-b');
        semilogx(MW,dw_dlogMW,plotlabel{lh})%'-g')%,DP,d,'-b');
        %title(strcat('DP Distribution after Scission
(random)',numberm_str));
        xlabel('MW');
        ylabel('dw/dlogMW');
        legend(plotlabel_run);
        hold on
        %figname=strcat('random',numberm_str);
        cd(randomscission_files);
%         saveas(gcf, figname, 'pdf');
%         saveas(gcf, figname, 'fig');
%         saveas(gcf, figname, 'jpeg');
        % MW
        % Storing data in Excel
        %=============================
        dw_dlogMW_SUCCESS =
xlswrite('C:\MATLAB\Random_scission_rawdata\Randomscissiondata.xlsx',dw
_dlogMW,'dw_dlogMW1000_100A',...
```

```
strcat(xlcol{lh},num2str(xlcol_num(1)),:,xlcol{lh},num2str(xlcol_num(en
d)))));
        MW_SUCCESS =
xlswrite('C:\MATLAB\Random_scission_rawdata\Randomscissiondata.xlsx',MW
,'dw_dlogMW1000_100A','A2:A2050');
        %===============================================
        lh=lh+1;
        %hold off




        %wt_frac=wt_frac*643;
        figure(4)
        semilogx(DP,wt_frac,plotlabel{lg})%'-g')%,DP,d,'-b');
        %title(strcat('DP Distribution after Scission
(random)',numberm_str));
        xlabel('DP');
        ylabel('Weight Fraction');
        legend(plotlabel_run);
        hold on
        %figname=strcat('random',numberm_str);
        cd(randomscission_files);
%        saveas(gcf, figname, 'pdf');
%        saveas(gcf, figname, 'fig');
%        saveas(gcf, figname, 'jpeg');

%        %Storing data in Excel
%        ===============================
%        WTFRAC_SUCCESS = xlswrite('C:\Users\Kazeem\Documents\My
Documents\MATLAB\Random_scission_rawdata\Randomscissiondata.xls',wt_fra
c','weightfraction',...
%
strcat(xlcol{lg},num2str(xlcol_num(1)),:,xlcol{lg},num2str(xlcol_num(en
d)))));
%        DP_SUCCESS = xlswrite('C:\Users\Kazeem\Documents\My
Documents\MATLAB\Random_scission_rawdata\Randomscissiondata.xls',DP','w
eightfraction','A2:A454');
%        %===============================================
         lg=lg+1;
        hold off




%


%


    end

    %MW=NMW;
```

```matlab
    TN(t)=sum(d); % Caculating the new total number of molecues after
each cycle

%



end


DW_DLOGMWA =
xlswrite('C:\MATLAB\Random_scission_rawdata\Randomscissiondata.xlsx',dw
_dlogMWA,'dw_dlogMWA');
%AREA_A = xlswrite('C:\Users\Kazeem\Documents\My
Documents\MATLAB\Random_scission_rawdata\Randomscissiondata.xlsx',SMWC'
,'SMWCT1000_100');

% figure(3)
% %plot(x,fracpdfNormal2);
% plot(DP,d,'-r')%,DP,d,'-b');
% title('DP Distribution after Scission');
% xlabel('DP');
% ylabel('# of Molecules and Probability');
% hold on

%cd('..');

% clear i j

end

%% center scission session
%========================================
%%(2)center scission:
%*****************************************
%polymer chain to be scissioned at the center
%%===================================================================
=====

% dc : degradation cycle
if center_scission==1
%dc=1;
% DP is the degree of polymerization
%dc=1;
fprintf('===================================');
fprintf('\nRunning center scissioning');
fprintf('\n===================================\n');
% DP is the degree of polymerization

mkdir('C:\MATLAB','Center_scission');
centerscission_files='C:\MATLAB\Center_scission';

mkdir('C:\MATLAB','Center_scission_rawdata');
randomscission_rawdata=('C:\MATLAB\Center_scission_rawdata');
```

```matlab
% DP=M/162;
to=0 % to : initial t
% step1 : randomly select a polymer chain for scissioning:
for t=1:dc

    % Calculating total number of bonds
    sTb=sum((DP-1).*d);



    % book keeping number of bonds at every cycle
    CsTb(t)=sum((DP-1).*d);
    %sTb=sum(d)-d(1);
    clear r;


    CP=vertcat(Chromresp,d,DP);

    DP=DP';
    % randomly selecting chain length for scission
    SDP=DP(1,ceil(length(DP)*rand));
    CSDP(t)=SDP;



    if SDP==1
        d=d;
        DP=DP';

    else SDP > 1  ;


        % Forming an array out of the selected DP (SDP)
        SBDP=1:SDP;

        % Forming an array of number of bonds from the selected DP
(SDP)
        NSBDP=1:SDP-1;

        % Checking if selected DP is odd or even and selecting bond to
        % break from the selected chain
        if mod(max(NSBDP),2)==0 % for even number of bonds
            SB=max(NSBDP)/2;
            SB1=SB-1;
            CDP=[SB+1 SB1+1];% DP=number of bonds +1; that is why SB+1
or SB1+1 are the new DPs

        else
            PSB=median(NSBDP); % for odd number of bonds
            SB=length(NSBDP)-PSB;
            SB1=SB;
```

```
            CDP=[SB+1 SB1+1]; % two new chains formed with DPs : SB+1
ans SB1+1
        end
        DP1=CDP(1); DP2=CDP(2);

        % Adding one more molecule to the number of molecules
corresponding to DP with equal size to the two
        % new DPs formed

        d=d';
        dp=find(DP==SDP);
        dp1=find(DP==DP1);
        dp2=find(DP==DP2);

        % decreasing number of molecules by 1 from the chain length
selected scissioned
        if d(dp)>=1
            d(dp)=d(dp)-1;
        else
            d(dp)=d(dp);
        end

        %increasing number of molecules by 1 for each new chain
        %length formed which

        if DP1==DP2

            d(dp1)=d(dp1)+2;
        else

            d(dp1)=d(dp1)+1;

            d(dp2)=d(dp2)+1;
        end

        DP=DP';
        d=d';

    end




    d=d; % array of new values for the number of molecules
    %Number_m1(:,t)=d;




    %Weight fraction in Dp
    wt_frac=(DP.*d)/sum(DP.*d);


    %Weight fraction in Mw
```

```
    Mwt_frac=((DP*162+180).*d)/sum((DP*162+180).*d);

    % Normalized height h/total_h also refers to dw/dv
    dw_dv=(d.*MW)/sum(d.*MW);

    %Number average MW:
    Mn(t)=sum(d/1E9.*MW)/sum(d/1E9);

    % DPn
    DPn(t) = (Mn(t)-18)/162;

    % Percentage of average bonds broken
    Percent_bond_broken(t) = ((iMn-Mn(t))/iMn)*100;


    %dw_dv=(NMW)/sum(NMW);
    %dw_dv=Mwt_frac;

    % Calibration equation from experiment is of the form logMW = A +
Bv;
    % where: A and B are intercept and gradient respectively; v is
elution volume;
    % dv/dlogMW equals the reciprocal of the gradient (constant-
linear)
    % therefore to obtain dw/dlogMW, we multiply dw/dv with dv/dlogMW
    % dw/dlogMW = dw/dv * dv/dlogMW
    dv_dlogMW = 643.3198705;

    dw_dlogMW = dw_dv*dv_dlogMW;

    dw_dlogMWA(1:end,t)=dw_dlogMW;

    %Differential fraction
    dw_frac=(log(10))*(DP).*Mwt_frac;

    lgMw=log10(DP*162);

    % Number fraction
    num_frac = d/sum(d);

    xlcol={'B' 'C' 'D' 'E' 'F' 'G' 'H' 'I' 'J' 'K' 'L' 'M' 'N' 'O' 'P'
'Q'};
    xlcol_num=2:5625;

    if mod(t,cystp)==0 || t==1
        figure(3)
        semilogx(MW,dw_dlogMW,plotlabel{lh})%'-g')%,DP,d,'-b');
        %title(strcat('DP Distribution after Scission
(random)',numberm_str));
        xlabel('MW');
        ylabel('dw/dlogMW');
        legend(plotlabel_run);
        hold on
%        figname=strcat('center',numberm_str);
```

```
            cd(centerscission_files);
%           saveas(gcf, figname, 'pdf');
%           saveas(gcf, figname, 'fig');
%           saveas(gcf, figname, 'jpeg');
%
            % Storing data in Excel
            %============================
            dw_dlogMW_SUCCESS =
xlswrite('C:\MATLAB\Center_scission_rawdata\Centerscissiondata.xlsx',dw
_dlogMW,'dw_dlogMW42000_4200C',...

strcat(xlcol{lh},num2str(xlcol_num(1)),:,xlcol{lh},num2str(xlcol_num(56
24)))));
            MW_SUCCESS =
xlswrite('C:\MATLAB\Center_scission_rawdata\Centerscissiondata.xlsx',MW
,'dw_dlogMW42000_4200C','A2:A5625');
            %===============================================
            lh=lh+1;
            %hold off

%


%


    end


    %TN(dc)=sum(d); % Caculating the new total number of molecues after
each cycle
    TN=sum(d);
    TN1(t)=sum(d);
    %d=TN*Probdf;
    %pause(4)

end


%

end

%% unzip scission session
%=========================================
%%(2)unzip scission:
%*****************************************
%polymer chain to be scissioned at the end (reducing end)
%%======================================================================
=====

% dc : degradation cycle
if unzip_scission==1
%dc=1;
```

```
% DP is the degree of polymerization
%dc=1;
fprintf('==================================');
fprintf('\nRunning unzip scissioning');
fprintf('\n==================================\n');
% DP is the degree of polymerization
mkdir('C:\Users\Kazeem\Documents\My Documents\MATLAB','Unzip_scission')
unzipscission_files='C:\Users\Kazeem\Documents\My
Documents\MATLAB\Unzip_scission';

mkdir('C:\Users\Kazeem\Documents\My
Documents\MATLAB','Unzip_scission_rawdata');
randomscission_rawdata=('C:\Users\Kazeem\Documents\My
Documents\MATLAB\Unzip_scission_rawdata');




% DP=M/162;
to=0 % to : initial t
% step1 : randomly select a polymer chain for scissioning:
for t=1:10

    % Calculating total number of bonds
    sTb=sum((DP-1).*d);




    % book keeping number of bonds at every cycle
    CsTb(t)=sum((DP-1).*d);
    %sTb=sum(d)-d(1);
    clear r;


    CP=vertcat(Chromresp,d,DP);

    DP=DP';
    % randomly selecting chain length for scission
    SDP=DP(1,ceil(length(DP)*rand));
    CSDP(t)=SDP;


    if SDP==1
        d=d;
        DP=DP';

    else SDP > 1  ;


        % Forming an array out of the selected DP (SDP)
        SBDP=1:1:SDP;
```

```matlab
        % Breaking off one bond from the end of the selected chain
        uzb=1; % number of unzip bonds from any of the chain ends
        SB=length(SBDP)-uzb;
        SB1=uzb;
        % Two different chains from scission
        CDP=[SB SB1];
        DP1=CDP(1); DP2=CDP(2);

        % Adding one more molecule to the number of molecules
corresponding to DP with equal size to the two
        % new DPs formed

        d=d';
        dp=find(DP==SDP);
        dp1=find(DP==DP1);
        dp2=find(DP==DP2);

        % decreasing number of molecules by 1 from the chain length
selected scissioned
        if d(dp)>=1
            d(dp)=d(dp)-1;
        else
            d(dp)=d(dp);
        end

        %increasing number of molecules by 1 for each new chain
        %length formed which

        if DP1==DP2

            d(dp1)=d(dp1)+2;
        else

            d(dp1)=d(dp1)+1;

            d(dp2)=d(dp2)+1;
        end

        DP=DP';
        d=d';

    end



    d=d; % array of new values for the number of molecules
    %Number_m1(:,t)=d;



    %Weight fraction in Dp
    wt_frac=(DP.*d)/sum(DP.*d);
```

```matlab
    %Weight fraction in Mw
    Mwt_frac=((DP*162+180).*d)/sum((DP*162+180).*d);

    % Normalized height h/total_h also refers to dw/dv
    dw_dv=(d.*MW)/sum(d.*MW);

    %dw_dv=(NMW)/sum(NMW);
    %dw_dv=Mwt_frac;

    % Calibration equation from experiment is of the form logMW = A +
Bv;
    % where: A and B are intercept and gradient respectively; v is
elution volume;
    % dv/dlogMW equals the reciprocal of the gradient (constant-
linear)
    % therefore to obtain dw/dlogMW, we multiply dw/dv with dv/dlogMW
    % dw/dlogMW = dw/dv * dv/dlogMW
    dv_dlogMW = 643.3198705;

    dw_dlogMW = dw_dv*dv_dlogMW;

    dw_dlogMWA(1:end,t)=dw_dlogMW;

    %Differential fraction
    dw_frac=(log(10))*(DP).*Mwt_frac;

    lgMw=log10(DP*162);


    % Number fraction
    num_frac = d/sum(d);

    xlcol={'B' 'C' 'D' 'E' 'F' 'G' 'H' 'I' 'J' 'K' 'L' 'M' 'N' 'O' 'P'
'Q'};
    xlcol_num=2:2050;



    if mod(t,cystp)==0 || t==1
%         figure(3)
%         %plot(x,fracpdfNormal2);
%         plot(DP,Number_m1);
%         title('DP Distribution after Scission (unzip)');
%         xlabel('DP');
%         ylabel('Number of molecules');
%         hold on
%
%         figure(4)
%         %plot(x,fracpdfNormal2);
%         plot(DP,P,'-r')%,DP,d,'-b');
%         title('DP Distribution after Scission (unzip)');
%         xlabel('DP');
```

```matlab
%        ylabel('Probability');
%        hold on


        figure(3)
        semilogx(MW,dw_dlogMW,plotlabel{lg})%'-g')%,DP,d,'-b');
        %title(strcat('DP Distribution after
Scission(unzip',az,'mer)',numberm_str));
        xlabel('MW');
        ylabel('dw/dlogMW');
        legend(plotlabel_run);
        hold on
        %figname=strcat('unzip_',az,'mers',numberm_str);
        cd(unzipscission_files);
%        saveas(gcf, figname, 'pdf');
%        saveas(gcf, figname, 'fig');
%        saveas(gcf, figname, 'jpeg');

         % Storing data in Excel
        %============================
        WTFRAC_SUCCESS = xlswrite('C:\Users\Kazeem\Documents\My
Documents\MATLAB\Unzip_scission_rawdata\Unzipscissiondata.xlsx',dw_dlog
MW,'dw_dlogMW2000_200',...

strcat(xlcol{lg},num2str(xlcol_num(1)),:,xlcol{lg},num2str(xlcol_num(en
d)))));
        DP_SUCCESS = xlswrite('C:\Users\Kazeem\Documents\My
Documents\MATLAB\Unzip_scission_rawdata\Unzipscissiondata.xlsx',MW,'dw_
dlogMW2000_200','A2:A2050');
        %==============================================

        lg=lg+1;


%

    end


    %TN(dc)=sum(d); % Caculating the new total number of molecues after
each cycle
    TN=sum(d); %
    TN1(t)=sum(d);
    %d=TN*Probdf;
    %pause(4)

end


% figure(3)
% %plot(x,fracpdfNormal2);
% plot(DP,d,'-r')%,DP,d,'-b');
% title('DP Distribution after Scission');
% xlabel('DP');
```

```
% ylabel('# of Molecules and Probability');
% hold on


cd('..');
% clear i j

end
```

REFERENCES

(1) Simmons, B. A.; Singh, S.; Holmes, B. M.; Blanch, H. W. Ionic Liquid Pretreatment. *CEP* **2010***, 106*, 50-55.

(2) Ladisch, M. R.; Mosier, N. S.; Kim, Y.; Ximenes, E.; Hogsett, D. Converting Cellulose to Biofuels. *CEP* **2010***, 106*, 56-62.

(3) U.S.D.O.E Biomass Multi-Year Program Plan Report. *http://www1.eere.energy.gov/biomass/pdfs/biomass_program_mypp.pdf*2007).

(4) Himmel, M. E., Ed.; In *Biomass Recalcitrance;* 2008; Vol. 1, pp 495.

(5) Ziegler, J. The Right to Food,". *United Nations General Assembly Report* **2007***, A/62/289*.

(6) Cortes-Caminero, M. Engineering Advanced Biofuels. *CEP* **2010***, 106*, 35.

(7) E.E.R.E PLANT/CROP-BASED RENEWABLE RESOURCES 2020. **1998***, DOE/GO-10097-385*, 1-24.

(8) U.S.D.O.E Biomass Multi-Year Program Plan Report. *http://www1.eere.energy.gov/biomass/pdfs/biomass_program_mypp.pdf* (accessed 03/25, 2010).

(9) U.S.D.A & U.S.D.O.E (2005) Biomass as Feedstock for a Bioenergy and Bioproducts Industry: The Technical Feasibility of a Billion-Ton Annual Supply. *http://www1.eere.energy.gov/biomass/pdfs/final_billionton_vision_report2.pdf* (accessed 11, 2007).

(10) Knauf, M.; Moniruzzaman, M. Lignocellulosic Biomass Process: A Perspective. *International Sugar Journal* **2004***, 106*, 147-150.

(11) Ehara, K.; Saka, S. Decomposition Behavior of Cellulose in Supercritical Water, Subcritical Water, and their Combined Treatments. *Journal of Wood Science* **2005***, 51*, 148-153.

(12) NEED In *Biomass;* Secondary Energy Infobook; Manassas, VA, 2007; pp 12-15.

(13) 106th Congress Public Law 106-224. **2000**, 301-310.

(14) Zhang, T. Glucose Production from Cellulose in Subcritical and Supercritical Water, The University of Iowa, 2008.

(15) Bruice, P. Y. In *Carbohydrates;* Folchetti, N., Mullaney, R., Kaveney, D., Lerner-Nelson, M. and Richards, M. J., Eds.; Organic Chemistry; Pearson Prentice Hall: Upper Saddle River, NJ, 2007; pp 1-2-1317.

(16) Krassig, H. A. In *The Fiber Structure;* Cellulose; Gordon and Breach Science: Amsterdam, The Netherlands, 1993; Vol. 11, pp 6-7-42.

(17) Jessop, P. G.; Leitner, W. In *Supercritical Fluids as Media for Chemical Reactions;* Jessop, P. G., Leitner, W., Eds.; Chemical Synthesis Using Supercritical Fluids; Wiley-VCH: Weinheim, Germany, 1999; pp 1-2-65.

(18) Linstrom, P. J.; and Mallard, W. G. National Institute of Standards and Technology, Gaithersburg MD, 20899. *http://webbook.nist.gov* (accessed 4/30, 2010).

(19) Linstrom, P. J.; and Mallard, W. G., Eds.; In *NIST Chemistry WebBook, NIST Standard Reference Database .;* Lemmon, E. W., McLinden, M. O. and and Friend, D. G., Eds.; "Thermophysical Properties of Fluid Systems"; .

(20) Baiker, A. Supercritical Fluids in Heterogeneous Catalysis. *Chem. Rev.* **1999***, 99*, 453-473.

(21) Li, L.; Kiran, E. Gas-Liquid Critical Properties of Methylamine + Nitrous-Oxide and Methylamine + Ethylene Binary-Mixtures. *J. Chem. Eng. Data* **1988***, 33*, 342-344.

(22) Savage, P. E.; Gopalan, S.; Mizan, T. I.; Martino, C. J.; Brock, E. E. Reactions at Supercritical Conditions - Applications and Fundamentals. *AICHE J.* **1995***, 41*, 1723-1778.

(23) Kiran, E., Debenedetti, P. G., and Peters, C. J., Ed.; In *Supercritical Fluids (Fundamentals and Applications);* Kluwer Academic Publishers: Dordrecht, The Netherlands, 1999; Vol. 366, pp 591.

(24) Yesodharan, S. Supercritical Water Oxidation: An Environmentally Safe Method for the Disposal of Organic Wastes. *Curr. Sci.* **2002***, 82*, 1112-1122.

(25) Schmieder, H.; Abeln, J. Supercritical Water: State of the Art. *Chem. Eng. Technol* **1999***, 22*, 903-904-908.

(26) Mesiano, A. J.; Beckman, E. J.; Russell, A. J. Supercritical Biocatalysis. *Chem. Rev.* **1999***, 99*, 623-633.

(27) Kajimoto, O. Solvation in Supercritical Fluids: Its Effects on Energy Transfer and Chemical Reactions. *Chem. Rev.* **1999***, 99*, 355-389.

(28) Jessop, P. G.; Ikariya, T.; Noyori, R. Homogeneous Catalysis in Supercritical Fluids. *Chem. Rev.* **1999***, 99*, 475-493.

(29) Brennecke, J. F.; Chateauneuf, J. E. Homogeneous Organic Reactions as Mechanistic Probes in Supercritical Fluids. *Chem. Rev.* **1999**, *99*, 433-452.

(30) Arthur E. Humphrey In *The Hydrolysis of Cellulosic Materials to Useful Products;* Brown, R. D., Jurasek, L., Eds.; Hydrolysis of Cellulose: Mechanisms of Enzymatic and Acid Catalysis; American Chemical Society: Washington, D. C., 1979; pp 25-53.

(31) Lipinsky, E. S. In *Perspectives on Preparation of Cellulose for Hydrolysis;* Brown, R. D., Jurasek, L., Eds.; Hydrolysis of Cellulose: Mechanisms of Enzymatic and Acid Catalysis; American Chemical Society: Washington, D. C., 1979; pp 1-24.

(32) Sasaki, M.; Adschiri, T.; Arai, K. Kinetics of Cellulose Conversion at 25 MPa in Sub- and Supercritical Water. *AICHE J.* **2004**, *50*, 192-202.

(33) Fan, L. T.; Gharpuray, M. M.; Lee, Y. -. In *Cellulose Hydrolysis;* Aiba, S., Fan, L. T., Fiechter, A., Klein, J. and Schugerl, K., Eds.; Springer-Verlag: Berlin Heidelberg, New York, 1987; Vol. 3, pp 197.

(34) Zhang, Y. P.; Lynd, L. R. Toward an Aggregated Understanding of Enzymatic Hydrolysis of Cellulose: Noncomplexed Cellulase Systems. *Biotechnol. Bioeng.* **2004**, *88*, 797-798-824.

(35) Sasaki, M.; Fang, Z.; Fukushima, Y.; Adschiri, T.; Arai, K. Dissolution and Hydrolysis of Cellulose in Subcritical and Supercritical Water. *Ind Eng Chem Res* **2000**, *39*, 2883-2890.

(36) Saeman, J. F. Kinetics of Wood Saccharification - Hydrolysis of Cellulose and Decomposition of Sugars in Dilute Acid at High Temperature. *Industrial and Engineering Chemistry* **1945**, *37*, 43-52.

(37) Girisuta, B.; Janssen, L. P. B. M.; Heeres, H. J. Kinetic Study on the Acid-Catalyzed Hydrolysis of Cellulose to Levulinic Acid. *Ind Eng Chem Res* **2007**, *46*, 1696-1708.

(38) Xiang, Q.; Lee, Y. Y.; Pettersson, P. O.; Torget, R. Heterogeneous Aspects of Acid Hydrolysis of Alpha-Cellulose. *Appl. Biochem. Biotechnol.* **2003**, *105*, 505-514.

(39) Wood, T. M.; McCrae, S. I. In *Synergism Between Enzymes Involved in the Solubilization of Native Cellulose;* Brown, R. D., Jurasek, L., Eds.; Hydrolysis of Cellulose: Mechanisms of Enzymatic and Acid Catalysis; American Chemical Society: Washington, D. C., 1979; pp 181-210.

(40) Kearsley, M. W.; Dziedzic, S. Z. In *Handbook of Starch Hydrolysis Product and their Derivatives;* Blackie Academy and Professional: 1996; , pp 275.

(41) Eremeeva, T.; Bikova, T.; Eisimonte, M.; Viesturs, U.; Treimanis, A. Fractionation and Molecular Characteristics of Cellulose during Enzymatic Hydrolysis. *Cellulose* **2001**, *8*, 69-79.

(42) Wald, S.; Wilke, C. R.; Blanch, H. W. Kinetics of the Enzymatic-Hydrolysis of Cellulose. *Biotechnol. Bioeng.* **1984**, *26*, 221-230.

(43) Saka, S.; Ueno, T. Chemical Conversion of various Celluloses to Glucose and its Derivatives in Supercritical Water. *Cellulose* **1999**, *6*, 177-191.

(44) Antal, M. J.; Allen, S. G.; Schulman, D.; Xu, X. D.; Divilio, R. J. Biomass Gasification in Supercritical Water. *Ind Eng Chem Res* **2000**, *39*, 4040-4053.

(45) Minowa, T.; Ogi, T.; Yokoyama, S. Hydrogen-Production from Wet Cellulose by Low-Temperature Gasification using a Reduced Nickel-Catalyst. *Chem. Lett.* **1995**, 937-938.

(46) Sakaki, T.; Shibata, M.; Miki, T.; Hirosue, H.; Hayashi, N. Decomposition of Cellulose in Near-Critical Water and Fermentability of the Products. *Energy Fuels* **1996**, *10*, 684-688.

(47) Matsumura, Y.; Sasaki, M.; Okuda, K.; Takami, S.; Ohara, S.; Umetsu, M.; Adschiri, T. Supercritical Water Treatment of Biomass for Energy and Material Recovery. *Combustion Sci. Technol.* **2006**, *178*, 509-536.

(48) Kabyemela, B. M.; Adschiri, T.; Malaluan, R. M.; Arai, K. Glucose and Fructose Decomposition in Subcritical and Supercritical Water: Detailed Reaction Pathway, Mechanisms, and Kinetics. *Ind Eng Chem Res* **1999**, *38*, 2888-2895.

(49) Zhang, T. Glucose Production from Cellulose in Subcritical and Supercritical Water, The University of Iowa, Iowa City, Iowa, USA, 2008.

(50) Nagamori, M.; Funazukuri, T. Glucose Production by Hydrolysis of Starch Under Hydrothermal Conditions. *Journal of Chemical Technology and Biotechnology* **2004**, *79*, 229-233.

(51) Rosen, S. L. In *Characterization of Molecular Weight;* Fundamental Principles of Polymeric Materials; John Wiley & Sons, Inc.: New York, 1993; pp 53-78.

(52) Trathnigg, B. In *Size-exclusion Chromatography of Polymers;* Encyclopedia of Analytical Chemistry; John Wiley & Sons Ltd: Chichester, 2000; pp 8008-8008.

(53) VARIAN, I. GPC/SEC Reference Guide. **2010**.

(54) Synder, L.; Kirkland, J. J. In *Introduction to Modern Liquid Chromatography;* John Wiley & Sons, Inc.: New York, 1979; .

(55) Chang, M.; Pound, T. C.; Manley, R. S. J. Gel-Permeation Chromatographic Studies of Cellulose Degradation .1. Treatment with Hydrochloric-Acid. *Journal of Polymer Science Part B-Polymer Physics* **1973**, *11*, 399-411.

(56) Berggren, R.; Berthold, F.; Sjoholm, E.; Lindstrom, M. Improved Methods for Evaluating the Molar Mass Distributions of Cellulose in Kraft Pulp. *J Appl Polym Sci* **2003**, *88*, 1170-1179.

(57) Kanda, T.; Nakakubo, S.; Wakabayashi, K.; Nisizawa, K. In *The Mode of Enzymatic Degradation of Cellulose Based on the Properties of Cellulase Components;* Brown, R. D., Jurasek, L., Eds.; Hydrolysis of Cellulose: Mechanisms of Enzymatic and Acid Catalysis; American Chemical Society: Washington, D. C., 1979; pp 211-236.

(58) Schnabel, W. In *Mechanistic Aspects;* Polymer Degradation, Principles and Practical applications; Macmillan Publishing Co., Inc.: New York, 1981; pp 13-24.

(59) Guaita, M.; Chiantore, O.; Luda, M. P. Monte-Carlo Simulations of Polymer Degradations .1. Degradations without Volatilization. *Macromolecules* **1990**, *23*, 2087-2092.

(60) Emsley, A. M.; Heywood, R. J. Computer Modeling of the Degradation of Linear-Polymers. *Polym. Degrad. Stab.* **1995**, *49*, 145-149.

(61) Bose, S. M.; Git, Y. Mathematical Modelling and Computer Simulation of Linear Polymer Degradation: Simple Scissions. *Macromolecular Theory and Simulations* **2004**, *13*, 453-473.

(62) Montroll, E. W.; Simha, R. Theory of Depolymerization of Long Chain Molecules. *Journal of Chemical Physics* **1940**, *8*, 721-722-727.

(63) Basedow, A. M.; Ebert, K. H.; Fosshag, E. Ultrasonic Degradation of Polymers in Mixed-Solvents. *Makromolekulare Chemie-Macromolecular Chemistry and Physics* **1978**, *179*, 2565-2568.

(64) Mostafa, M. A. K. Degradation of Addition Polymers by Ultrasonic Waves. *Journal of Polymer Science* **1956**, *22*, 535-548.

(65) Glynn, P. A. R.; Vanderho.Bm; Reilly, P. M. General Model for Prediction of Molecular-Weight Distributions of Degraded Polymers - Development and Comparison with Ultrasonic Degradation Experiments. *Journal of Macromolecular Science-Chemistry* **1972**, *A 6*, 1653-1664.

(66) Ballauff, M.; Wolf, B. A. Degradation of Chain Molecules .1. Exact Solution of the Kinetic-Equations. *Macromolecules* **1981**, *14*, 654-658.

(67) Ballauff, M.; Wolf, B. A. Degradation of Chain Molecules .2. Thermodynamically Induced Shear Degradation of Dissolved Polystyrene. *Macromolecules* **1984**, *17*, 209-216.

(68) Yoshioka, T.; Motoki, T.; Okuwaki, A. Kinetics of Hydrolysis of Poly(Ethylene Terephthalate) Powder in Sulfuric Acid by a Modified Shrinking-Core Model. *Ind Eng Chem Res* **2001**, *40*, 75-79.

(69) Yoshioka, T.; Okayama, N.; Okuwaki, A. Kinetics of Hydrolysis of PET Powder in Nitric Acid by a Modified Shrinking-Core Model. *Ind Eng Chem Res* **1998**, *37*, 336-340.

(70) ASTM Standard D 1795-96 In *Standard Test Method for Intrinsic Viscosity of Cellulose;* Annual Book of ASTM Standards; 1997; Vol. 05.01, pp 345-350.

(71) He, C.; Wang, Q. Viscometric Study of Cellulose in PF/DMSO Solution. *J. M. S. - Pure Appl. Chem. ,* **1999**, *A36*, 105-114.

(72) Merienne, S.; Busnel, J. P.; Fricoteaux, F.; Prudhomme, J. C. Size Exclusion Chromatography of Dextrans in DMSO as Eluent. *J. Liq. Chromatogr. Rel. Technol.* **2000**, *23*, 1745-1746-1756.

(73) Striegel, A. M.; Timpa, J. D. Size Exclusion Chromatography of Polysaccharides in Dimethylacetamide-Lithium Chloride. *Strategies in Size Exclusion Chromatography* **1996**, *635*, 366-378.

(74) Dadi, A. P.; Varanasi, S.; Schall, C. A. Enhancement of Cellulose Saccharification Kinetics using an Ionic Liquid Pretreatment Step. *Biotechnol. Bioeng.* **2006**, *95*, 904-910.

(75) Kamiya, N.; Matsushita, Y.; Hanaki, M.; Nakashima, K.; Narita, M.; Goto, M.; & Takahashi, H. Enzymatic in Situ Saccharification of Cellulose in Aqueous-Ionic Liquid Media. *Biotechnol. Lett.* **2008**, *30*, 1037-1038-1040.

(76) Remsing, R. C.; Swatloski, R. P.; Rogers, R. D.; Moyna, G. Mechanism of Cellulose Dissolution in the Ionic Liquid 1-n-Butyl-3-Methylimidazolium Chloride: A C-13 and Cl-35. *Chemical Communications* **2006**, 1271-1273.